2007

Synthesis and Adsorption Studies of the MIcro-Mesoporous Material Sba-15

Eunyoung You
University of Massachusetts Amherst

SYNTHESIS AND ADSORPTION STUDIES OF THE MICRO-MESOPOROUS MATERIAL SBA-15

A Thesis Presented

by

EUNYOUNG YOU

Submitted to the Graduate School of the
University of Massachusetts Amherst in partial fulfillment
of the requirements for the degree of

MASTER OF SCIENCE IN CHEMICAL ENGINEERING

September 2007

Chemical Engineering

SYNTHESIS AND ADSORPTION STUDIES OF THE MICRO-MESOPOROUS MATERIAL SBA-15

A Thesis Presented

by

EUNYOUNG YOU

Approved as to style and content by:

W. Curtis Conner, Jr., Chair

Scott Auerbach, Member

David M. Ford, Member

T. J. Lakis Mountziaris, Department Head
Department of Chemical Engineering

ACKNOWLEDGMENTS

I would like to thank my advisor, Professor W. Curtis Conner, Jr. for his guidance, encouragement, support and patience throughout the years. He was always willing to put his hands on the troublesome adsorption instruments when I was having trouble and giving me helpful suggestions on solving problems in the lab.

I would also like to thank Professor Scott Auerbach for his guidance and advice with this project and my graduate school life. I am grateful to Professor David Ford for being a part of my thesis committee and his valuable comments for my thesis.

My thanks go to all past and present Conner group members. Dr. Tompsett has taught me, in many ways, so that I can adapt to the research environment quickly and has given me great suggestions for this project. He amazes a lot of people with his great literature searching skills. I am in great debt to Karl for his help in the lab and bright comments on my thesis. I value his great effort to organize things in the lab and his sense of humor which made the lab work enjoyable.

I am grateful for people from the Chemical Engineering department at UMass: My friends, Bing, Miguel, Monica, Sarvesh, Seo (and his lovely wife Seungeun), Xiaoming (alphabetic order) and many more. Without them, graduate life would have never been the same. Many of the departmental secretaries, Bobbie, Ellen, Lisa, and Margie, and the workshop staffs, Gary, Joe and Les have provided lots of warm help which made my steps toward this work smoother and lighter.

Many thanks go to my friends from the Amherst Korean Church. I have gained lifelong friendships that I won't forget. They will be in my thoughts and prayers.

I would also like to thank my family who always believed in me and provided me with incessant love and prayers.

Lastly, but above all, I praise my Lord, Jesus Christ for guiding me, encouraging me and loving me always. "*The Lord is my strength and my song; he has become by salvation"*

ABSTRACT

SYNTHESIS AND ADSORPTION STUDIES OF
THE MICRO-MESOPOROUS MATERIAL SBA-15

September 2007

EUNYOUNG YOU

B.E., KOREA UNIVERSITY

M.S., UNIVERSITY OF MASSACHUSETTS AMHERST

Directed by Professor W. Curtis Conner, Jr.

Over the past decades, there have been worldwide efforts to synthesize new types of ordered porous materials for catalysis, separations, etc. Among those, mesoporous material with microporous walls are promising in a sense that while mesopores act as channels for the reactant transport with little diffusion limitation, micropores in the wall act as active sites for reactions or storage of the molecules.

In this study, we focused on the SBA-15 material, which is a highly ordered mesoporous silica material with micropores present in the wall. We have studied the synthesis of the material by manipulating various factors that are known to have influence on the porous characteristic of the material. We have aimed our studies particularly on the micropores present in the material. Unlike zeolite materials, which have regular, well characterized pore structures, micropores in the SBA-15 are not ordered, thus may have a very broad pore size distribution. We have synthesized sets of mesoporous silica materials that have characteristics similar to those reported in the literature. Using microwave heating, we were able to synthesize the target material within a short period of time, about

10 to 12-fold reduction of the conventionally known synthesis time. The synthesized materials were initially characterized using XRD and SEM. Adsorption studies were then undertaken on the materials to determine the surface area and pore structure. The interpretation of micropores has heretofore been problematic and the models are ambiguous. Relatively simply ordered, 1-dimensional channel type, zeolite materials were also studied; MTW, MTT, TON, ATS, VET frameworks. Adsorption isotherms of these materials were obtained and simple empirical models were developed to determine the pore size distribution.

Further, a sequential adsorption technique, using *n*-nonane as a preadsorbate, was used to evaluate the realistic external surface areas of zeolite materials and mesopore surface areas of micro-mesoporous materials. Applying this technique to "multidimensional pore system" will provide another way to obtain the realistic surface area and mesopore size distribution.

TABLE OF CONTENTS

Page

LIST OF TABLES

LIST OF FIGURES

CHAPTER 1

INTRODUCTION

1.1 Motivation

In the last few decades, remarkable advances have been made in the synthesis of novel nanoporous solids for use in catalysis, separations etc. A variety of microporous silica based materials, namely zeolites were discovered by many researchers and at the same time, the theoretical studies of the assessment of zeolite structures were being developed. However, regardless of the growing needs in the application of zeolite materials, single zeolite crystals cannot be used directly for these applications. Zeolite crystallites need to be formed into pellets or need to be grown into a membrane. Therefore, we are not only dealing with micropores, which are an inherent characteristic of zeolites but also with the meso- macro-pores that are formed in the process. Systems that have both micropores and mesopores are called "multidimensional nanoporous networks." Hence, studying the structural characteristic of complex nanoporous networks is more practical, since it is one step closer to the real system that is employed in industry e.g. membrane. Micropores and mesoporous materials cannot be studied individually. To meet this need, therefore it is necessary to investigate mesoporous materials that also have micropores.

1.2 Objective

- The objective of the current work includes the synthesis of the nanoporous networks that have both micropores and mesopores. We studied the structural characterization

of a porous silica material with micropores and mesopores, namely SBA-15. Specifically, the analysis and interpretation of physical adsorption techniques for pore size determination and surface area assessment are our goal.

- To develop an analytical approach to extract the micropore volume influence on the measurement of mesoporous material that has micropores within the pore walls.
- To develop an empirical model using standard 1-dimensional zeolites to quantitatively determine the micropore dimension of the SBA-15 materials.
- To introduce a new technique, sequential adsorption, to assess the external surface area of microporous materials and the mesoporous surface area for multi-scale nanoporous networks.

1.3 Systems of Interest and Approach

To achieve these objectives, we will examine two different types of porous materials namely, microporous crystalline solids and mesoporous materials with micropores in the mesopore walls.

Zeolites are the most commonly known microporous materials with well characterized regular pore sizes. We selected MFI, MTT, MTW, TON, VET, and ATS type framework zeolites as standard microporous materials. As for the first framework, MFI, we used commercially available silicalite samples (from Union Carbide) for the study and the rest of the framework samples were kindly provided by Stacey Zones from Chevron Research and Technology, Richmond, California, USA.

As for the micro- mesoporous material, we extensively worked on SBA-15. We synthesized SBA-15 by varying different synthesis conditions. Samples were initially characterized by X-ray diffraction (XRD) and scanning electron microscopy (SEM) and primarily with physical adsorption using readily available adsorption instruments, AUTOSORB®-1-C (an automated adsorption system manufactured by Quantachrome Instruments, Boynton Beach, FL, USA) and VAS (Vallee Adsorption System, assembled by Steven Vallee in Conner research group, Univ. of Massachusetts, Amherst, USA). Physical adsorption characterization involves the analysis of collected isotherms with software provided by Quantachrome Instruments. An in-house Microsoft Excel® spreadsheet template will also be used for the modified adsorption analysis of zeolite materials.

CHAPTER 2

BACKGROUND

2.1 Nanoporous Network

Porosity, which is the fraction of pore volume, is the major characteristic required for a solid to be used in catalysis, storage and separation, because it gives rise to a high surface area of the material. Porous materials are categorized into three different types according to their pore sizes. Dubinin[1] originally proposed the classification and it was officially accepted by the International Union of Pure and Applied Chemistry (IUPAC).[2] If the pore width is less than 2 nm the pores are called *micropores*, if they are between 2 and 50 nm, *mesopores*, and if they are more than 50 nm, *macropores*. When different sized pores are mixed, we call the system a multi-scale porous network or nanoporous network.

2.2 SBA-15

2.2.1 Background

There have been growing demands for new types of mesoporous materials after discovering that M41S materials[3-7] have poor thermal stress properties. A novel material, SBA-15, was first synthesized by the research group lead by Stucky[8, 9]at UC-Santa Barbara. SBA-15 earned much attention in the last decade owing to its excellent thermal stability, variable pore sizes, and tailored particle morphology. The pore topology consists of a two dimensional mesoporous network of uniform dimensions formed by microporous walls. Compared to zeolites which have pores in the micro-range (4~14Å), SBA-15 material is a

new type of mesoporous material with micropores, hence it is expected to lower the diffusion limitation that a microporous material typically experiences. Zeolites are crystalline while SBA-15's pore walls are essentially amorphous, however, the mesopores of SBA-15 material are regularly spaced due to the templates liquid crystal micelle arrangement.[10]

2.2.2 SBA-15 Synthesis

SBA-15 is synthesized by the use of amphiphilic triblock copolymers, poly(ethylene oxide)-*b*-poly(propylene oxide)-*b*-poly(ethylene oxide) or PEO-PPO-PEO as the organic structure directing agent (template). PEO blocks are hydrophilic, while PPO blocks are hydrophobic. Hence, direct formation of cylindrical micelles with the PEO blocks on the outside can be achieved in the aqueous solution. The aqueous silica cations locate themselves within the hydrophilic regions of the self-assembled system and associate preferentially with the PEO blocks. Removal of the polymer results in a mesoporous solid due to the hexagonal arrangement of cylindrical polymer aggregates and also microporosity generated by PEO segments. [10, 11] Figure 1 shows the hexagonally arranged SBA-15 with and without the template.

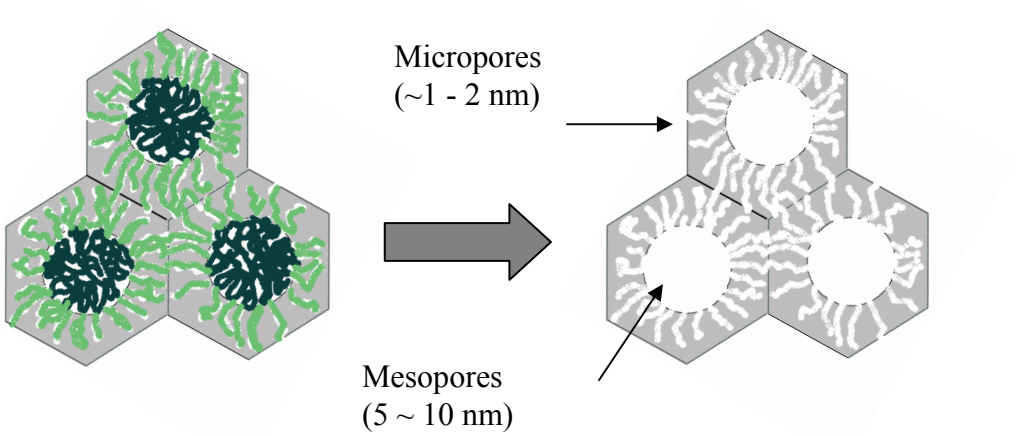

Figure 1 Schematics of SBA-15 as synthesized (left) and after the removal of template (right)

A simplified procedure for typical SBA-15 synthesis is depicted in the following figure (Figure 2).

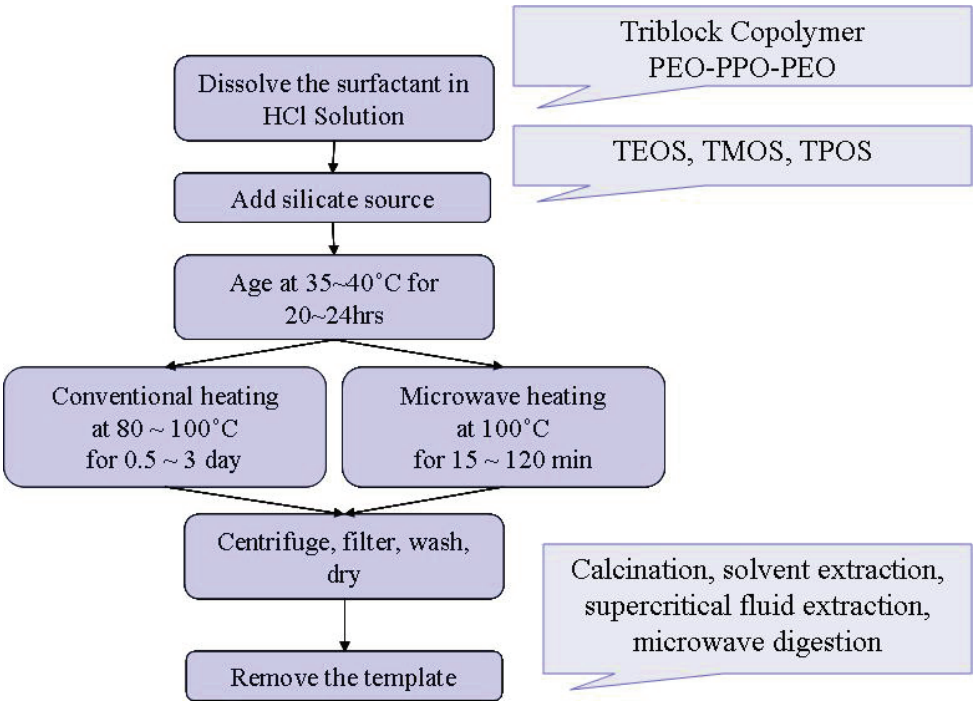

Figure 2 A simplified procedure to obtain SBA-15 samples

The process to obtain solid powder SBA-15 involves dissolving of template polymer in acidic solution, adding a silica source, which is typically either tetraethyl orthosilicate (TEOS), tetramethyl orthosilicate (TMOS), or sodium silicate. The mixed solution is aged at a temperature slightly above room temperature for 20 to 24 hours and heated up to 80 to 100 ^{o}C either in a conventional oven or in a microwave oven for an appropriate amount of time. Precipitated solids are centrifuged, washed and dried. Finally, the organic polymer is removed by calcination (e.g. 550 ^{o}C for 24 hours); by extraction using a solvent or a supercritical fluid[12]; or by microwave digestion.[13]

2.2.2.1 *In situ* studies of the formation mechanism of SBA-15

Due to its structurally interesting properties and potential applications, there is a growing interest to investigate and engineer the structural properties of SBA-15 at optimized synthesis conditions. This motivated the studies on the formation mechanism of SBA-15. Results from *in situ* SAXS[14]/XRD[15, 16], time-resolved NMR and TEM[15, 17], and EPR[18] studies gave us the insight that the hexagonally packed structure is obtained within 2 hours after the addition of the silica source. Flodström *et al*.[17] have concluded that "*for Pluronic P123 amphiphiles as structure directing agents, the polymerization of the silica leads to the introduction of an attractive force between micelles due to a bridging mechanism. This attraction leads to the formation of flocs of micelles, and these flocs eventually reach a critical size where they precipitate. There is a continuing structural change within these clusters involving the coalescence of micelles that tend to form cylindrical aggregates, which order in a two-dimensional hexagonal pattern.*" Fulvio and

coworkers[19] synthesized SBA-15 with TEOS and sodium metasilicate with an aging time of 2 hours, which is 10 to 12-fold reduction of commonly known aging time (20~24 hours). Aged samples were heated at a higher temperature (100 ^{o}C) for longer period of time (12~48 hours). Thus, prepared samples exhibited a p6mm space group which is the characteristic feature for hexagonal structure with X-ray diffraction. Two of the samples exhibited similar surface areas. However, SBA-15 prepared with TEOS showed slightly larger pore volumes than that formed using sodium metasilicate. Sodium metasilicate precursor resulted in SBA-15 with higher microporosity and thicker pore walls. They have also found that the samples' specific surface area decreased with increasing time and temperature of the hydrothermal treatment. However, the mesopore size distributions became narrower and the mesopore widths and volume increased as a function of hydrothermal reaction time and temperature.[20]

2.2.2.2 Control of the microporosity

There have been a great number of studies on controlling the microporosity of SBA-15 materials. When SBA-15 was first synthesized by Stucky *et al.*,[8] there were controversies among research groups over whether SBA-15 is simply an array of uniform mesopores or a network of mesopores and micropores[10]. However, Ryoo *et al*.,[10] for the first time, reported that SBA-15 synthesized with P123 not only consists of ordered mesopores but also of micropores and even smaller mesopores that give the connectivity between the ordered mesopores. It was later found that micropores exist in the silica walls of the ordered mesopores of SBA-15 using gas adsorption, SAXS, and HRTEM.[10, 11, 21-24]

Nowadays, it is acknowledged that the material is mesoporous, and at the same time, it can also be ultra-high-microporous,[25] microporous, or micropore-free,[26] depending on the synthesis conditions. Microporosity of the material can be tuned by many different factors: a) the source of silica (e.g. TEOS, TMOS, sodium silicate, sodium metasilicate), b) the polymer chain length of block copolymers used for the template[27], c) heating method (conventional hydrothermal heating or microwave heating), d) the synthesis temperature[22, 28] and time, e) the H^+/Si molar ratio (pH value),[25] f) the silica source/surfactant ratio,[29] g) the addition of cosolvent(ethanol) and salt[26] etc. It is not easy to understand how each factor influences the microporosity, since the factors typically are not independent.

As briefly mentioned earlier, the microporosity originates from the PEO block in the triblock copolymer, which penetrates into the silica wall and leaves micropores upon removal.[23] As the synthesis temperature increases, the micropore volume decreases. This is due to the partial dehydration of the PEO blocks at elevated temperature, consequently, it decreases the interaction between micelles through the PEO chains so that these become less occluded into the silica wall, resulting in the microporosity reduction.[23, 30]

Newalkar and Komarneni[26] have accomplished the synthesis procedure by heating the precursor solution with microwaves, resulting in a micropore-free SBA-15. Miyazawa and Inagaki[29] demonstrated control over the microporosity within the pore walls of SBA-15 by varying the synthesis temperature and the TEOS/surfactant ratio. When the synthesis temperature was reduced from 100^{o}C to 80^{o}C the micropore volume increased,[29, 30] and when the TEOS/P104 ratio was increased, the micropore volume was increased.[29] However, increasing the micropore volume by adjusting the silica source to surfactant ratio

needs to be carried out with care. 3D TEM studies[31] found that increasing the TEOS to template (P123) ratio would result in not only the increase of the microporosity but also increase of the mesopore axial curvature within the SBA-15 particle. Hence, the diffusion path length through the mesopores cannot be estimated in a straight forward manner from the particle size. This needs to be considered when using the particle size as the characteristic length for the diffusion studies for this typeof material, especially when the sample being studied was synthesized with high TEOS/P123 ratio, such as plugged hexagonal templated silicas (PHTS).[32, 33]

PHTS is proposed to contain microporous nanocapsules or plugs inside the mesoporous channels. These plugs are formed by the use of excess silica source (TEOS) in the synthesis and its rapid hydrolysis during the synthesis. It is claimed by the authors[32, 33] that the microporosity of the plugs are also directed by Pluronic triblock copolymers. The template copolymers are in fact polydisperse, hence, they contain numerous diblock copolymers and free PO chains. Some of these might have been involved in the process of nanoplug formation giving rise to micropores. Compared to normal SBA-15 materials, PHTS are claimed to be mechanically and hydrothermally more stable. And due to the presence of microporous nanocapsules inside the mesopore, it was obvious that the micropore volume was much higher.

Based on these findings, we studied, in detail, the microporosity of SBA-15 and related micro-mesoporous network materials.

2.2.3 Application of SBA-15

Due to its distinct structure, it was claimed that SBA-15 will provide an ideal reactor or catalyst support[34]. While mesopores act as channels for the reactant transport with little diffusion limitation, micropores in the wall act as active sites for reactions.[35] Hence, SBA-15 silica has a high potential for application in various areas of catalysis, separations, sensors, and template[36] for synthesis of novel mesoporous materials.

2.3 Characterization of Pore Structure

Characterization of the pore structure of materials is essential, since many of their properties are determined or strongly influenced by these characteristics. For this reason, considerable effort has been undertaken to extensively characterize the pore structure.[37]

2.3.1 Physical Adsorption

Perhaps physical adsorption is the most extensively used method to determine the textural properties of a solid material in a relatively straightforward manner. Adsorption is the attachment of a species, the *adsorbate* or *adsorptive*, to a surface, the *adsorbent*. If the adsorbent-adsorbate interaction does not involve the formation of chemical bonds, the process is called *physisorption*; if chemical bonds are formed, then the process is *chemisorption*. The reverse process of adsorption is called desorption.

As for the choices of the adsorptive and the temperature to acquire adsorption isotherm, the nitrogen adsorption at its boiling temperature, 77 K, is the standard. Nitrogen adsorption at liquid nitrogen temperature enables the high resolution adsorption experiment

so far as the instrument allows (Low pressure reading gauges and turbomolecular pump are essential). The next candidate is argon adsorption at its boiling point, 87 K (or 77 K). While liquid argon comes at a higher cost, it provides many advantages. Argon adsorption by micropores occurs at least an order of magnitude higher relative pressure (P/P_o where P_o is the saturation pressure) than with nitrogen adsorption at 77 K. Hence, as far as pressure readings from the pressure transducers are concerned, argon adsorption gives more reliable data.[38] Argon adsorption at 87 K (or 77 K) is suggested as being preferred over nitrogen adsorption at 77 K possibly due to the presence of quadrupolar moment in nitrogen.[39, 40] The quadrupolar moment could result in an enhanced interaction of the nitrogen molecule with the heterogeneous surface of the zeolite framework that might lead to difficulty when differentiating zeolites with different pore sizes.

2.3.2 Measuring Adsorption Isotherms

When an empty porous solid is exposed to a gas in a closed volume, the solid starts to adsorb the gas and the process is accompanied by the increase in the weight of the solid and a decrease in the pressure of the gas. After some time, this process reaches an equilibrium, and one can calculate the amount of gas adsorbed by applying the ideal gas law, under one condition; the volume of the vessel and the solid should be known prior to this process. This is a simple description of a static volumetric adsorption experiment.

The amount of gas adsorbed by a sample of solid, n, is proportional to the mass, m, of the sample, and it depends on the temperature, T, the pressure of the gas, P, and the nature of both the solid and the gas. Hence, we can say that,

$$n = f(P, T, gas, solid) \quad (1)$$

For a given gas adsorbed on a particular solid maintained at a fixed temperature, this becomes,

$$n = f(P)_{T, gas, solid.} \quad (2)$$

If the temperature is below the critical temperature of the gas, P/P_o, instead of P is usually employed, where P_o is the saturation pressure of the adsorptive at the fixed temperature

Hence, the equation more simplifies to,

$$n = f(P/P_o)_{T, gas, solid} \quad (3)$$

The amount of gas adsorbed, n, can be expressed in many ways; mass of gas (mg), volume of gas reduced to STP (cm^3 (STP)), or moles. Construction of an adsorption isotherm, therefore, means constructing the above relation or plotting n versus P/P_o. . For physical adsorption, different sorbents often give rise to similar volume adsorbed vs. P/P_o data.

2.3.3 Analysis of Adsorption Isotherm

Experimental isotherms are analyzed for surface area and porosity measurement. There are various theories and models proposed to transform the obtained adsorption data into structural information, as discussed below.

2.3.3.1 Surface Area Measurement

The Brunauer-Emmett-Teller (BET) method[41] is the most widely used procedure for the surface area measurement of solid materials. This involves the use of BET equation such as the following.

$$\frac{P/P_o}{V_a(1-P/P_o)} = \frac{1}{V_m C} + (P/P_o)\frac{(C-1)}{V_m C} \tag{4}$$

where, V_a is the volume adsorbed, P/P_o is the relative pressure, equilibrium pressure to saturation pressure ratio, V_m is the monolayer volume, C is the BET constant.

Plotting the left hand term versus P/P_o yields a straight line with slope $\frac{(C-1)}{V_m C}$ and intercept, $\frac{1}{V_m C}$.

The monolayer volume, V_m and BET constant C can be calculated easily from the obtained slope and intercept.

The surface area of 1g of the solid, A can be expressed as the following equation.

$$A = n_m a_m N_{AV} \tag{5}$$

where, n_m is the moles of adsorbate per gram of adsorbent, a_m is the average area occupied by a molecule in the completed monolayer, N_{AV} is the Avogadro's constant. If the volume of gas (reduced to STP), V_m is used instead, the equation becomes,

$$A = \frac{V_m}{22414} a_m N_{AV} \times 10^{-20} \tag{6}$$

assuming that A is in m^2/g and a_m in $Å^2$/molecule units. It is widely accepted that for N_2 at 77 K, a_m = 16.2 $Å^2$,[37] for Ar at 87 K, a_m = 14.3 $Å^2$.[37]

The BET constant, C, reflects the difference in the energy of adsorption for the first layer compared to the difference in adsorption of subsequent layers on top of those already adsorbed. C can be expressed as,[37]

$$C = 1 + \frac{\text{slope}}{\text{intercept}} = \frac{a_1 v_2}{a_2 v_1} e^{-(E_1 - E_2)/RT} \quad (7)$$

The pre-exponential term is composed of a_i, a condensation coefficient (fraction of incident molecules which actually condense), and v_i, the frequency of oscillation of adsorbed molecules in a direction normal to the surface, where i=1 or 2 for the first and second adsorbed layer, respectively. E_1 is an energy of adsorption between the surface and the first layer and E_2 is that of second and subsequent layers. In practice, the BET constant C is almost always taken as,

$$C = 1 + \frac{\text{slope}}{\text{intercept}} = e^{-(E_1 - E_2)/RT} \quad (8)$$

The BET model can be applied to the restricted relative pressure ranges from 0.05 to 0.3, and Gregg and Sing[37] suggested that the BET analysis is credible only if the obtained C constant values are between 20 and 400.

2.3.3.2 Micropore Pore Size Analysis

The micropore size is most often estimated using Horvath-Kawazoe (HK)[42] and/or Saito-Foley (SF)[43]models. These models are relatively simple in terms of concept and

mathematics, thus they provide easy analysis of micropore structures using the adsorption isotherms. The foundation of these methods is the potential energy of interaction between the adsorbate and adsorbent molecules. The difference between the two is the geometry of the adsorbent pore structure; HK method[42] is developed based on slit-like pores, usually for carbon based materials whereas the SF method[43] was developed for oxide materials with spherical and cylindrical pores. Both methods provide the relations between the relative pressure and the effective pore diameter (width), d_{eff}, thereby enabling the transformation of $V_a = f(P/P_o)$ relation to $V_a = g(d_{eff})$ relation. Therefore, a pore size distribution can be obtained by differentiating the volume of gas adsorbed relative to the total uptake (V_a / V_t, where V_t is the total pore volume), with respect to the pore diameter.

The final expressions of each model equation are given below.

For HK, slit model,

$$RT \ln \frac{P}{P_o} = N_{AV} \frac{N_A A_{A-A} + N_E A_{E-A}}{\sigma^4 (L - 2d_o)} \times \left[-\frac{\sigma^4}{3(L-d_o)^3} - \frac{\sigma^{10}}{9(L-d_o)^9} - \frac{\sigma^4}{3d_o^{\,3}} + \frac{\sigma^{10}}{9d_o^{\,9}} \right] \qquad (9)$$

For SF, cylindrical model with line-averaged,

$$\ln \frac{P}{P_o} = \frac{3}{4} \frac{\pi N_{AV}}{RT} \frac{(N_A A_{A-A} + N_E A_{E-A})}{d_o^{\,4}} \times \sum_{k=o}^{\infty} \left[\frac{1}{2k+1} \left(1 - \frac{d_o}{r_p} \right)^{2k} \left\{ \frac{21}{32} \alpha_k \left(\frac{d_o}{r_p} \right)^{10} - \beta_k \left(\frac{d_o}{r_p} \right)^4 \right\} \right] \qquad (10)$$

For SF with area-averaged,

$$\ln\frac{P}{P_o}=\frac{3}{4}\frac{\pi N_{AV}}{RT}\frac{(N_A A_{A-A}+N_E A_{E-A})}{{d_o}^4}\times\sum_{k=o}^{\infty}\left[\frac{1}{k+1}\left(1-\frac{d_o}{r_p}\right)^{2k}\left\{\frac{21}{32}\alpha_k\left(\frac{d_o}{r_p}\right)^{10}-\beta_k\left(\frac{d_o}{r_p}\right)^{4}\right\}\right] \quad (11)$$

, where the expansion coefficients α_k and β_k are expressed as:

$$\alpha_k=\left(\frac{-4.5-k}{k}\right)^2\alpha_{k-1} \quad (12)$$

$$\beta_k=\left(\frac{-1.5-k}{k}\right)^2\beta_{k-1} \quad (13)$$

with α_0 and β_0 both equal to one.

R is the gas constant, T is the temperature, P/P_o is the relative pressure, and N_{AV} is the Avogadro's constant. Subscript A refers to the adsorbate, while E refers to the adsorbent. N is number of molecules per unit area, A is the dispersion constant between two molecules, d_o is the arithmetic mean of the diameters of adsorbent and adsorbate, L is the distance between the nuclei of the two parallel layers, σ is 0.858 d_o and r_p is the pore radius. The detailed information on these parameters can be found in the literature.[43]

2.3.3.3 Micropore volume evaluation

The most used methods for microporosity evaluation are comparison plots, i.e., t-plots and α_s plots. They both involve the use of isotherm for a standard sample, i.e., a standard isotherm, where standard sample is a nonporous solid having the same surface chemistry as that of the test sample, e.g., a silica.

t-plot[44] is based on the t-curve, which is constructed by plotting the standard isotherm with t, the statistical thickness of the film. t is evaluated by the following equation.[45]

$$t = \frac{n}{n_m}\sigma \tag{14}$$

where, σ is the thickness of a single molecular layer. For nitrogen at 77 K, this is equal to 3.54 Å, assuming that the molecules in the film are hexagonally closed packed[45]. Then, the experimental, or test sample's isotherm is transformed into a t-plot. The amount adsorbed, n, is replotted against t at the corresponding P/P_o.

The t relation could be also obtained from the de Boer equation[1],

$$t(\text{Å}) = \left[\frac{13.99}{\log(P_o/P) + 0.034}\right]^{1/2} \tag{15}$$

or the Halsey equation[46] which, for nitrogen adsorption at 77 K can be expressed as

$$t(\text{Å}) = 3.54 \times \left[\frac{5}{2.303\log(P_o/P)}\right]^{1/3} \tag{16}$$

or in a generalized form as,

$$t(\text{Å}) = a\left[\frac{1}{\ln(P_o/P)}\right]^{1/b} \tag{17}$$

Where the pre-exponential term, a, and the exponential term, b, are 6.0533 and 3.0 for nitrogen adsorption at 77 K.

When miropores are present, the t-plot will exhibit a positive intercept. Converting this intercept to a liquid volume would result in micropore volume.

α_s plots[37] are constructed in a similar manner, however, instead of using n_m which is BET analysis dependent value, this method uses n_s, amount adsorbed at a preselected relative pressure. Typically, it is taken at $(P/P_o)_s = 0.4$. Following this manner, one can construct the α_s-curve. This time, α_s is evaluated by the following equation.

$$\alpha_s = \frac{n}{n_s} \tag{18}$$

Then, the α_s-plot can be constructed in an analogous manner to the t-plot.

2.3.3.4 Pore Size Distribution for Mesopores

For cylindrical pores, capillary condensation occurs during adsorption via a "cylindrical meniscus" while capillary evaporation occurs during desorption via a "hemispherical meniscus." Therefore, the pores of a specific size are filled at a higher pressure and emptied at lower pressures, and thus hysteresis is observed.[37]

It is controversial whether to use adsorption branch or desorption branch to correctly assess the mesopore size distribution. Groen *et al.*[47] have reviewed on the use of either adsorption and desorption branch for pore size distribution calculation. It is believed that desorption branch is often more affected by pore network effects than the adsorption branch.[48, 49] Ravikovitch and coworkers[50] suggest to use desorption isotherm branch to perform the pore size distribution calculation when a hysteresis is observed. They find that desorption isotherm corresponds to the thermodynamic equilibrium evaporation predicted by theoretical model. Therefore, for a purely mesoporous material, using desorption

isotherm branch is favored for mesopore size distribution calculation, otherwise, it needs to be carefully decided on which isotherm to base the pore size calculation.

BJH method[51] is the most often used for estimating mesopore size distribution. This model is based on the Kelvin equation and corrected for multilayer adsorption using statistical film thickness.

Pore radius r_p is the summation of Kelvin radius, r_K and the statistical film thickness, t.

$$r_p = r_K + t \tag{19}$$

where, r_K is calculated from Kelvin equation.

$$r_K = \frac{-2\gamma V_L}{RT\ln(P/P_o)} \tag{20}$$

where, γ and V_L are the surface tension and molar volume of the liquid adsorbate, respectively. For nitrogen adsorption at 77 K and argon adsorption at 87 K, the Kelvin equation is reduced to the following expressions where r_K is in unit of Å.

N_2 at 77 K: $$r_K = \frac{-4.14}{\log(P/P_o)} \tag{21}[51]$$

Ar at 87 K $$r_K = \frac{-3.76}{\log(P/P_o)} \tag{22}[52]$$

Statistical film thickness, t, is determined from the standard isotherm (t-plot).

The BJH method is conventionally employed on materials with well defined cylindrical pores. However, this method does not take into account the influence of solid-

fluid interactions on capillary condensation, hence, it underestimates the real pore size.[24] Nevertheless, it is still widely used in the characterization of porous materials.

Nonlocal density functional theory (NLDFT)[24, 53] is recognized as an alternative method to characterize micro- and mesopores. While conventional methods such as BJH[51], SF[43] and HK[42] cannot give a realistic description of micropore filling or even narrow mesopore filling, density functional theory (DFT) provides molecular level description of adsorption and phase behavior of fluids in narrow pores.

CHAPTER 3

SYNTHESIS OF MICRO-MESOPOROUS MATERIAL

3.1 Overview

The general structure of this chapter includes the preparation of different micro-mesoporous samples and their structural characterization. Characterization tools include X-ray diffraction, scanning electron microscopy and physical adsorption.

X-ray Diffraction

All samples of micro-mesoporous material were characterized with X-ray diffraction (XRD). X-ray diffractograms were recorded on a PANalytical X'Pert PRO X'Celerator using Ni filtered CuKα radiation (λ = 1.54187 Å). The data was collected with 2θ varying from 0.501^{o} to 5.999^{o}, with an increment of 0.002089^{o}. X-ray diffraction typically gives information on the crystal structure of a material. In the case of SBA-15, the mesopores have a regular hexagonal order giving rise to small angle X-ray peaks. Typically, the XRD patterns of calcined SBA-15 samples exhibit three clear peaks which are characteristic of hexagonally ordered structures (p6mm space group), namely the (100), (110), and (200) crystal planes. The (100) d-spacing from the diffraction pattern was calculated to obtain the a-parameter (denoted as *a*), which is the mesopore center-to-center distance ($a = 2/\sqrt{3}\ d(100)$). The calculated a-parameter value will be combined with adsorption results to further calculate the thickness of mesopore wall (t = a – D, where t is wall thickness and D is the mesopore size). Kruk and Jaroniec[23] reported XRD pattern interpretation studies and its relationship to pore wall thickness. They claim the pore wall

thickness (relative to the unit cell size) tends to decrease as the intensity of the (200) peak relative to the (110) peak decreases.

Scanning Electron Microscopy

Scanning electron microscopy (SEM) enables one to study a crystal's topography. SEM images were obtained for some of the synthesized SBA-15 samples using a JEOL JEM-5400 scanning electron microscope. The micrograph shows the particle size and its morphology. However, a morphological study is beyond the scope of this work and therefore will not be discussed in detail. The particle size will be of relevance, however, for transport studies of frequency response and zero length chromatography.

Physical Adsorption

Adsorption experiments were performed using nitrogen and argon at 77 K and 87 K, respectively, on the prepared samples using an AUTOSORB®-1-C and VAS[54] adsorption instruments. Ultra high purity grade helium (for dead space calculation), nitrogen and argon gas cylinders were obtained from Merriam-Graves. Samples of 30~90 mg were placed in a glass adsorption sample cell (6 mm outside diameter stem). The samples were outgassed prior to the adsorption experiment at 300^{o}C for 4 to 20 hours depending on the sample. This step is required to eliminate any possible remaining adsorbate from earlier adsorption run and/or molecules that adsorbed when the sample was exposed to the air.

A more highly ordered material gives a higher pore volume.[55] Hence, we can determine whether a material is highly ordered or not from the adsorption isotherm in

conjunction with the XRD pattern. Typical SBA-15 adsorption isotherms exhibit hysteresis loops with sharp adsorption and desorption branches. The sharpness of the adsorption branch indicates a narrow mesopore size distribution.[23]

Measured isotherms were processed for the data reduction using Quantachrome Inc. software AS1WIN v1.51 to estimate the BET surface area and BET C constant,[41] BJH mesopore diameter,[51] wall thickness, HK pore width,[42] SF pore diameter,[43] NLDFT mesopore width,[24] micropore volume based on the α_s method, total pore volume calculated at $P/P_o = 0.99$ (or sometimes at 0.95). They will be denoted as $SA_{BET}(m^2/g)$, C_{BET}, $D_{BJH}(Å)$, t(Å), $d_{HK}(Å)$, $d_{SF}(Å)$, $D_{NLDFT}(Å)$, $V_{\mu}(cc/g)$, and $V_{total}(cc/g)$,respectively. All the pore diameters are determined from the peak position in the pore size distribution. Ar zeolite/silica equilibrium transition kernel at 87 K was used for NLDFT model. Standard nitrogen adsorption isotherm at 77 K[56] and argon adsorption isotherm at 87 K[57] were used for α_s method and are provided in the Appendix.

3.2 Standard SBA-15 Samples

3.2.1 Objective

A set of SBA-15 materials were synthesized according to the procedure reported in the literatures[58, 59] to set as standard SBA-15 samples. A sample S1 was synthesized with conventional heating method and a sample S2 was synthesized with microwave heating. The set of standard samples were accordingly synthesized and characterized with the tools described as to the aforementioned methods and settings.

3.2.2 Conventional Synthesis of Standard Sample, S1

A detailed synthesis procedure for SBA-15 has been reported by Zhao *et al*.[8] However, the current work was based on the synthesis procedure used by Luan *et al*.,[58] which is briefly outlined here.

First, 2 g of Pluronic P123 (Aldrich) was dissolved in 15 g of deionized water and 60 g of 2 M HCl solution (Fisher Scientific) while stirring. Then 4.25 g of tetraethyl orthosilicate (TEOS, 98 wt %, Aldrich) was added to the solution while stirring. This mixture was continuously stirred for 24 hours while the container was immersed in a silicone oil bath that was maintained at 40^{o}C. The gel mixture was then transferred to a Teflon-lined autoclave and kept static at 100^{o}C for two days. The product was centrifuged at 11000 rpm and washed with deionized water several times, and dried in air at 80^{o}C. The material was calcined in static air at 550^{o}C for 24 hours to remove the polymer template and to obtain the white powder SBA-15 we called standard sample S1.

3.2.3 Microwave Synthesis of Standard Sample. S2

Newalkar *et al*.,[59] reported the microwave-assisted synthesis of SBA-15. Conventional synthesis of SBA-15, typically requires approximately 24 hours of aging at 35~40^{o}C in order for the structure directing agent (SDA), or template, to self-assemble, and heating of the solution to 80~100^{o}C for a further 12 hours to two days for crystallization to occur. Newalkar and coworkers'[59] preparation of SBA-15 takes considerably less time. We prepared SBA-15 using microwave based on Newalar's preparation method. The gel was obtained by dissolving the amphiphile template, Pluronic P123 ($PEO_{20}PPO_{70}PEO_{20}$; MW

5800, Aldrich), in acidic solution, then adding the silicate source, tetraethylorthosilicate (TEOS, 98 wt % Aldrich). The gel was then heated with the microwave at 100 ^{o}C for a period of 15-120 minutes.

Newalkar *et al.*[59] claimed that they were able to synthesize the SBA-15 material that has textural properties that are similar to those prepared by conventional methods. Microwave-assisted synthesis, however, enabled them to make structurally similar SBA-15 material, in 120 min rather than 2 days.[8]

We have performed a similar preparation procedure to obtain another standard sample prepared with microwave heating which hereafter will be referred to as standard sample S2. Microwave hydrothermal heating was performed using a MARS 5® (CEM Corporation, Matthews, NC) microwave oven using the ramp-to-temperature mode. The microwave oven operates at a frequency of 2.45 GHz. A maximum power input of 300 W was set using a two-minute ramp from room temperature to 100^{o}C. About 80 mL of precursor solution was put into a cylindrical 30 mm diameter reaction vessel (100 mL GreenChem Teflon autoclave supplied by CEM Corporation) and heated for 120 min.

It should be noted that, in general, the maximum power input affects the ramp time in conjunction with the amount of aged precursor solution put in the reaction vessel. When the precursor solution is large in amount, using the low power setting will be insufficient to reach the reaction temperature in a given ramp time. Hence, it should be emphasized that when heating the precursor solution with microwaves, the maximum input power is a key factor in the initial temperature control. However, in our case, heating 80 mL of aged

precursor solution at room temperature to 100^{o}C with 300 W maximum power input was achieved within 1 minute and 30 seconds.

3.2.4 X-ray Diffraction

Figure 3 shows the XRD patterns of the standard samples, S1 and S2. Each pattern shows the peaks that correspond to the hexagonal structure, P6mm. However, we can see that S1 is more highly ordered than S2, since (110) and (200) peaks are more distinct. (100) peak for S2 occurring at higher 2θ than 21 indicates a smaller a-parameter value for S2 which is prepared using microwave heating.

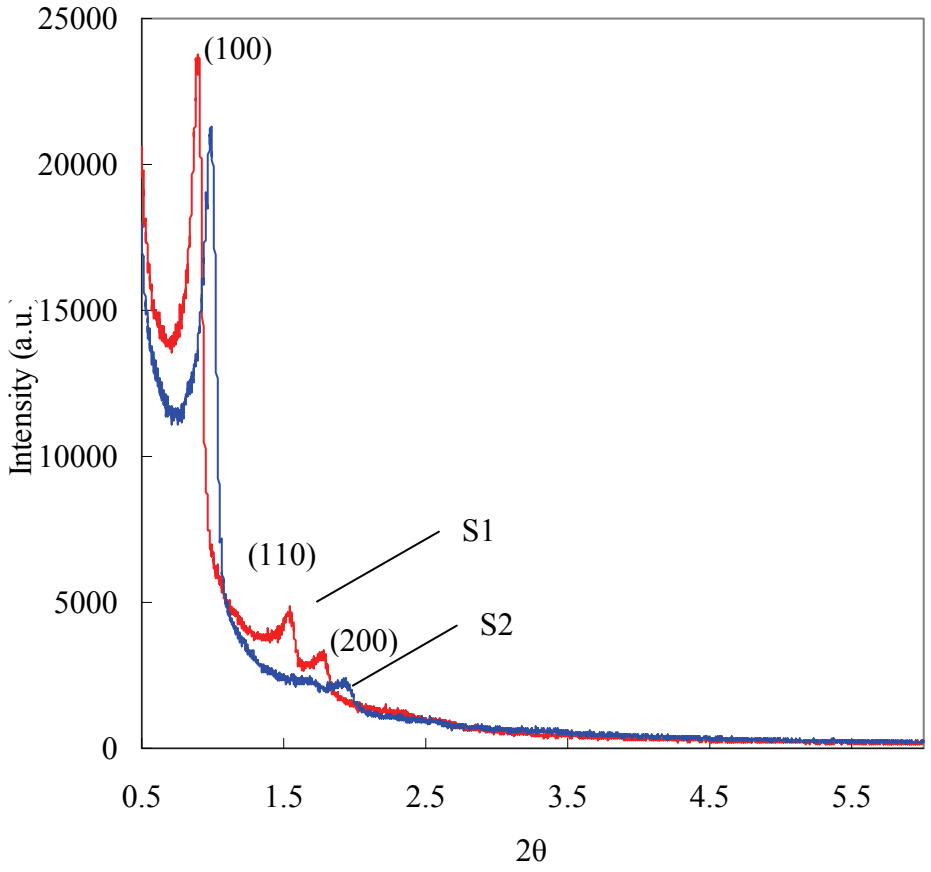

Figure 3 XRD pattern of standard SBA-15 samples S1 and S2

3.2.5 Scanning Electron Microscopy

An SEM image of the standard sample S1 is shown below in Figure 4. The particle size is approximately one micron as can be seen in the figure. It exhibits irregular spherical shape.

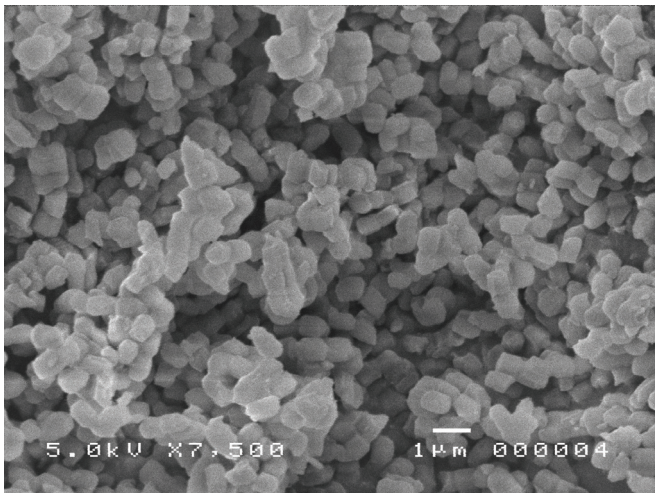

Figure 4 SEM image of SBA-15, standard sample S1

3.2.6 Physical Adsorption

Argon adsorption at 87 K on the standard samples is shown in Figure 5. The adsorption isotherms on standard SBA-15 materials exhibit a well-defined hysteresis loop of type H1 according to the IUPAC classification.[37] This type of hysteresis loop is observed for the open ended cylindrical mesopores during the adsorption and desorption.

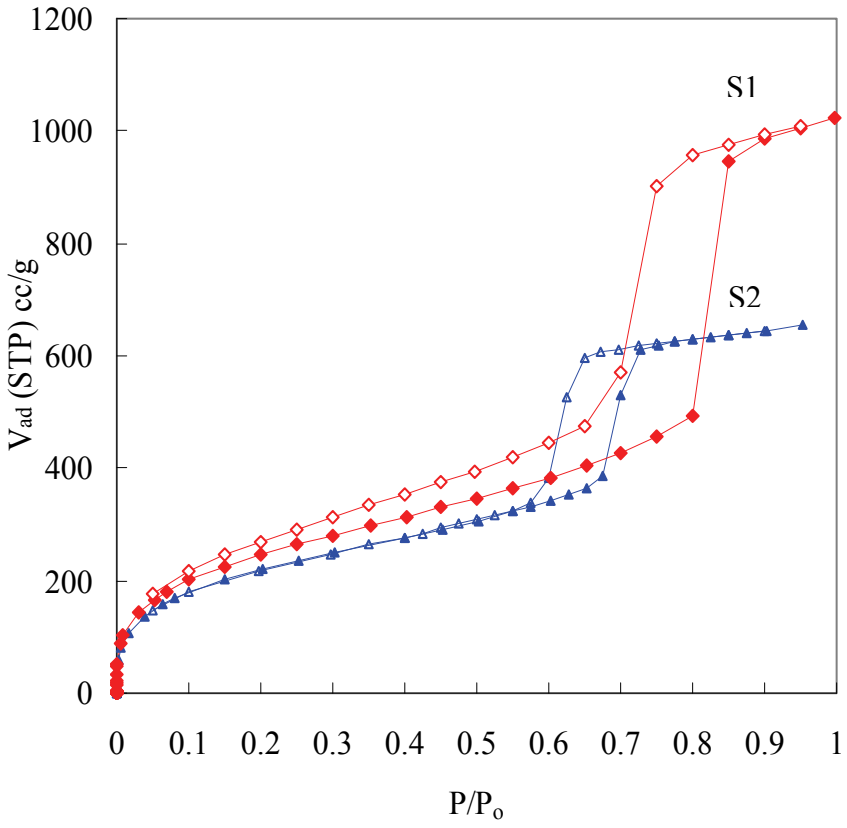

Figure 5 Adsorption isotherms of argon at 87 K on standard samples S1 and S2

We infer that S1 has much higher mesopore volume compare to S2. Up to the relative pressure where the hysteresis begins, the volume adsorbed difference between two isotherms is less than 100 cc/g. However, the difference becomes abruptly high as the mesopores are filled, giving the difference as large as 370 cc/g. We learn that conventionally heated sample, S1 has higher pore volume compare to microwave synthesized sample, S2

3.2.7 Results and Discussion

The structural properties of standard samples are obtained from both XRD and physical adsorption analysis and are shown in Table 1.

Table 1 Structural properties of standard samples obtained from XRD and adsorption isotherms

Sample	*a* (Å)	D_{BJH}(Å) ad/de	t(Å) ad/de	SA_{BET} (m^2/g)	C_{BET}	d_{SF}(Å)	D_{NLDFT} (Å)	V_{μ} (cc/g)	V_{total} (cc/g)
S1	110.7	131.4/83.2	?/27.5	785.1	65.7	7.1	87.8	0.108	1.303
S2	102.6	72.2/57.4	30.4/45.2	694.4	71.27	8.13	70.9	0.096	0.836

It can be seen that conventionally heated sample exhibit larger pore sizes, surface area, micropore volume and total pore volume than that prepared with microwave heating. The wall thickness calculation based on the adsorption branch could not be obtained for S1 since the pore diameter was higher than the a- parameter. The desorption branch finally closed for sample S1 but we can see the closure point is at low relative pressure where the normal point is around 0.42 relative pressure. This might be the experimental error during the sorption isotherm measurement.

3.3 SBA-15 Samples Synthesized with Microwave Heating

3.3.1 Objective

There are many parameters we can manipulate in the microwave hydrothermal synthesis, such as ramping mode, ramping time, hold time, maximum power, frequency of the microwave energy and reactor geometry. We aim to examine the effect of some of these parameters on structural properties of SBA-15 samples.

3.3.2 Synthesis

We have synthesized a set of SBA-15 samples by heating the precursor solutions (~20 mL each) with microwaves to 100^{o}C by varying the ramp time (2 min or 10 min), hold time (90 min or 120 min) and the maximum power input (300 Wor 600 W). Sample names and the conditions used are tabulated in Table 2. The rest of the conditions for synthesizing the precursor solution and the remaining steps to obtain the solid powder were the same as the preparation of sample S2. (refer section 3.2.3)

Table 2 Microwave synthesis methods used to prepare SBA-15 samples by changing ramp time, hold time, maximum power input

Sample ID	Ramp time (min)	Hold time (min)	Maximum Power (W)
MW-rhp	2	90	300
MW-RHp	10	120	300
MW-RhP	10	90	600
MW-rHP	2	120	600
MW-Rhp	10	90	300
MW-rHp	2	120	300
MW-rhP	2	90	600
MW-RHP	10	120	600

For the sake of simplicity, each sample was identified based on the case of initials of ramp time, hold time, and maximum power input. A case sensitive nomenclature was used, such that r is short ramp time, 2 min, and R is longer ramp time, 10 min. Similarly, hold time is denoted, h or H and maximum power as, p or P. Thus, for example, MW-rHp was prepared in the microwave oven with short ramp time, 2 min, long hold time, 120 min, and small power input, 300 W.

3.3.3 X-ray Diffraction

As-obtained samples were subject to XRD characterization and the low angle range diffraction pattern of each sample is shown in Figure 6. The XRD patterns have well-

resolved peaks, which confirms that the materials are structurally similar to SBA-15 and that they can indeed be synthesized in less than 2 hours using microwave energy.

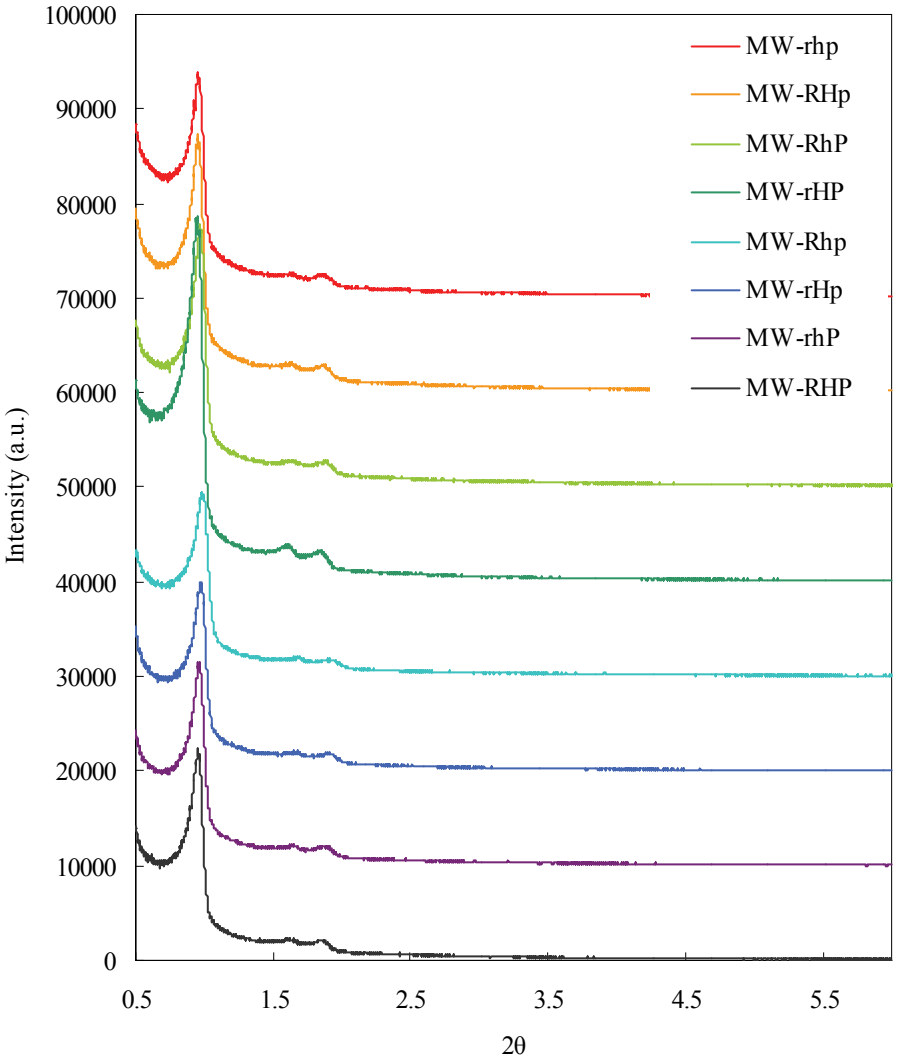

Figure 6 XRD patterns of SBA-15 synthesized in microwave oven with different synthesis conditions

3.3.4 Physical Adsorption

The SBA-15 samples prepared in section 3.3.2 were characterized using argon adsorption. Isotherms at 87 K were obtained using an AUTOSORB®-1-C. (Quantachrome

Instruments) Figure 7 shows the overlay of the argon adsorption isotherms of microwave synthesized samples at 87 K. Individual samples' isotherms are shown in the Appendix. (Figure 33 - 40) Especially, the high resolution adsorption isotherms can be found in the appended isotherms. The micropore filling starts in the $2 \times 10^{-6} \sim 4 \times 10^{-6}$ relative pressure region. All the isotherms exhibit typical H1 type hysteresis which confirm that they possess open-ended cylindrical mesopores.[37]

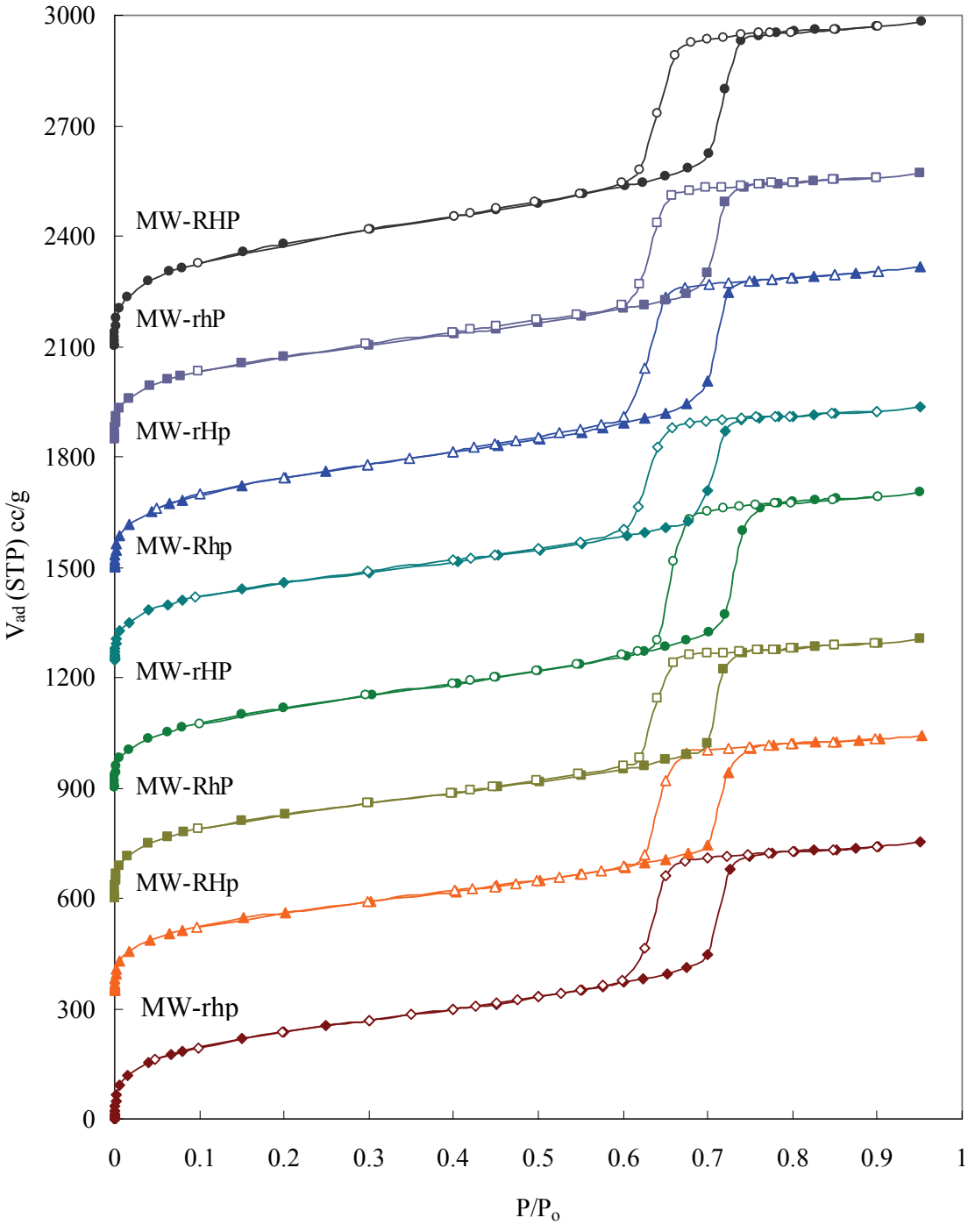

Figure 7 Argon adsorption isotherms at 87 K on microwave-synthesized samples
The isotherms for samples MW-RHp, MW-RhP, MW-rHP, MW-Rhp, MW-rHp, MW-rhP, and MW-RHP were offset vertically by 350, 600, 900, 1250, 1500, 1850, and 2100 cc/g, respectively.

3.3.5 Results and Discussion

The structural properties calculated from both XRD and Ar adsorption isotherm are tabulated in Table 3.

Table 3 Textural properties of microwave synthesized SBA-15 samples obtained from XRD and adsorption isotherms

Sample ID	a (Å)	D_{BJH} (Å) ad/de [a]	t (Å) ad/de [b]	SA_{BET} (m^2/g)	C_{BET}	d_{HK} (Å)	d_{SF} (Å)	D_{NLDFT} (Å)	V_{μ} (cc/g)
MW-rhp	107.3	78.7/ 61.9	28.6/ 45.4	744.6	86.6	5.0	7.5	70.9	0.101
MW-RHp	106.8	78.8/ 61.8	28.0/ 45.0	668.9	75.9	5.0	7.9	70.9	0.086
MW-RhP	105.4	78.0/ 60.4	27.4/ 45.0	714.2	93.3	4.9	5.0	68.3	0.109
MW-rHP	107.5	84.1/ 64.0	23.4/ 43.5	700.2	56.1	5.1	8.0	73.5	0.066
MW-Rhp	103.5	78.1/ 60.3	25.4/ 43.3	658.8	68.9	5.0	8.0	68.3	0.075
MW-rHp	104.6	78.8/ 61.9	25.9/ 42.8	776.1	59.1	4.9	5.0	68.3	0.082
MW-rhP	105.3	78.1/ 60.3	27.2/ 45.0	705.3	69.3	5.1	7.6	68.3	0.089
MW-RHP	106.9	78.2/ 64.2	28.8/ 42.7	879.8	74.6	5.0	7.9	68.3	0.122

[a] D_{BJH} calculated based on adsorption isotherm (ad) and desorption isotherm (de). [b] Wall thickness t obtained from a-parameter by subtracting calculated D_{BJH} which was based on adsorption isotherm (ad) and desorption isotherm (de).

In order to verify the effects of ramp time, hold time, and input power on each property, we can compare the sets of samples as follows: for ramp rate, compare _hp, _Hp, _hP, _HP; for hold time, compare r_p, R_p, r_P, R_P; for power, compare rh_, Rh_, rH_, RH_. For example, to learn the effect of ramp rate, compare _hp set, which consists of samples MW-Rhp and MW-rhp.

As for the a-parameters, we can draw careful generalizations from these experiments. Faster ramp rates (small ramp time) result in larger a-parameters. Samples prepared with longer hold times tend to result in larger a-parameters. Changing the maximum power input had a negligible or indeterminable influence on the a-parameters.

Surprisingly, all eight samples showed nearly same BJH mesopore diameter, D_{BJH}, 78 Å, except the sample MW-rHP.

BET surface areas of the microwave-synthesized samples were between 650 and 900 m^2/g. Longer hold time yielded higher BET surface areas, while other variables had negligible or indeterminable consequences. The BET C constants were all within the applicable range for BET analysis (20~400).[37]

Micropore sizes based on HK[42] and SF[43]models were similar for all samples with pore size distribution peaks positioned near 5 and 8 Å, respectively. No evident effects of varying ramp time, hold time or maximum input power were observed for micropore size.

The influences of hold time and maximum input power on the micropore volumes were not conclusive. However, we observed a tendency of slow ramp rates (longer ramp intervals) to give rise to higher micropore volumes. It is claimed by van Bavel *et al*.[33] that in the aging period, the preliminary structure of the silica material is formed and it is consolidated upon heating at 100^{o}C. As discussed in section 2.2.2, the hydrophobicity of occluded PEO segments of triblock copolymers increases as the temperature is elevated. For this reason, we propose that there is a competition between the rate of retraction of PEO blocks and the consolidation of the silica structure during the temperature ramp stage. Slower ramp rates means that the PEO chains that give rise to the microporosity within the mesopore walls are slowly withdrawn while the consolidation occur, hence they show higher micropore volumes. On the other hand, faster ramp rates mean that PEO segments become hydrophobic and withdrawn from the wall in a relatively short time, then the consolidation follows. This is a possible reason why Newalker *et al*.[26, 59, 60] have obtained low microporosity SBA-15 materials with microwave heating; although, they have not given the details about the ramp rates used to synthesize their samples.

It is generally known that microwave heating is a dielectric heating process which leads to the rapid heating with fast ramp rates.[61] However, one can manipulate the ramp rate flexibly with commercially available microwave ovens. This versatility will enable future studies of how the ramp rate influences the synthesis of organic or inorganic materials, including zeolites and mesoporous silicate materials.

3.3.6 Summary

A study of ramp time, hold time, and maximum power input influence on the synthesis of SBA-15 materials using microwave heating was performed.

The ramp rate tends to have a strong influence on the a-parameter and the microporosity of the samples: the greater the rate, the larger the a-parameter, and the slower the rate, the higher the microporosity.

Hold time appears to effect the BET surface area monotonically in the sense that reacting at higher temperatures for prolonged periods of time gives a higher surface area.

Maximum power input had minor or insignificant effects on the structural properties of synthesized SBA-15 materials. Rather, power is relevant to the ramp rate to the set temperature. Higher power is required for faster ramp rates, particularly with large amounts of precursor solution in the reaction vessel. In this case, the maximum power of 300 W was sufficient to heat the given solution up to the set temperature of 100^{o}C with in 2 minutes.

3.4 SBA-15 Samples Prepared with Shorter Synthesis Time

3.4.1 Objective

Newalkar and coworkers[59] have successfully synthesized SBA-15 using much shorter periods of time using microwave heating, however, the details of the actual syntheses were not provided. It is also unclear whether an aging step was used. As discussed in section 2.2.1, that recent studies on the mechanism revealed that SBA-15 mesopore structures were already obtained within two hours of heating the precursor solution at 40^{o}C.[19]

We planned our experiment based on the combination of the two results obtained previously to shorten the overall synthesis time to less than four hours.

3.4.2 Synthesis

We have performed the experiments according to the method described in Table 4 in order to meet the objective of synthesizing SBA-15 in a relatively short time.

Table 4 Preparation of SBA-15 samples within shorter synthesis time by combining conventional and microwave heating

Sample ID	Heating method for aging step	Time (hrs)	Heating method for reaction step	Time (hrs)
C24M2	Conventional	24	MW (2min/600W)	2
C24C2	Conventional	24	Conventional	2
C24	Conventional	24	No heating	0
M2M2	MW (10sec/600W)	2	MW (2min/600W)	2
C2M2	Conventional	2	MW (2min/600W)	2
C2	Conventional	2	No heating	0
C2C2	Conventional	2	Conventional	2
C2m2	Conventional	2	MW (100min/300W)	2

Samples were identified based on the heating method employed and the time of heating. There are normally two heating steps involved in the synthesis of SBA-15: heating at 40^{o}C with stirring and heating at 100^{o}C without stirring. Since the aging is defined as the period between the mixing of reagents and the onset of heating to the crystallization temperature (100^{o}C), we will define the first heating step as "aging" and the second as normal "heating." If the sample was heated inside the oil bath maintained at 40^{o}C during the "aging" period, it is denoted C. If the sample was heated inside the conventional heating oven, in which the hot air is blown, during the "heating" period, it is also denoted C. If heated in the microwave oven, it is denoted as M. Hence, the sample identification is such as CxMy or CxCy, where x represents the duration of aging time (in hours) and y represents the duration of heating time (in hours) in the corresponding heating methods. It should be noted that in the stage of microwave "heating," the ramp rate and the power are variables. In most cases, the ramp time was set to 2 minutes using maximum power of 600 W.

Sample C2m2 was intended to replicate the synthesis conditions of C2C2, except that it was heated in the microwave oven during the "heating" stage. In order to realize this, we measured the temperature of the precursor solution using a similar reaction vessel set up used for microwave heating (refer Figure 31 in the Appendix). The temperature vs. time profiles of C2C2 and C2m2 precursor solutions are shown in Figure 9.

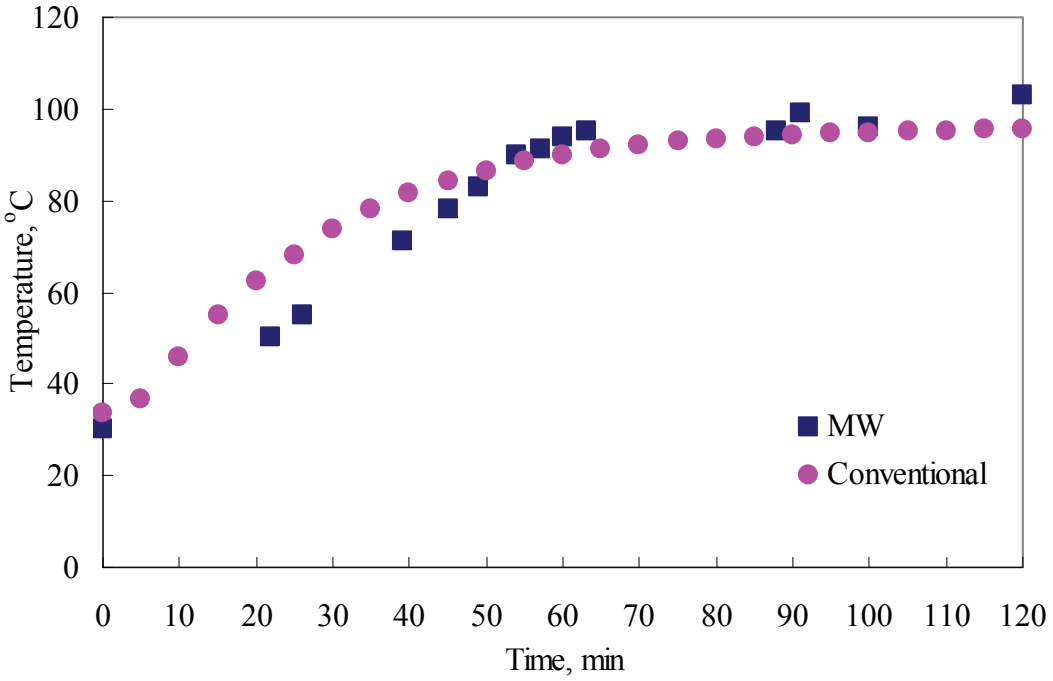

Figure 8 Temperature profiles of the precursor solutions in the conventional oven and the microwave oven.

It was difficult to control the precursor temperature in the microwave reactor. To obtain C2m2, the ramp time was set to 100 minutes using a maximum power of 300 W. It may have been better to divide the ramping stage into several 10-minute increments rather than one step of 100 minutes; this would have provided better replication of the temperature profile of the conventional oven synthesis, C2C2. However, the feedback controller of the microwave oven was less effective when the operating temperature was below 100°C. This ineffectiveness was evident when synthesizing M2M2. Aging temperature of 40°C was far below the microwave oven's control limit, hence the temperature during the aging stage was abruptly changing continuously, mostly at values above 40°C (temperature profile not shown).

3.4.3 X-ray Diffraction

Synthesized samples were subject to XRD characterization. The XRD patterns are plotted in Figure 9 and the enlarged section between $2\theta = 1.3 – 2.5$ is shown in Figure 10 for an expanded view of the d(110) and d(200) peaks. We can see from Figure 10 that the higher order peaks are observed only after the precursor solution was heated at the elevated temperature (100^{o}C).

The a-parameters for each sample based on the obtained XRD patterns are tabulated in Table 5. XRD data shows that there are no significant differences between aging for 24 hours and 2 hours as far as the a-parameter is concerned; compare C24M2 and C2M2, C24C2 and C2C2, C24 and C2. Rather, sample C2M2, which was synthesized within four hours by combining conventional and microwave heating, has the most well resolved peaks compared to the other samples (Figure 9 and 10). And the sample M2M2, which was synthesized solely in the microwave oven, has the largest a-parameter among the samples.

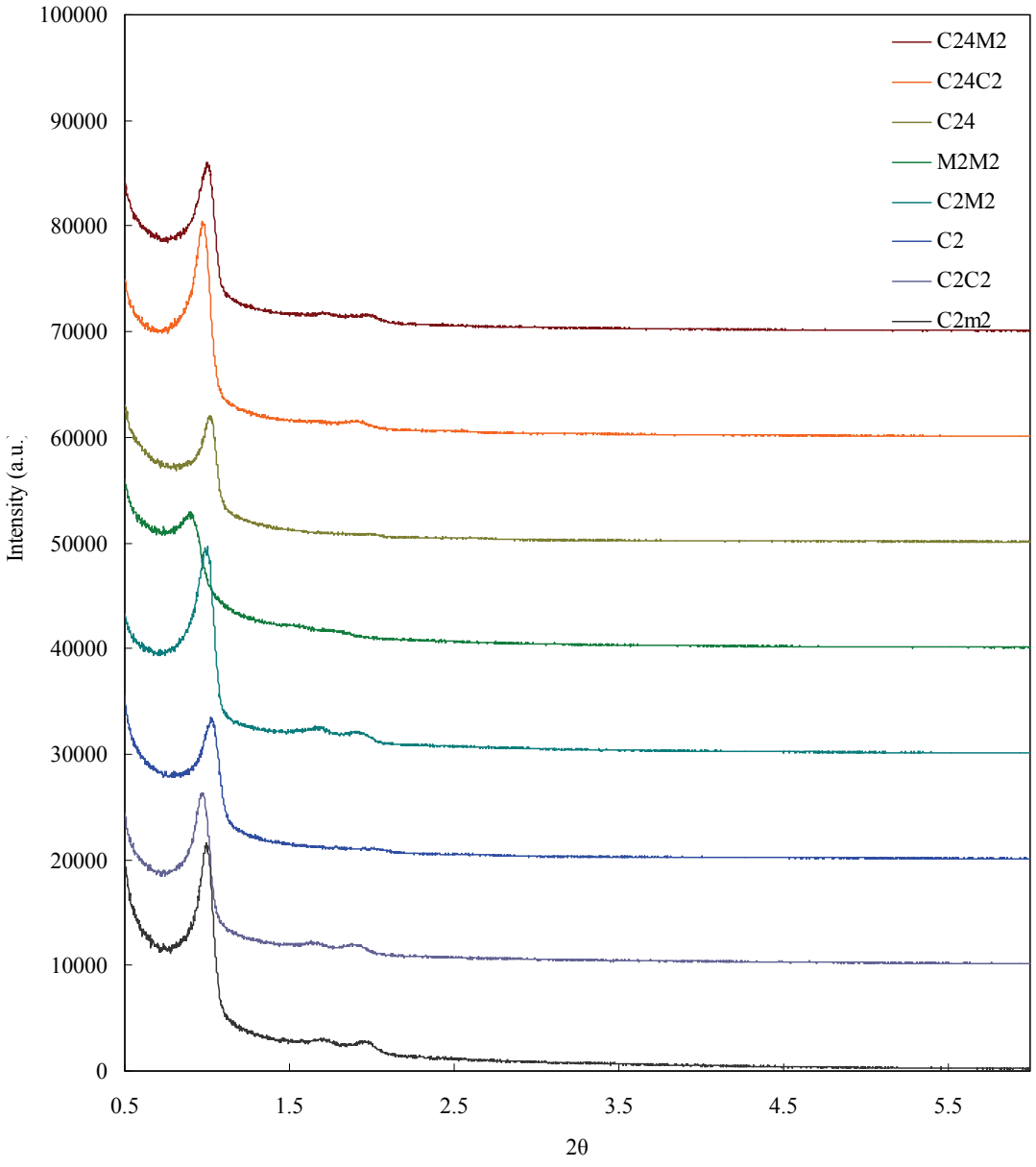

Figure 9 XRD patterns for short synthesis time experiment

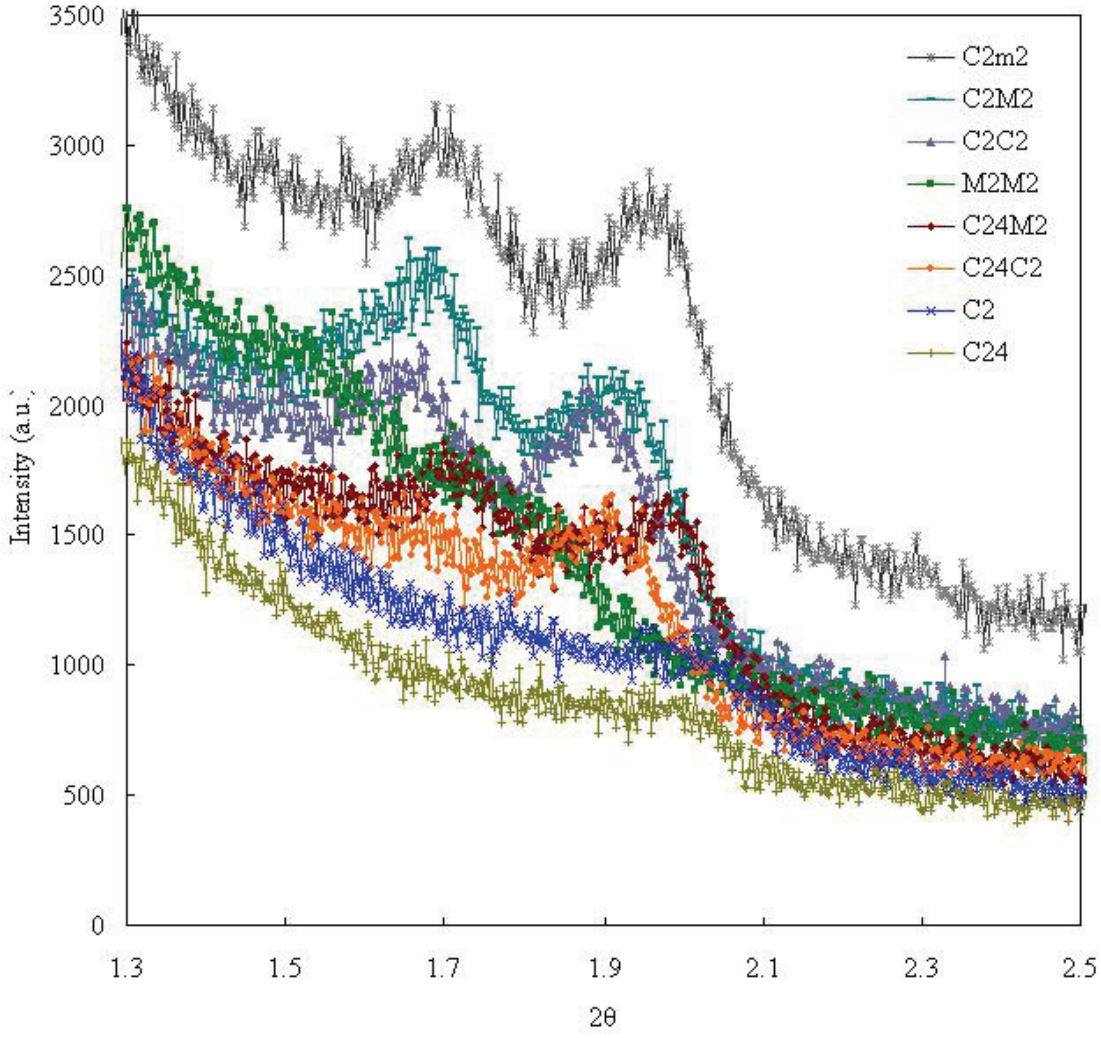

Figure 10 Enlarged XRD patterns for short synthesis time experiment.

Table 5 a-parameters of SBA-15 samples synthesized within shorter synthesis time

Sample ID	a-parameter (Å)
C24M2	101.9
C24C2	104.8
C24	100.2
M2M2	113.5
C2M2	101.7
C2	99.8
C2C2	105.2
C2m2	102.6

3.4.4 Physical Adsorption

Argon adsorption at 87 K on each sample prepared in section 3.4.2 was performed on AUTOSORB®-1-C adsorption instrument. Figure 11 shows the overlay of the adsorption isotherms.

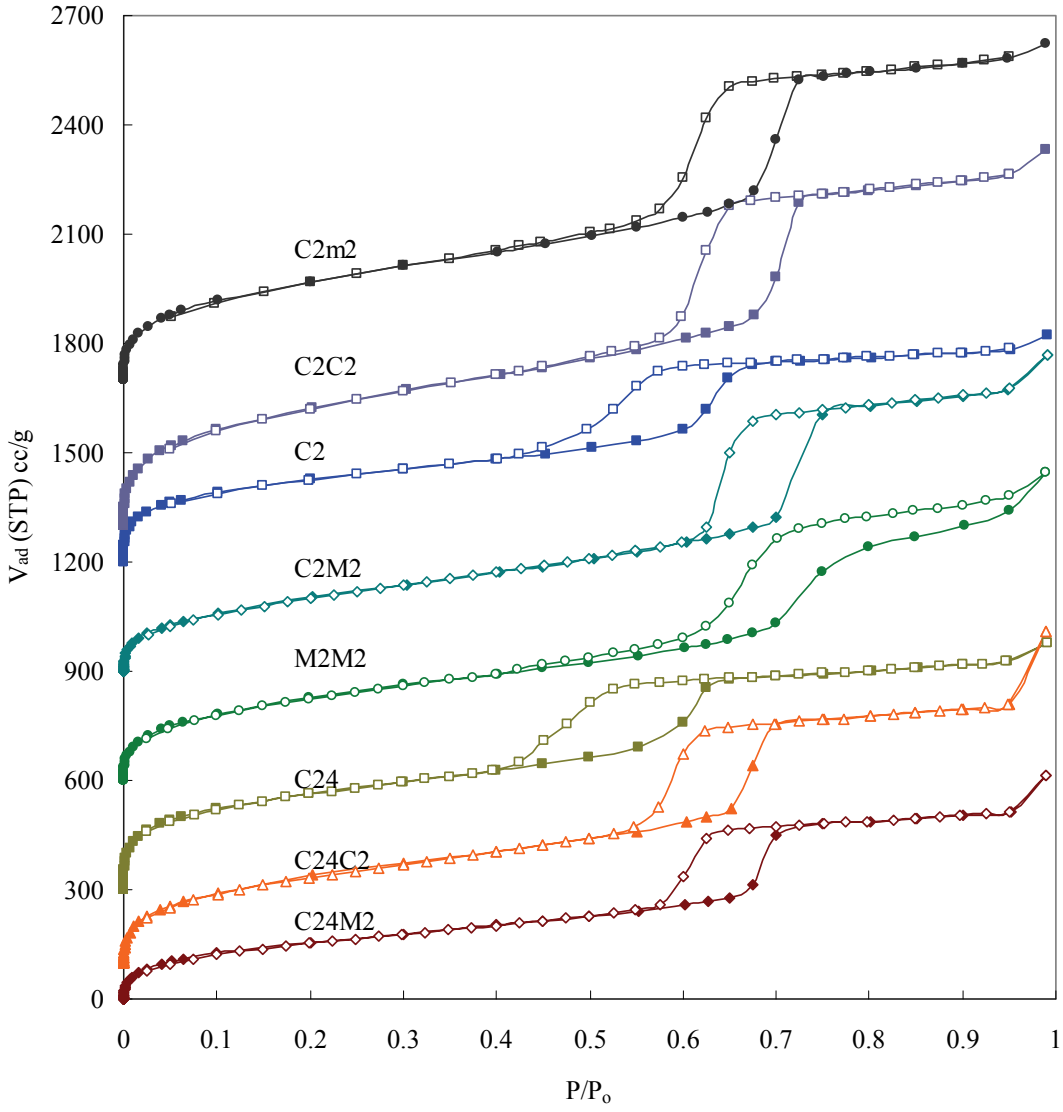

Figure 11 Argon adsorption isotherms at 87 K on SBA-15 samples prepared in shorter synthesis time

The isotherms for samples C24C2, C24, M2M2, C2M2, C2, C2C2, and C2m2 were offset vertically by 100, 300, 600, 900, 1200, 1300, and 1700 cc/g, respectively.

Individual samples' isotherms including the high resolution adsorption isotherms are also shown in the Appendix. Most sorption isotherms exhibit typical H1 hysteresis with varying steepness of the adsorption isotherm, however, sample M2M2 shows a different

hysteresis loop from the other samples. From the steepness of the adsorption isotherm, we can see that the mesopore structure in M2M2 is not well ordered and has a broad pore size distribution.

We can distinguish the samples only treated at low temperature (40 ^{o}C), C2 and C24 have relatively broad pore size distribution and lower transition point of relative pressure, which in turn would give smaller pore sizes. We will discuss this more in the next section.

3.4.5 Results and Discussion

The structural parameters determined from both XRD and argon adsorption for SBA-15 samples prepared in section 3.4.2 are tabulated in Table 6.

Table 6 XRD and Ar adsorption results for SBA-15 samples prepared in shorter synthesis time

Sample ID	a (Å)	D_{BJH} (Å) ad/de	t (Å) ad/de	SA_{BET} (m^2/g)	C_{BET}	d_{SF} (Å)	D_{NLDFT} (Å)	V_{μ} (cc/g)
C24M2	101.9	72.2/57.5	29.7/44.5	502.2	54.0	7.9	66.0	0.045
C24C2	104.8	66.8/53.5	38.0/51.3	761.9	58.3	8.4	61.5	0.084
C24	100.2	57.3/41.7	42.9/58.6	814.9	13.0	7.1	51.4	0.122
M2M2	113.5	83.0/66.7	30.5/46.8	734.3	52.8	5.0	76.2	0.090
C2M2	101.7	83.1/61.8	18.6/39.9	668.1	42.4	5.0	70.9	0.032
C2	99.8	61.6/47.0	38.2/52.8	698.3	114.1	7.2	57.0	0.083
C2C2	105.2	78.8/57.4	26.4/47.8	1027.0	67.2	7.8	68.3	0.132
C2m2	102.6	72.3/57.5	30.2/45.1	871.4	54.3	7.9	68.3	0.081

3.4.5.1 Effect of Aging Time

In order to determine aging time effects, we compared C24M2/ C2M2, C24C2/ C2C2, and C24/ C2. As it was briefly discussed earlier in 3.4.3, the a-parameters were almost same for samples aged for 2 or 24 hours. BJH mesopore diameters tended to be

bigger for samples aged for two hours, these samples, in turn, have thinner walls. Similar tendencies for BET surface area and microporosity could not be found.

3.4.5.2 Effect of Heating Method at "Aging" Step

When we synthesized samples C2M2 and M2M2, we hoped to see the influence of microwave heating during the aging period. At the same time, we wished to accomplish the "rapid one-pot synthesis of SBA-15" with a microwave heating method. However, care is required when comparing C2M2 with sample M2M2. As was mentioned in section 3.4.2, M2M2 actually experienced higher temperatures during the aging period. Hence, direct comparisons of those two samples to draw conclusions of microwave effects during the aging period should be undertaken with caution. Looking at the data provided in Table 6 for those two samples, we recognize that M2M2 has larger values for all the properties. The argon adsorption isotherm of M2M2 is quite different from other samples in that the hysteresis closes at a higher relative pressure (Figure 11). Amphiphilic triblock copolymer micelles arranged during the aging period may be irregular leading to broader pore size distribution.

3.4.5.3 Effect of Heating Method at "Heating" Step

Sample C2C2 has a slightly larger a-parameter than C2m2. The BJH pore diameter based on the adsorption isotherm is larger for C2C2 than C2m2, whereas that based on the desorption isotherm is the same. Sample C2C2 has a much higher BET surface area and more microporosity than C2m2, even though the isotherms look very much alike.

These C2C2 and C2m2 samples were synthesized with the same ramp rate. However, we were unable to avoid the temperature control problem within the microwave oven (section 3.4.2). Hence, we have to allow for the possibility that the structural property differences we observe are due to a specific microwave heating mechanism or to temperature variations during the "heating" that the samples experienced.

3.4.5.4 Effect of Ramp Rate in Microwave "Heating" Step

When determining the effect of ramp rate, we can use C2m2 with more confidence. C2M2 and C2m2 had almost the same a-parameters. Sample C2M2 showed a bigger mesopore diameter, which implies a smaller wall thickness. Even though both samples were heated with microwaves for the same amount of time, C2m2 had a larger BET surface area and a higher amount of microporosity than C2M2. We observe that slow ramp rates result in high microporosity and large surface area. This result clearly supports our argument made in the synthesis of SBA-15 with microwave heating (section 3.2.5) that ramp rate during the synthesis impacts the structural properties of SBA-15.

3.4.5.5 Effect of "Heating" Step

In order to understand the effect of the "heating" step, we individually studied two sets of samples; C24/C24M2/C24C2 and C2/C2M2/C2C2. Comparing samples within each set, in general, we find that as we heat the aged precursor solution, we obtain a slightly larger a-parameter, larger mesopores, thinner walls, smaller surface area, and lower

microporosity. Sample C2C2 was an exception in terms of surface area and microporosity; it showed the largest value.

3.4.6 Summary

Within 2~4 hours, we have successfully synthesized micro-mesoporous materials that are structurally similar to SBA-15. The a-parameter values are nearly constant during the aging period and gradually increase with additional heating at higher temperature and longer times. Depending on the presence, duration, and ramp rate to the heating step, the mesopore sizes are determined.

3.5 Synthesis of Plugged Hexagonal Templated Silica

3.5.1 Background

As discussed earlier, Plugged Hexagonal Templated Silica (PHTS) has a very high volume fraction of micropores in its structure. Also its adsorption isotherm, especially the desorption branch, exhibits unique behavior: the adsorption isotherm is similar to that of SBA-15, except that desorption isotherm has *two* steps in the hysteresis loop.

3.5.2 Synthesis

The PHTS sample, PSBA_1, was prepared in accordance with the procedure described by van der Voort *et al*.[32] The synthesis procedure is the same as those for the standard sample S1, except for the silica source to template ratio, the aging conditions, and the heating conditions, which are tabulated in Table 7. The fact that PSBA_1 was prepared

under different conditions to standard sample S1 means that direct comparison is not possible. Therefore, we synthesized PSBA_2 with the same conditions as standard sample S1.

Table 7 Preparation of PHTS samples by changing TEOS/P123 and heating temperature

Sample ID	TEOS/P123	Aging temperature, ^{o}C	Aging time, hrs	Heating temperature, ^{o}C	Heating time, hrs
PSBA_1	146	40	8	100	16
PSBA_2	146	40	24	100	48

3.5.3 X-ray Diffraction

Figure 12 shows the XRD patterns of the PHTS samples PSBA_1 and PSBA_2. Each of the samples has three clear peaks for d(100), d(110), and d(200) spacing which conforms to the hexagonally ordered structure.

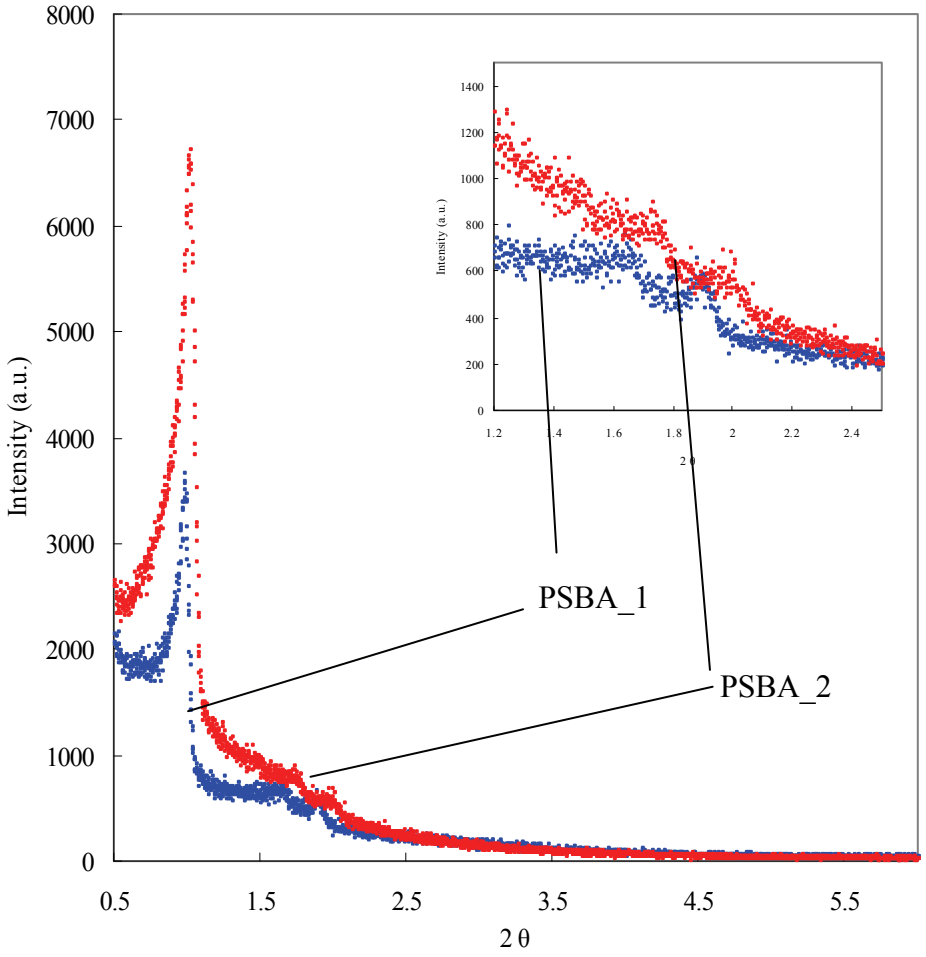

Figure 12 XRD patterns of the PHTS samples with enlarged diffraction pattern section shown in inset

3.5.4 Physical Adsorption

Nitrogen adsorption isotherms at 77 K on synthesized plugged hexagonal templated silica samples were obtained from the AUTOSORB®-1-C. The samples were synthesized with a silica source to template ratio (TEOS/P123) of 146, whereas typical SBA-15 materials are normally synthesized with a ratio of 59. Figure 13 shows the corresponding adsorption isotherms. Desorption isotherms of synthesized samples showed two steps in the

hysteresis. As mentioned earlier, this might be a consequence of the existence of microporous plugs inside the mesopore channel. It has been proposed that the first step in the higher relative pressure region is the desorption of gas from the open mesopores and the second step in the lower relative pressure region comes from the mesopores that were blocked by the microporous plug.[32]

At present, few people have paid attention to the high resolution adsorption studies of the SBA-15 materials. This is partly due to the fact that the micropore sizes of SBA-15 are broadly distributed and thus a distinct adsorption step could not be observed. However, in the case of PHTS samples, we observed that step-like adsorption in the low relative pressure region (around 2×10^{-6} P/P_o) for N_2 at 77 K (Figure 13 inset). Even though the micropore size is not uniformly distributed, due to its high micropore volume, we observe a small step in the high resolution adsorption isotherm as seen for zeolite isotherms.

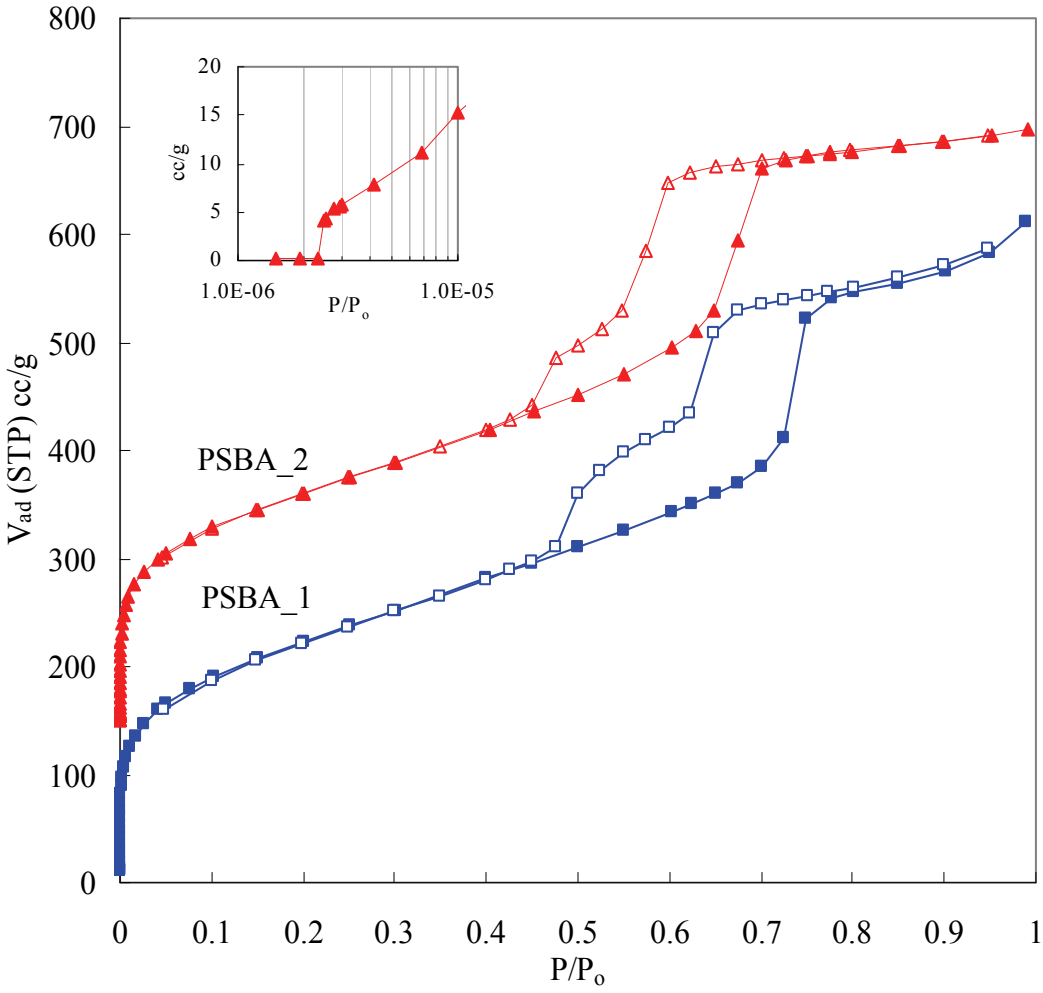

Figure 13 Nitrogen adsorption isotherm at 77 K on PSBA_1 and PSBA_2 and corresponding high resolution adsorption isotherm of PSBA_2 (inset)
The adsorption isotherm for PSBA_2 was offset vertically by 150 cc/g

3.5.5 Results and Discussion

The results from XRD and nitrogen adsorption isotherms are tabulated in Table 8. Alpha-s plot analysis was attempted to determine the microporosity of the synthesized PHTS samples, however the analysis gave negative values. According to the work done by van der Voort *et al.*,[32] the micropore volumes of the PSBA samples should be largest

among all SBA-15 related samples synthesized in the present work, due to the presence of the microporous nanoplugs within the mesoporous channels. However, the result from alpha-s plot analysis was beyond our expectation, it gave us negative values for micropore volume. Hence, we applied t-method. de Boer equation[1] was used to calculate statistical thickness t, instead of t-curve, which is based on the standard adsorption isotherms. Still, the micropore volumes were far less than the reported values (0.17~0.30 cc/g).[32]

Table 8 Structural properties of PSBA samples obtained from XRD and nitrogen adsorption isotherms at 77K

Sample	a (Å)	D_{BJH} (Å)	t (Å)	SA_{BET} (m^2/g)	C_{BET}	d_{SF} (Å)	D_{NLDFT} (Å)	V_{μ} (cc/g)
PSBA_1	103.9	81.1	22.8	787.8	144.6	5.2	73.1	0.083
PSBA_2	100.7	62.7	38	749.0	127	5.7	63.2	0.032

3.6 Conclusion

We have studied various factors that influence the microporosity of SBA-15 materials during the synthesis. We have synthesized SBA-15 extensively with microwave heating; although, we could not detect any clear trends in the microwave effect on the synthesized SBA-15 materials other than the ramp rate effect.

We find that the silica precursor to template ratio (TEOS/P123), ramp rate to the synthesis temperature, and duration of heating time influence the micropore volume and the BET surface areas of micro-mesoporous SBA-15. In order to obtain higher microporosity, higher ratio of TEOS to P123, slower ramp rate to the synthesis temperature, shorter heating time at elevated temperature are required.

How can we evaluate the irregular micropore size of micro-mesoporous samples from the simple gas adsorption measurement? We understand that the presence of the microporosity partly reflects the BET surface area of micro-mesoporous material. Then, how can we separate the micropore contribution of the BET surface area and mesopore size evaluation? We seek to answer these questions throughout the rest of this thesis.

CHAPTER 4

EMPIRICAL MODELS FOR THE CHARACTERIZATION OF MICROPOROUS MATERIALS

4.1 Objective

In order to study micro-mesoporous materials in more detail, we studied inherent microporous materials, namely, zeolites. We attempt to develop empirical models for low pressure isotherms. We then applied these models to SBA-15 materials, which are micro-mesoporous materials, to estimate their micropore size.

4.2 Samples to Study

We have chosen relatively simple-structured (one dimensional channel structure) zeolite samples for this analysis. Samples of synthetic zeolites were supplied by Stacey Zones, Chevron Research and Technology Company, Richmond, California, USA. These samples are listed in Table 9 along with the detailed structure information.

Table 9 Selected zeolite samples and dimensions

Zeolite	Structure, space group	Ring size	Channel type	Pore Shape	Pore size from X-ray crystallography (Å)	Ref
ZSM-23 (MTT)	Orthorhombic, $Pmn2_1$	10 MR	1D	Elliptical	4.5 × 5.2	[62]
SSZ-20 (TON)	Monoclinic, Cmcm	10 MR	1D	Elliptical	4.6 × 5.7	[62]
ZSM-12 (MTW)	Monoclinic, C12/c1	12 MR	1D	Elliptical	5.6 × 6.0	[62]
SSZ-41 (VET)	Monoclinic, P-4	12 MR	1D	Circular	5.9 × 5.9	[62]
SSZ-55 (ATS)	Monoclinic, $Cmc2_1$	12 MR	1D	Elliptical	6.5 × 7.5	[62]

Here to after, for simplicity, we will refer to the zeolite samples by their three letter IZA (International Zeolite Association) codes. Further information on the structures of these zeolite samples can be found on the International Zeolite Association structure database.[62, 63]

4.3 Development of Empirical Correlations for Micropore Size Estimation

4.3.1 Background

Zeolite materials have well defined micropores. The pore sizes of zeolite materials are compiled by the International Zeolite Association.[63] Zeolites may be grouped into types based on the pore dimensions i.e., 0 D for enclosed porosity without channels; 1 D for one pore type in one direction; 2 D for two pore types in 2 directions; 3 D for two or more pore types in two or more directions, which creates a network of porosity. Pores may also be classified according to the shape of the pore, namely, circular, ellipsoidal or irregular.

As we have reviewed in Chapter 2, physical gas adsorption is extensively used in the characterization of porous materials and its interpretation is considered relatively straightforward. Typically, a zeolite material's adsorption isotherm exhibits step-like feature in the relative pressure range of 10^{-6} ~10^{-2}. This steep increase of adsorbed volume, or "step" in the isotherm, corresponds to the micropore filling. Thus, the "step" in the adsorption isotherm will shift in relative pressure depending on the pore size, dimension or shape. Figure 14 illustrates the definition of "step" for an ideal adsorption isotherm. In Figure 14, P_B and P_E are denoted for the relative pressure where the "step" begins and ends, respectively, and Pc is denoted for the relative pressure where the slope of the curve is the

maximum. Mathematically speaking, P_C is the relative pressure where the peak center is positioned, when the slope of the isotherm curve, $\frac{dV_{ad}}{dP/P_o}$, is plotted against the relative pressure.

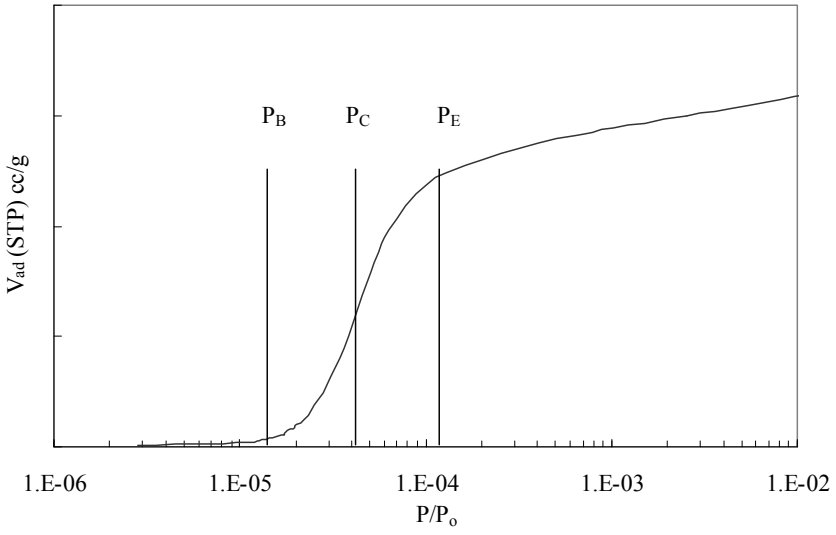

Figure 14 Idealized schematic plot of the low pressure isotherm "step" observed for zeolite materials

Many different models for the micropore size determination from the low pressure isotherms have been developed over the past decades with refinements for differing pore shapes and materials compositions: HK method,[42] SF method,[43] and etc. It is shown by Maglara[64] that, there lies a large discrepancy between the calculated pore size from the models (HK and SF) and the actual pore size determined from crystallographic techniques. An empirical model using the relative pressure at the "step", P_C, and the pore size from crystallography of a set of standard microporous materials, would give a correlation of size versus relative pressure directly from experimental data rather from theoretical models.

Hence, a simplistic correlation may be used instead of complicated models to give a more realistic pore size estimation of an unknown sample.

As mentioned previously (section 4.2), one dimensional zeolite samples were chosen with circular or elliptical shape as a set of standard microporous materials in order to obtain correlations between the pore filling pressure from the adsorption isotherm and the crystallographic pore diameter. The shape of the pores, the dimension and the degree of networking may affect the pore filling pressure and the number of steps observed in the low pressure isotherm.

The crystallographic pore sizes are calculated using assumed atomic radii. Cook and Conner[65] discussed the dimensions of zeolite pores using different estimations for the silicon and oxygen radii. They carried out calculations on cluster models of silica rings which indicate that Norman radii for silicates are 1.2 Å for silicon and 1.0 Å for oxygen. Therefore, the net effect is to increase the pore size by ~0.7 Å. In Table 10, the pore sizes reported from X-ray crystallographic measurements are compared with those calculated using a covalent oxygen radii and Norman radii of selected zeolite materials.

Table 10 Zeolite pore size using ionic and Norman oxygen radii

Zeolite	Pore size from X-ray crystallography (ionic radii, O^{2-} = 1.35Å) (Å)	Norman radii adjusted pore size (O = 1.0Å, Si = 1.2 Å) (Å)
ZSM-23 (MTT)	4.5 x 5.2	5.2 x 5.9
SSZ-20 (TON)	4.6 x 5.7	5.3 x 6.4
ZSM-12 (MTW)	5.6 x 6.0	6.3 x 6.7
SSZ-41 (VET)	5.9 x 5.9	6.6 x 6.6
SSZ-55 (ATS)	6.5 x 7.5	7.2 x 8.2

4.3.2 Argon Adsorption at 87 K on Selected Zeolite Samples

Argon adsorption isotherms of MTT, TON, MTW, VET and ATS type zeolites at 87 K were obtained over a low relative pressure ranges (from 10^{-7} to 0.3 P/P_o) using a AUTOSORB®-1-C adsorption instrument. AUTOSORB®-1-C adsorption instrument is equipped with a turbomolecular pump and 1 Torr pressure transducer that enables the high resolution adsorption measurement in low relative pressure ranges ($P/P_o > 10^{-7}$). Liang [66] has claimed that at low pressures, where the nitrogen and argon micropore characterizations are performed, the phenomenon called thermal transpiration can give rise to a pressure measurement error if not taken into account. The software provided by Quantachrome Instruments along with the AUTOSORB®-1-C has an option to include this thermal transpiration calculation on to construct the adsorption isotherm. However, in this work, this option was not selected for the adsorption isotherm construction.

4.3.2.1 Adsorption Isotherms

Argon adsorption isotherms of selected zeolite framework samples are shown in Figure 15. Each isotherm exhibits, to somewhat degree, the "step" in the adsorption isotherm, where the micropores are filled.

.

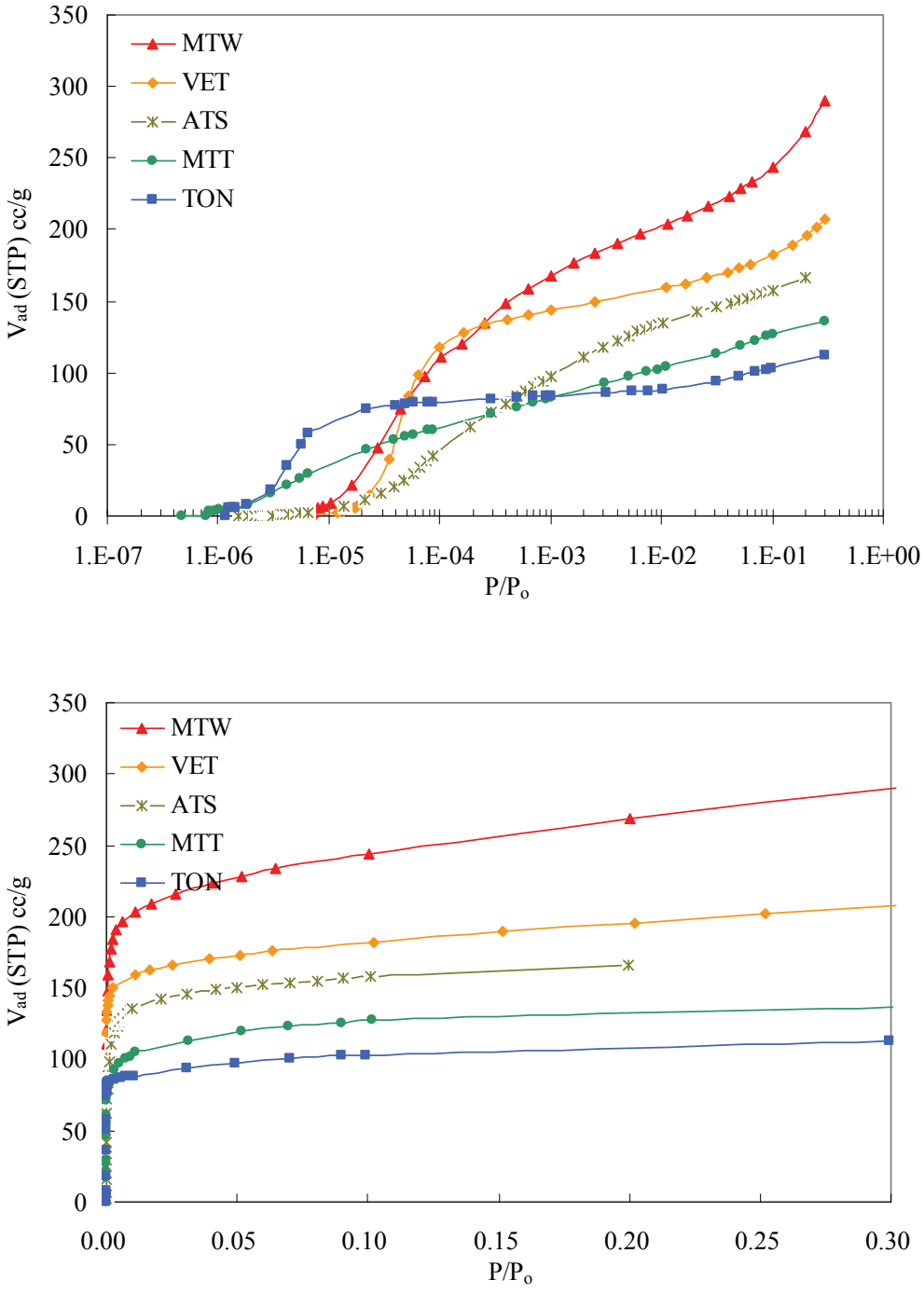

Figure 15 Low pressure argon adsorption isotherms at 87 K of selected zeolite framework samples logarithmic scale (top) and linear scale (bottom).

4.3.2.2 Data Reduction

The isotherms were characterized using several standard analysis techniques, including BET for surface area measurement (SA_{BET} (m^2/g) and C_{BET}), α_s- plot for micropore volume evaluation (V_μ (cc/g)), and HK, SF, and BJH models for micropore size estimation (d_{HK}, d_{SF}, and d_{BJH} (Å), respectively). The calculations were carried out using the Quantachrome Instruments, AUTOSORB®-1-C software, ASWIN version 1.51. The micropore size for each model was obtained from the pore size distribution, where the peak is positioned.

Table 11 Zeolite micropore dimensions from X-ray crystallography and argon adsorption analysis

Zeolite	Pore dimensions from X-ray crystallography (Å)[62]	SA_{BET} (m^2/g)	C_{BET}	d_{HK} (Å)	d_{SF} (Å)	d_{BJH} (Å)	V_μ (cc/g)
MTT	4.5 x 5.2	352.4	-63.3	4.3	5.6	5.1	0.144
TON	4.6 x 5.7	291.9	-68.3	5.6/6.8/10.6	5	5.1	0.122
MTW	5.6 x 6.0	770.7	-148.9	4.3	6.2	5.6	0.219
VET	5.9 x 5.9	551.5	-88.2	4.3	6.5	5.3	0.181
ATS	6.5 x 7.5	497.2	-148.6	4.3	6.5	5.9	0.170

BET surface area of the selected zeolite samples are in the range of 300 and 800 m^2/g. Corresponding BET constants were all negative values, which raises the question of validity of BET calculation for these microporous materials. As we have shown in detail in Section 2.3.3.1, neither pre-exponential nor exponential terms can be negative values. Therefore, negative C_{BET} values do not have any physical meaning. The BET method cannot be applied reliably in this case.

Horvath-Kawazoe calculation, HK, gives the pore width in the range of 4 to5 Å. Only TON framework exhibited poly disperse pore size distribution. HK calculation appears to underestimate the pore sizes. SF calculation gives the pore diameters of 5 to 6 Å, which somewhat agrees with the actual pore diameters.

4.3.3 Development of Empirical Correlations for Micropores

Empirical correlations between the pore diameters, which are estimated from X-ray crystallographic techniques,[63] and the logarithm of the relative pressure at the "step", P_C, in the low-pressure region is developed by first tabulating the relation. (Table 12)

Table 12 Pore diameters and the relative pressures, P_c, where the maximum slope is observed in the adsorption "step" for selected zeolite samples

Zeolite	Pore diameter from X-ray crystallography (Å)[62]	Average pore diameter (Å)	Smallest pore diameter (Å)	P_C
MTT	4.5 x 5.2	4.85	4.5	4.00E-06
TON	4.6 x 5.7	5.15	4.6	7.07E-06
MTW	5.6 x 6.0	5.8	5.6	1.63E-05
VET	5.9 x 5.9	5.9	5.9	3.02E-05
ATS	6.5 x 7.5	7.0	6.5	5.00E-05

We find that, in general, P_C occurs at increasingly high pressure as the zeolite pore size increases. Smaller pores are filled at lower relative pressure than larger pores. These 1-D zeolites show uniform correlation of micropore size to filling relative pressure.

Figure 16 is obtained by plotting P_C versus the average pore diameter and the smallest pore diameter. Fitting the plotted data gives the lines with reasonable R squared values (R^2>0.9).

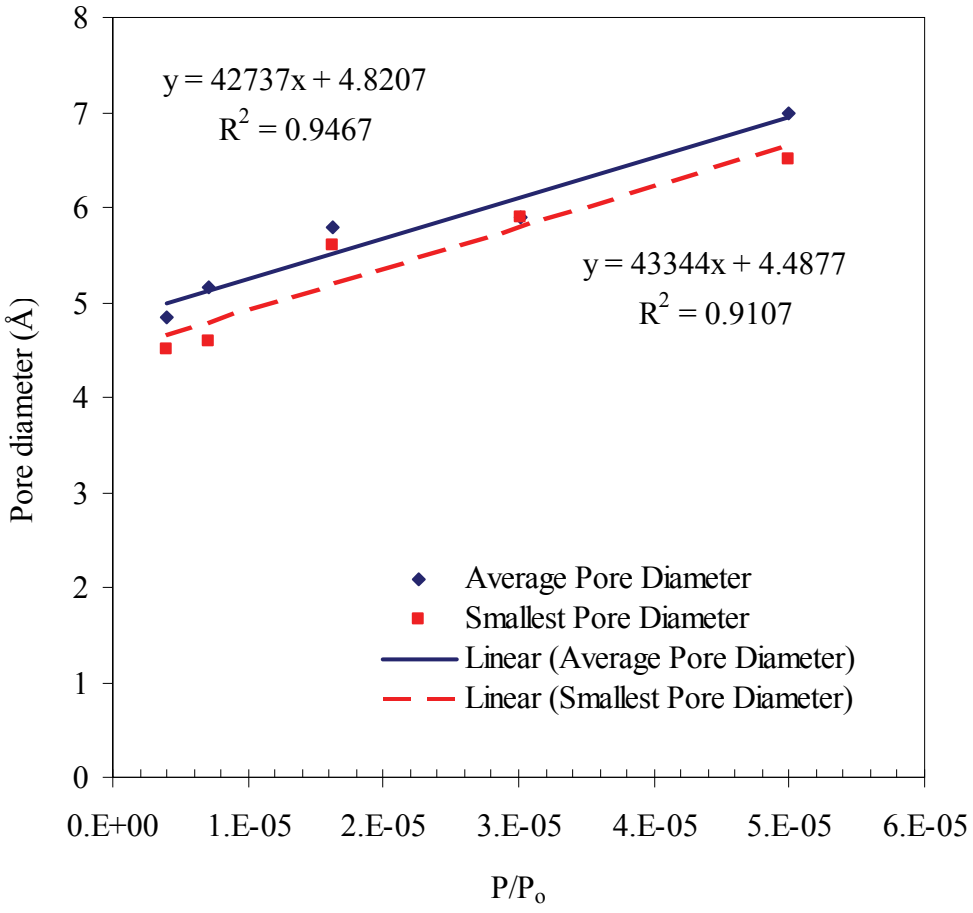

Figure 16 Correlation between pore diameter (average pore diameter and smallest pore diameter) and relative pressure for zeolites, MTT, TON, MTW, VET, and ATS, measured with argon at 87 K

The low pressure argon isotherms at 87 K, from the literature of zeolite materials were reviewed and the data for the isotherm "step" are listed in Table 13. Three additional one dimensional zeolite samples, namely, $AlPO_4$-5 (IZA code, AFI), $AlPO_4$-11 (AEL), and VPI-5 (VFI) are taken into account to determine a correlation between pore diameter and

step pressure. The argon adsorption isotherms taken at 87 K on those additional zeolite samples were obtained from the work of Cheng and Yang.[67]

Table 13 Average pore diameter and the relative pressure, P_C, where the step is formed for selected 1 D zeolite samples combined with literature

Zeolite	Average pore diameter from X-ray crystallography (nm)[62]	Norman radii adjusted pore diameter (nm)	P_C	Reference
MTT	0.485	0.555	4.00E-06	This work
TON	0.515	0.585	7.07E-06	This work
MTW	0.58	0.65	1.63E-05	This work
VET	0.59	0.66	3.02E-05	This work
ATS	0.7	0.77	5.00E-05	This work
AEL	0.53	0.60	3.00E-05	Cheng and Yang[67]
AFI	0.73	0.8	1.50E-04	Cheng and Yang[67]
VFI	1.27	1.34	2.00E-03	Cheng and Yang[67]

In Figure 17, all the experimental data for 1D pores tabulated in Table 13 are compared with the different models. The relationships between the relative pressure and the pore diameter were obtained for HK model and SF model by calculating equations (9) and (11), respectively for a range of pore sizes. The appropriate constants were used as they were published in the work by Saito and Foley.[43] The BJH calculation was performed using equation (19) and equation (22). Since the t-plot we have so far used does not include low relative pressure data, an alternative t-plot reported by Kruk and Jaroniec[52] was used. It seems that the models do not fit the actual experimental data. Therefore, we have needs to develop empirical correlations that better represent the experimental data obtained from both adsorption isotherm and X-ray crystallographic technique.

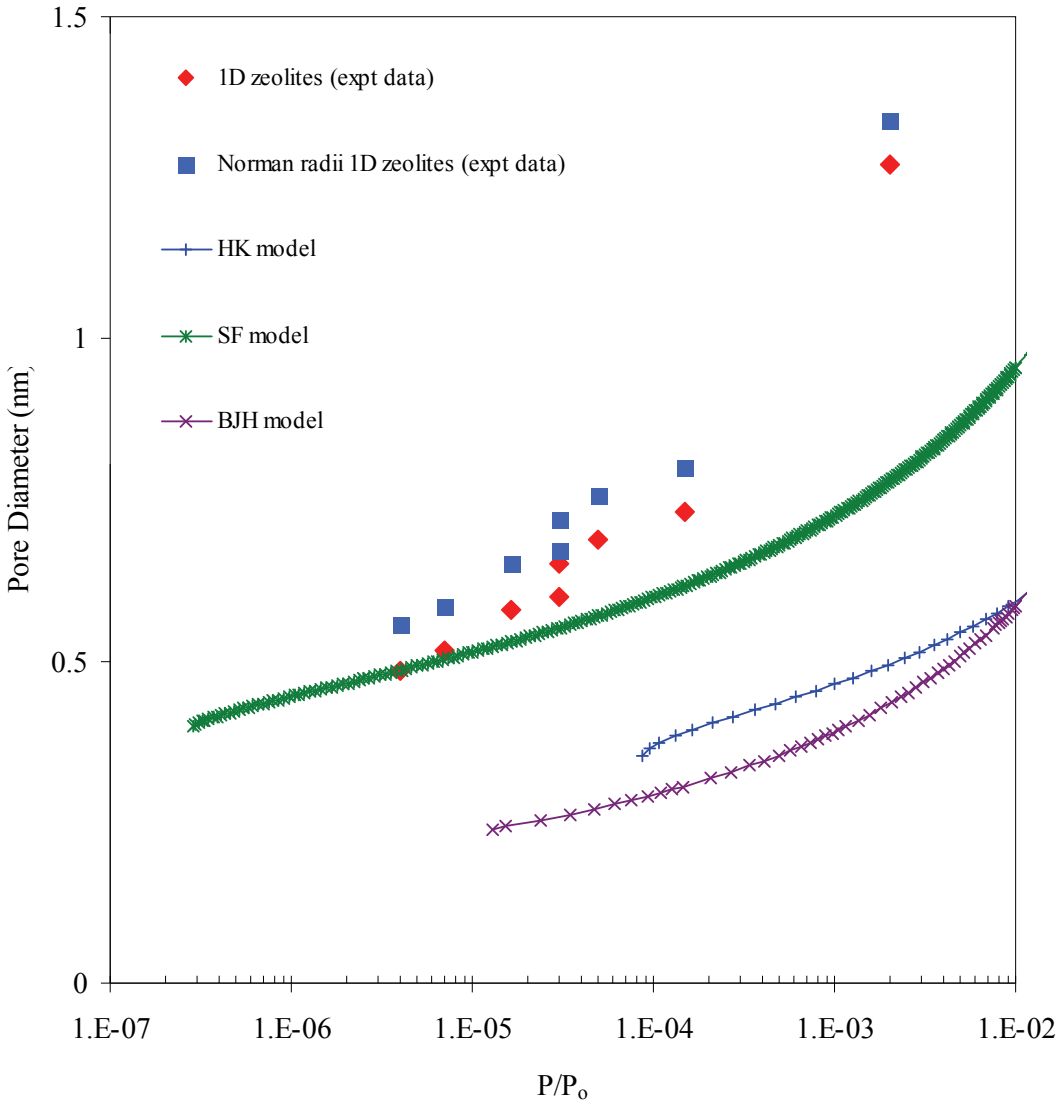

Figure 17 Pore sizes according to different models compared to experimental data

Empirical correlation equations for the relative pressure of pore filling with pore dimensions can be given by the following equations. These equations, based on real

experimental data, without Norman radii adjustment, give a simplistic approach for estimation of the micropore diameter, D_μ (nm).

(1) Power law relation,

$$D_\mu = A(P/P_o)^a$$

By fitting the experimental data to the power law relation above, parameters are obtained for A=3 and a=0.15 with R^2 of 0.9651.

(2) Kelvin type relation,

$$D_\mu = \frac{-B}{\ln(P/P_o)}$$

Kelvin type relation gives the parameters as B= 6.86 with R^2 of 0.8959.

(3) Halsey type relation,

$$D_\mu = C\left[\frac{-1}{\ln(P/P_o)}\right]^{1/c}$$

Experiment data fitting to the Halsey type relation resulted in C=15 and c=0.73 with R^2 of 0.9805.

Data fitting procedures to three relations are depicted in the Figure 18.

(a) Power type

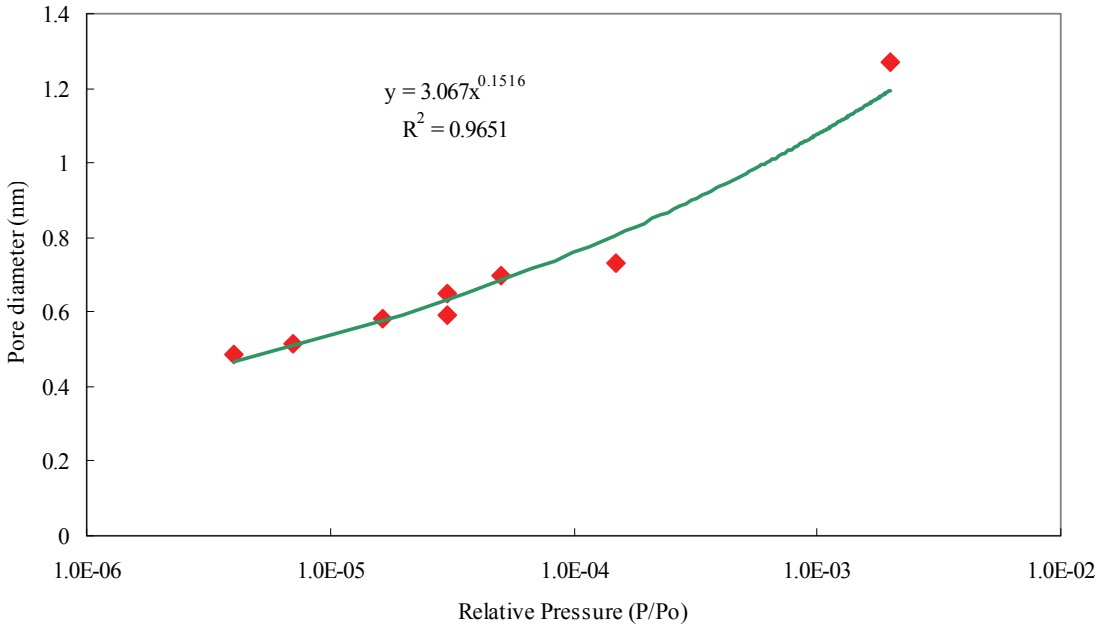

(b) Kelvin type

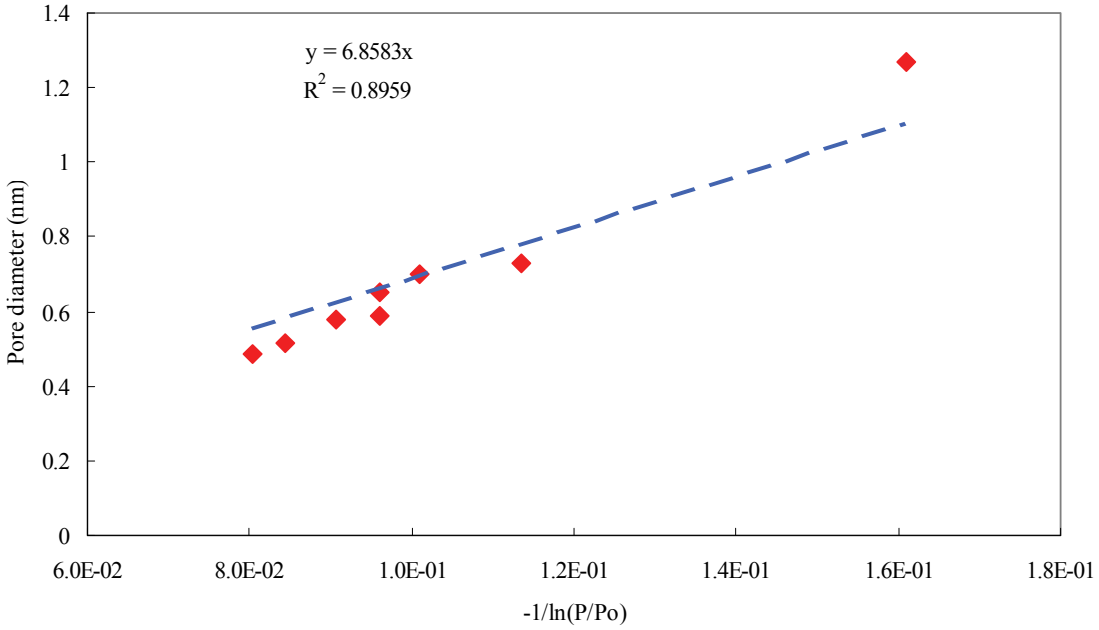

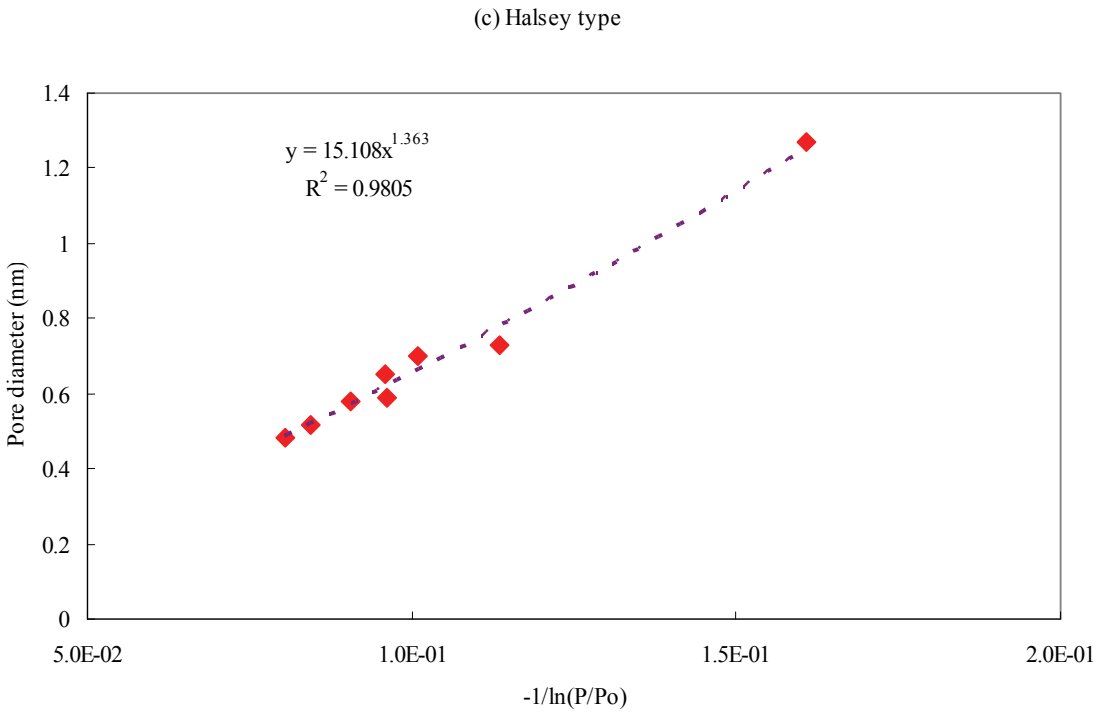

Figure 18 Fitted plots with (a) power law type; (b) Kelvin type; (c) Halsey type equations to obtain the coefficients in the assumed equations

Also, the results obtained are tabulated in Table 14.

Table 14 Empirical equations for micropore size estimation from the relative pressure where the "step" occurs in the adsorption isotherms

Type	Empirical relation of D_μ (nm) to P/P_o
(1) Power law	$D_\mu = 3(P/P_o)^{0.15}$
(2) Kelvin	$D_\mu = \dfrac{-6.86}{\ln(P/P_o)}$
(3) Halsey	$D_\mu = 15\left[\dfrac{-1}{\ln(P/P_o)}\right]^{1/0.73}$

The correlations between pore diameter and relative pressure for 1D zeolites with three types of mathematical equation fits, Kelvin, Halsey, and power law, are shown in Figure 19.

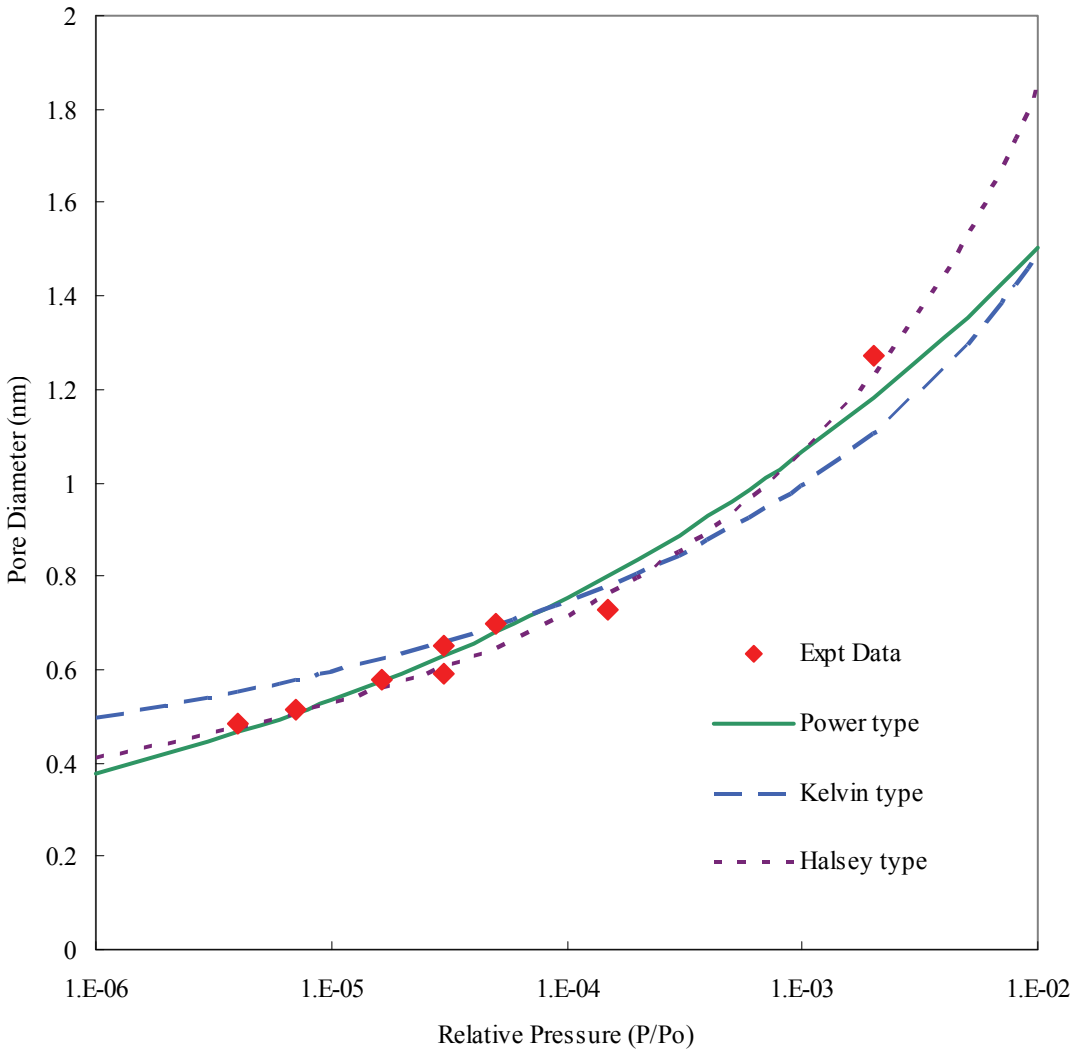

Figure 19 Correlation between pore diameter and relative pressure for 1D zeolites, with three types of mathematical correlation fits, Kelvin, Halsey, and power law type relations

From Figure 19, we infer that, in general, all three types of relation represent the trends of the experimental data well. Among the three, Halsey type relation shows the best fit. The Kelvin type relation tends to overestimate for the smaller pore sizes and underestimate at large pore sizes.

Figure 20 summarizes all the results and we find that our empirical correlations better estimate the pore sizes compared to the theoretical models presented.

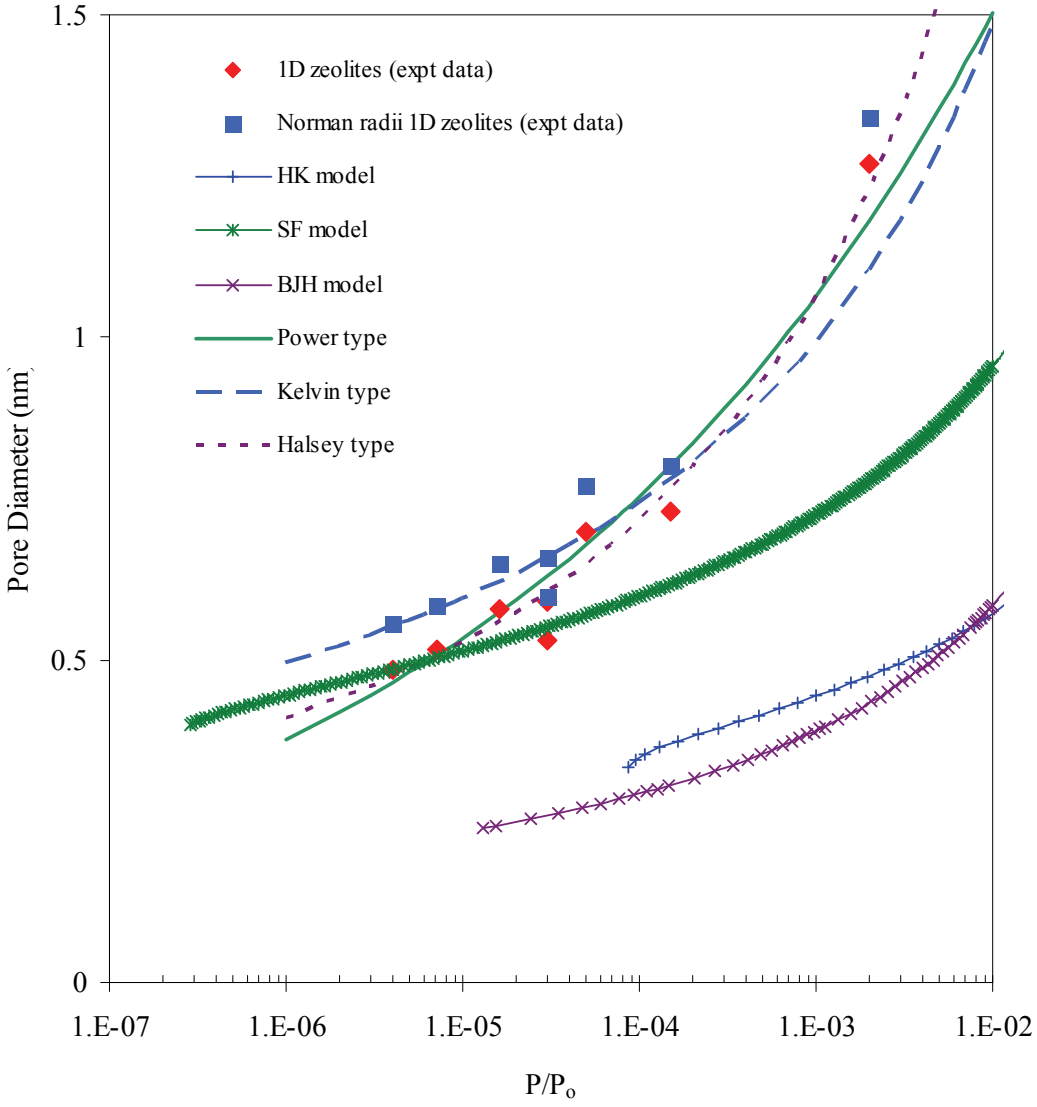

Figure 20 Comparison of theoretical models and developed empirical correlations with experimental data based on the relative pressure and the pore size

4.3.4 Micropore Size Estimation for Micro-Mesoporous System

The empirical correlations developed in this study can be used to estimate the micropore size in unknown materials, such as the micro-mesoporous SBA-15 materials we have synthesized.

Although adsorption isotherm[23] and small angle X-ray scattering (SAXS)[35] curves were used to verify the existence of the micropores, direct observation and measurement of the micropore size were not possible. High-resolution transmission electron microscope (HRTEM)[68] study enabled the direct observation of micropores present in the mesopores. Liu *et al.*[68] claim that the micropores of SBA-15 are approximately spherical cages rather than one-dimensional channel with a diameter of ~5 Å. This is close to the values from the SF method based calculation for SBA-15 synthesized in Chapter 2. However, micropores of SBA-15 studies by HRTEM should be done in detail to attempt to detect the microporosity. Although it was not explicitly given in Liu and coworker's work, we estimated the microporosity with t-plot shown in the supporting information.[68] The micropore volume is estimated to be 0.06 cc/g. One of the SBA-15 samples synthesized with slow ramp time and high micropore volume would be another suitable sample to perform the HRTEM study to observe the micropore structure and to estimate the sizes.

The empirical correlations we developed from our date were applied to estimate the pore sizes of the synthesized SBA-15 samples.

Conventionally synthesized sample S1 and microwave synthesized sample MW-RHP were selected. (Refer Chapter 3 for detailed synthesis conditions.)

The high resolution argon adsorption isotherm at 87 K for each sample is again plotted in the figure below. (Fig. 21)

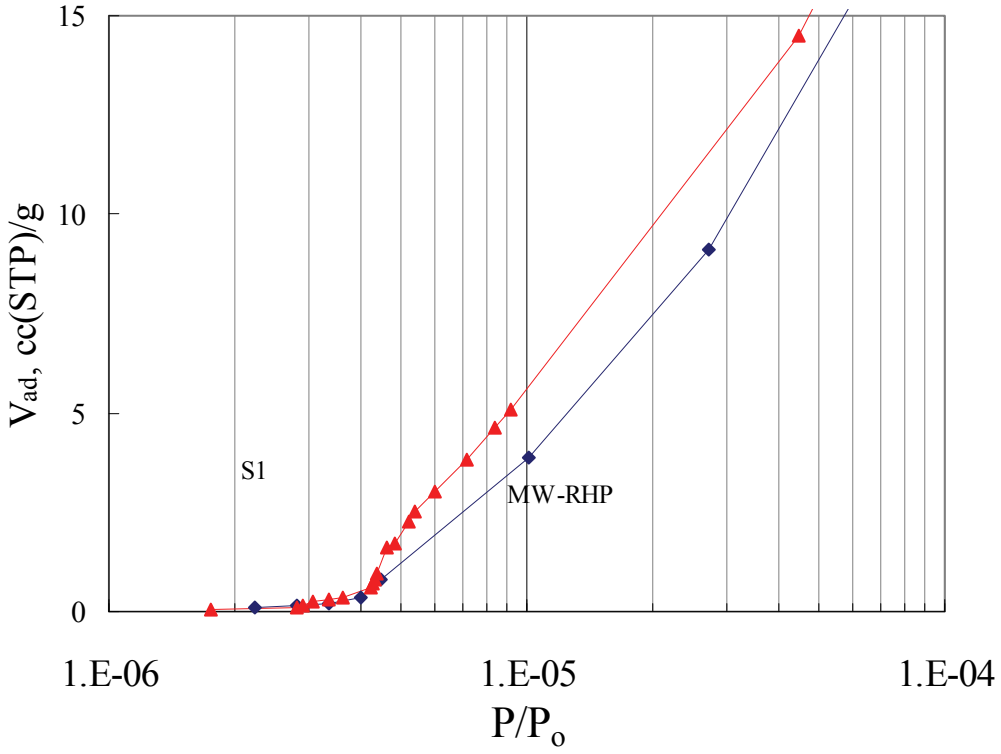

Figure 21 High resolution argon adsorption isotherm at 87 K for SBA-15 samples, S1 and MW-RHP

When these adsorption isotherms were converted to d V_{ad} /d (P/P_o) vs. P/P_o, the following pore size distributions (PSD) are obtained. (Figure 22)

(a) (b)

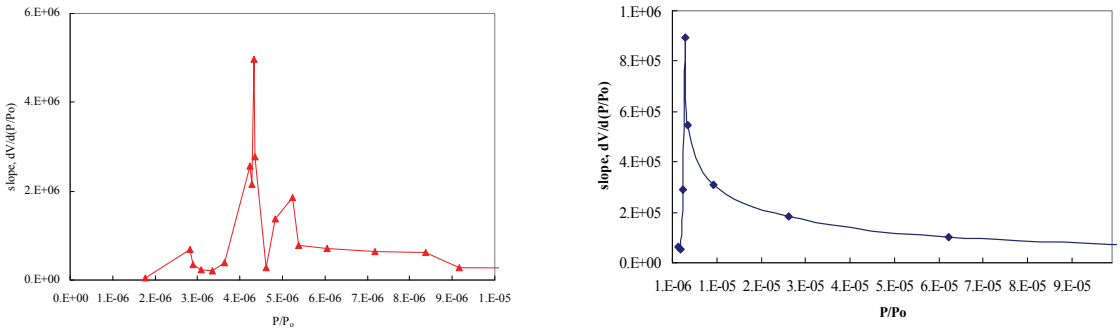

Figure 22 $d(V_{ad})/d(P/P_o)$ vs. P/P_o for S1 (a) and MW-RHP (b)

The PSD 'peak' in Figure 22 is positioned at P/Po = 4.3 x 10^{-6} for S1 and P/P_o = 4.02 x10^{-6} for MW-RHP sample. Applying the relation tabulated in Table 14 provides an estimate of the micropore size. The results for each sample employing the three different type model correlations are shown in Table 15.

Table 15 The micropore size estimation of SBA-15 samples using three different empirical correlations

Sample	Power Type (Å)	Kelvin Type (Å)	Halsey Type (Å)
S1	4.7	5.6	5.0
MW-RHP	4.7	5.5	5.0

The pore size is around 5 Å for all estimates, which is consistent with the result provided by HRTEM[68] and SAXS[35] study. The micropore size appears to be consistent from sample to sample which is consistent with the template PEO branch dictating the micropore dimensions.

4.4 Summary and Conclusion

We have developed a new simple method to estimate the pore sizes of micropores using standard zeolite samples with known pore geometry and dimensions. We have correlated the pore dimensions of these standard zeolites to their pore filling pressures based on the argon adsorption isotherms. We found that empirical correlations we have developed provide a better estimate of the pore sizes than widely used theoretical models *i.e.*, HK, SF, and BJH models. We then applied the empirical models to the high resolution isotherms of the multi-dimensional nanoporous network, SBA-15, a system whose micropore sizes are not known from crystallography. Comparing the estimated pore sizes to the result from the direct observation data, we find that the models give a reasonable estimation.

We conclude that the empirical models developed in this study can be used to accurately estimate the micropore sizes of new structures from their sorption isotherms.

CHAPTER 5

REALISTIC SURFACE AREA MEASUREMENT

5.1 Objective

The presence of the microporosity partly obfuscates the calculation of the BET surface area of micro-mesoporous materials, thus prevents one to correctly estimate the surface area of the material. Then, how can we separate the micropore contribution to the calculated BET surface area? We seek to answer this question in this chapter.

5.2 External Surface Area of a Microporous Material

Due to their high micropore volume, the BET surface area calculations for microporous materials are inappropriate. The micropores are filled before the first layer of adsorbate forms on the surface. BET analysis depends on a model for the adsorption process wherein a monolayer is formed at a relative pressure $0.05 < P/P_o < 0.3$. Therefore, the BET surface area values calculated for microporous materials do not represent the real surface area. However, these values are continually tabulated and published.

Sayari *et al.*[69] redefined the *external* surface area as the micropore-contribution excluded BET surface area. Zeolites exhibit shape-selectivity which make them important materials in catalyses and separations for many reactions.[70-72] Determination of the external surface area is of practical relevance in a sense that it is related to the extent shape-selectivity within the pores and deactivation rate of the zeolite material. A zeolite with a smaller external surface area provides higher shape-selectivity since external active sites

would not exhibit shape-selectivity. However, smaller external surface area can result in higher rate of deactivation due to the limited number of pore openings for entrance of reactants into the active internal surface.[73]

There are several methods proposed to determine the external surface areas of micro-porous materials. These include:

- Geometrical area measured directly by SEM
- Mercury porosimetry[37]
- Preadsorption method[69, 73, 74]
- Adsorption kinetic method[73, 74]
- Electron paramagnetic resonance[75]

We attempted to calculate the actual surface area of materials that are purely microporous and apply these approaches to the materials that already possess micropores within the mesopores such as SBA-15. The zeolite samples, MTT, TON, MTW, VET, ATS structures, provided by Stacey Zones, Chevron-Texaco, are used for external surface area measurement studies.

5.3 Geometric Area of Zeolite Samples Calculated Based on SEM Images

Geometrical surface area can be directly measured from particle sizes observed by SEM image for perfect uniform crystalline zeolite samples. However, in reality, zeolite samples are often less than perfect crystals and may possess inter-crystalline mesopores. Hence, their external surface areas can be much higher than their geometrical surface area.[69]

SEM images of the selected zeolite samples were obtained by JEOL JEM-5400 scanning electron microscope. Figure 23 shows the SEM micrographs of zeolite samples we studied. MTT and MTW zeolite samples have sphere-like morphology with relatively even particle size distribution whereas TON and ATS zeolite samples have bar-like morphology with uneven particle size distribution. VET zeolite exhibits needle-like shapes.

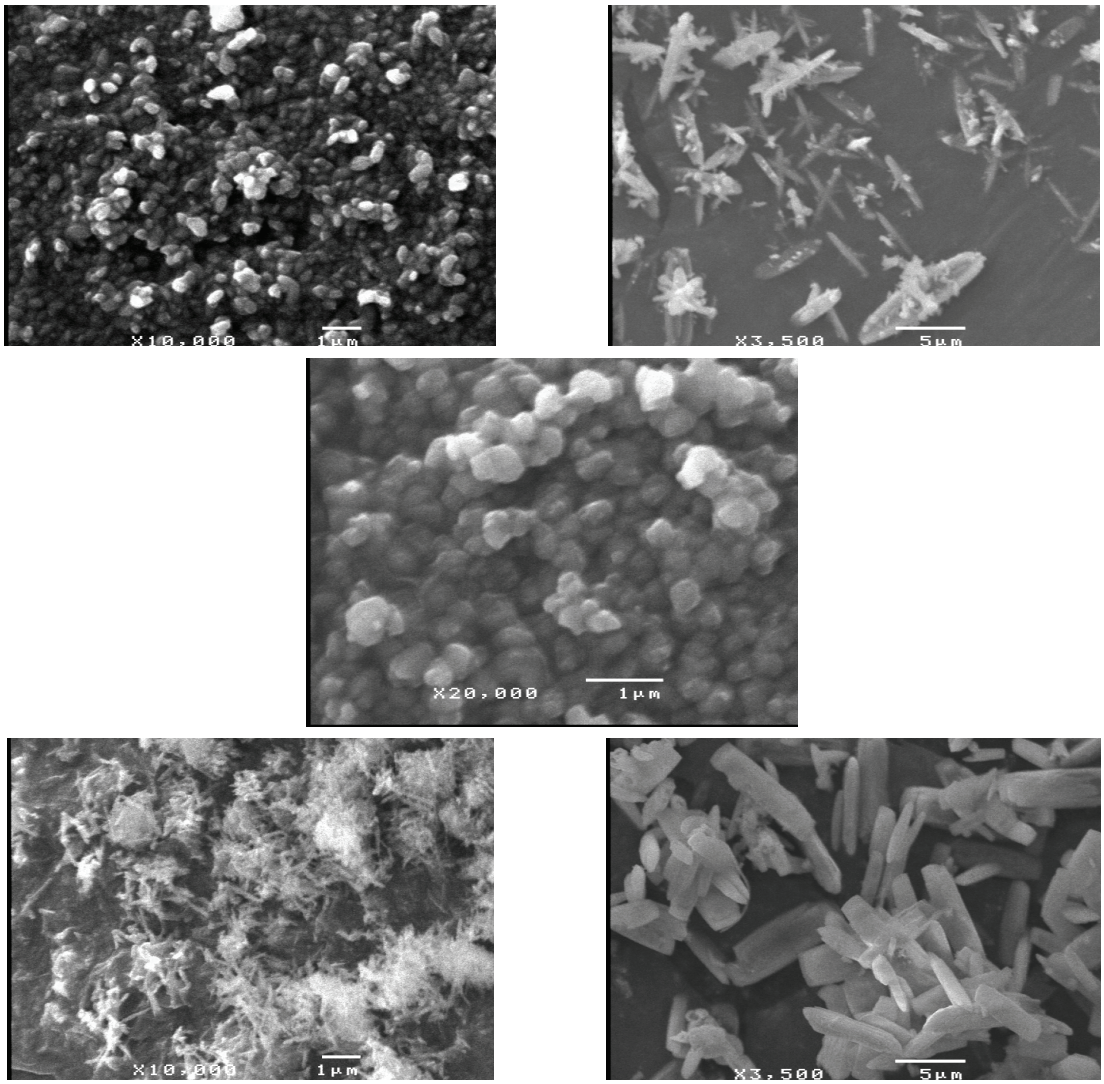

Figure 23 SEM images of selected zeolite samples: MTT (upper left), TON (upper right) MTW (center), VET (lower left), and ATS (lower right)

With the SEM images we obtained for each zeolite sample, we made estimations of external surface area. As mentioned before, geometric surface area of particle estimation based on SEM images is only a rough *estimation* since there are many assumptions involved in the derivation of the surface area calculation. For instance, we assume the particle shape as simple sphere, rectangular cube, or rod, etc. Then we assume that the surface is perfectly smooth, which is a simplified view. Most of the time, we do not have a uniform particle size distribution, hence statistical error can occur in this estimation.

Table 16 shows the estimation of external surface areas of zeolite samples from the SEM image. The density of each zeolite samples were calculated based on the framework density, FD_{Si}, values from the "Atlas of Zeolite Framework Types."[62] According to the IZA,[63] the framework density is defined as the number of tetrahedrally coordinated atoms (in our case, Si) per 1000 $Å^3$. The relation used to convert density from FD_{Si} is as follows:

T atoms	1 $Å^3$	1 m^3	SiO_2 molecule	(28.086 Si + 2 x 15.999 O)g
1000 $Å^3$	10^{-30} m^3	10^6 cc	1 T atom	6.0221415 x 10^{23} molecules

Average particle volume and external surface area are calculated from the particle size obtained from the SEM image based on the assumed shape. Then, the average particle weight was calculated by multiplying the calculated density with the average particle volume. The resulting average particle weight was finally divided from the average particle external surface area to evaluate the average external surface area of the zeolite sample.

Table 16 External surface areas of zeolite samples based on SEM images

Zeolite	FD_{Si} [62] T atoms /1000Å^3	Calculated Density g/cm^3	SEM Particle Shape	Particle Size, Length µm	Particle Size, Diameter µm	Average Particle Volume, cm^3	Average Particle External Surface Area, m^2	Average Particle Weight, g	Average External Surface Area m^2/g
MTT	20.1	2.01	Sphere	-	0.366	2.567E-14	4.208E-13	4.661E-14	9.03
TON	19.7	1.97	Rod	4	0.556	9.712E-13	7.472E-12	1.754E-12	4.26
MTW	19.4	1.94	Sphere	-	0.499	6.506E-14	7.823E-13	1.181E-13	6.62
VET	19.8	1.98	Rod	0.872	0.088	5.304E-15	2.532E-13	1.069E-14	23.69
ATS	16.4	1.64	Rod	6.468	1.502	1.146E-11	3.406E-11	1.841E-11	1.85

5.4 BET Surface Area Analysis on Modified Adsorption Isotherms

Argon adsorption isotherms of MTT, TON, MTW, VET and ATS type samples at 87 K were obtained for a low relative pressure range from 10^{-7} to 0.3 (Figure 15). These isotherms were analyzed using the BET surface area method. Our BET analysis gives surface areas in the range from 300 to 800 m^2/g with corresponding BET C constants outside the range of accuracy (20~ 400),[37] in fact, the C constants are negative values. Surface areas determined from BET theory for micropore materials are invalid since the theory does not account for adsorption at low pressures.

We wished to determine if a simplistic modification of the BET analysis could be performed in order to determine realistic surface areas for microporous materials. We performed a basic analysis described as follows. Since it is well known that micropores are fully filled at the relative pressure (P/P_o) of $10^{-3}$for N_2 and Ar, we subtracted the volume adsorbed at that relative pressure from the volume adsorbed for the rest of the relative pressures to create a modified isotherm. BET analyses were then undertaken on these

modified isotherms using subtraction of volumes adsorbed at different relative pressures, namely, $P/P_o = 10^{-2}$, 10^{-3}, 10^{-4} and a visual best fit relative pressure, P_E (Refer Figure 14 for the definition of P_E). This was carried out for each of the zeolite samples. The analysis procedure for VET type zeolite is depicted below as an example (Figure 24).

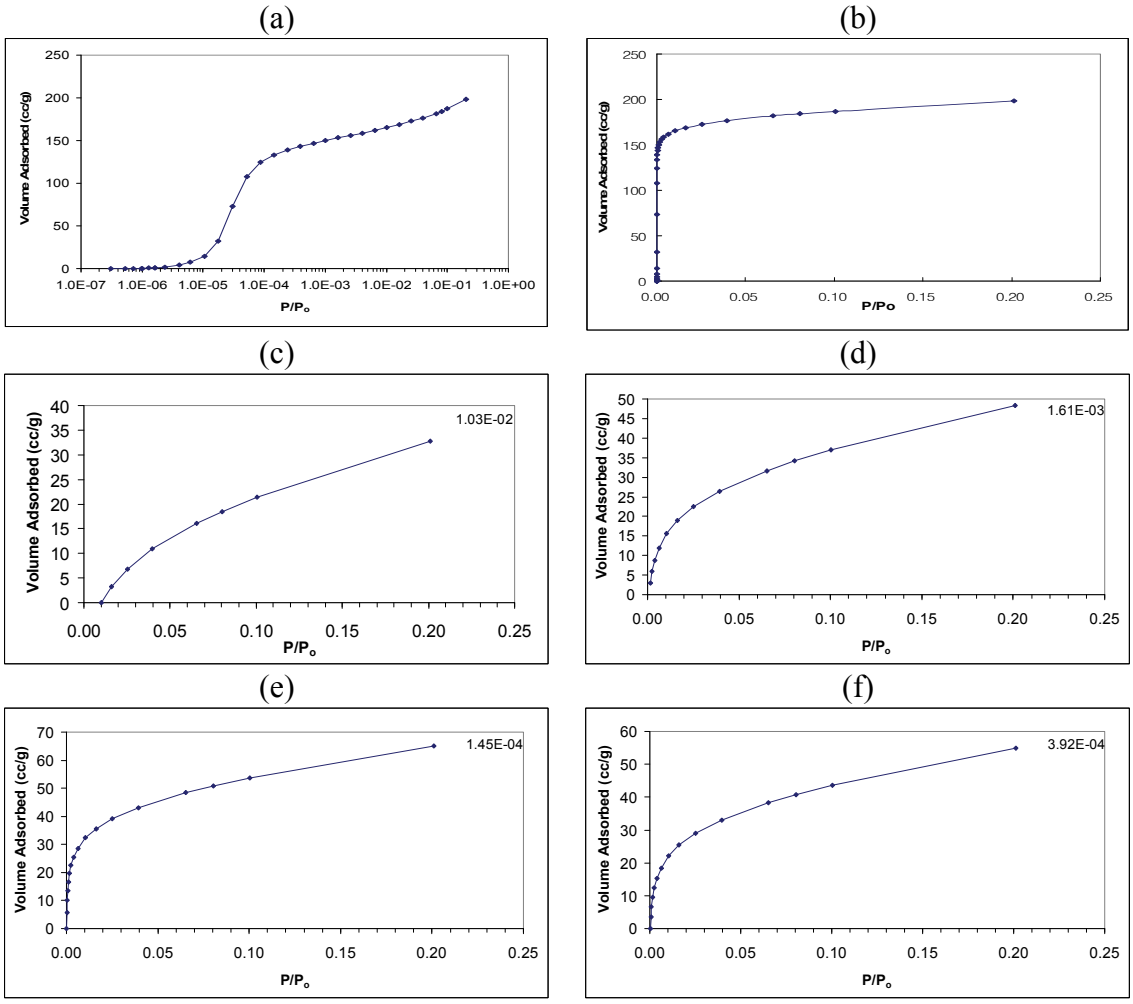

Figure 24 Construction of modified isotherms for BET analysis on VET framework zeolite

(a) Original isotherm (logarithmic scale); (b) original isotherm (normal scale); Modified isotherm constructed by subtracting the volume adsorbed at $P/P_o = 1.0 \times 10^{-2}$ (c); $P/P_o = 1.0 \times 10^{-3}$ (d); $P/P_o = 1.0 \times 10^{-4}$ (e); at the $P/P_o = P_E$ (refer Figure 14 for definition of P_E) (f).

Table 17 shows the tabulated results of the BET surface area analyses for all zeolite samples.

Table 17 BET analyses of selected zeolite samples before and after modifying the adsorption isotherm

Zeolite	Original		$P/P_o = 10^{-4}$		$P/P_o = 10^{-3}$		$P/P_o = 10^{-2}$		$P/P_o = P_E$		
	SA_{BET}	**C_{BET}**	**SA_{BET}**	**C_{BET}**	**SA_{BET}**	**C_{BET}**	**SA_{BET}**	**C_{BET}**	**SA_{BET}**	**C_{BET}**	P_E
MTT	**400.3**	**-213.1**	**195.3**	**151.7**	**163.9**	**77.2**	**117.6**	**14.9**	**225.4**	**326.9**	8.66×10^{-5}
TON	**323.5**	**-183.9**	**89.8**	**32.8**	**85.5**	**26.1**	**80.9**	**14.3**	**98.8**	**47.1**	4.87×10^{-5}
MTW	**1082.7**	**-978.5**	**539.2**	**48.5**	**475.1**	**29.4**	**477.5**	**7.5**	**506.0**	**38.3**	4.91×10^{-4}
VET	**596.8**	**-226.8**	**283.7**	**67.2**	**186.1**	**32.0**	**158.9**	**10.0**	**206.3**	**44.0**	3.92×10^{-4}
ATS	**513.3**	**-411.6**	**376.6**	**732.5**	**250.3**	**128.2**	**136.1**	**16.6**	**180.4**	**53.0**	3.00×10^{-3}

We find from Table 17 that, when the volume adsorbed at $P/P_o=10^{-3}$ was subtracted to construct a modified isotherm, the modified isotherm results in a surface area with BET C constant in valid range (20~400). Analyses performed based on the best visual fit also gave appropriate BET C constants. The BET surface areas, calculated after this analysis, were 2- to 3-fold reduced values compared to those calculated without modifying the isotherms. However, the estimates are still considerably higher then the estimates from microscopic analyses.

From Figure 24 and Table 17, we observe that as we increase the relative pressure at which we set the baseline of the volume adsorbed, *i.e.*, that corresponding to filled micropores, the BET C constant increases and the modified isotherms level off.

We are certain that the BET constants are within a valid range as we modify the adsorption isotherms by subtracting volumes at elevating relative pressures. However, we can see that the calculated surface areas are somewhat large (orders of magnitude) as

compared to the result from the external surface area calculation base on the SEM images. (Table 16). We still need to ask ourselves the question whether "cutting down" the volume adsorbed at lower relative pressures would resolve the "true" micropore volume effect on the surface area calculation. We continue our study using a different approach, sequential adsorption, with this question in mind.

5.5 Sequential Adsorption

5.5.1 Background

"Sequential adsorption" is also known as preadsorption. The preadsorption method was first introduced by Gregg and Langford[76] in 1969 to evaluate the microporosity of a carbon black. In preadsorption, as can be inferred from its name, a preadsorbate is adsorbed by the adsorbent prior to the normal adsorption. According to Gregg and Langford, the objective was to fill the micropores of an adsorbent with normal nonane (refer to as *n*-nonane hereafter), while leaving the wider pores and exterior surface still available for the adsorption of nitrogen at 77 K. *n*-nonane was chosen for the preadsorptive due to the fact that it has a relatively large heat of adsorption which means, in turn, that there is a high activation energy and slow rate for desorption. (P_o = 4.7 Torr at 298K)[37] As a consequence, high temperatures are required to remove the *n*-nonane molecules from the narrow pores at a measurable rate. Moreover, it is known that the minimum kinetic diameter of *n*-nonane is 0.43 nm[77] and the cross-section is approximately 0.34 nm.[78] Therefore, the long-chain molecules of *n*-nonane are able to enter narrow micropores of widths as low as 0.4 nm, which is not the case with more bulky hydrocarbon molecules. The selected material for the

adsorbent in Gregg and Langford's study was carbon black which had been oxidized in order to produce micropores in its constituent particles. The nitrogen isotherm at 77 K was determined both before and after the micropores had been filled with *n*-nonane by adsorption from the vapor phase, and also after the micropores had been partially emptied by evacuating at elevated temperature. The schematic of the preadsorption system is illustrated in Figure 25.

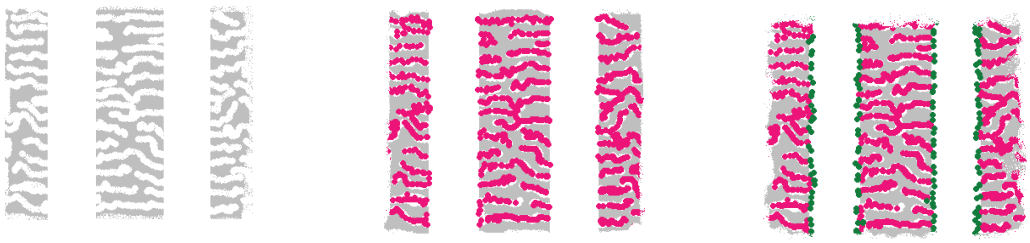

1. Outgas the porous sample at elevated temperature

2. Preadsorb with preadsorbate at room temperature and evacuate

3. Sequentially adsorb N_2 at 77 K (or Ar at 87 K)

Figure 25 Schematics of Sequential Adsorption

Gregg and Langford's[76] experimental procedure is as listed below.

1. Outgas the sample

2. Preadsorb *n*-nonane vapor at room temperature (25°C) for 30 minutes

3. Re-outgas the sample at room temperature for 6 hours

4. Determine the nitrogen isotherm at 77 K

5. Outgas the sample at a number of increasingly higher temperatures and determine nitrogen isotherms successively after each stage of outgassing until the *n*-nonane had been completely removed.

Hence, constructed isotherms should be parallel to each other. The distance between the parallel branches of the nitrogen isotherms, corresponding respectively to the sample filled and emptied of *n*-nonane, should give a value for the micropore volume.

Suzuki *et al*.[73, 74] have furnished a "filled pore method," which is a slight alteration of the preadsorption method, but basically the same concept. Instead of microporosity evaluation, they used this method for external surface area determination of zeolite materials. They filled the internal pores of zeolite, with different filling substances (butane, ethane, water, propane, 2,2-dimethyl-propane) and performed typical nitrogen adsorption experiments. BET analyses were applied based on the isotherms obtained which, in turn, gave an estimate of the external surface areas of zeolite materials.

The concept of filling the internal micropores of microporous material with another adsorbate can be applied to a micro-mesoporous system, where micropores will be filled with preadsorbate and the mesopores still will be available for the sequential adsorption of nitrogen or argon. Applying BET analysis will consequently provide a more realistic surface area of the remaining mesopores. Göltner and coworkers[35] used *n*-nonane preadsorption method on mesoporous molecular sieves, in order to show the mesopore system with micropores selectively blocked. However, they did not continue their study to the quantitative measurement of the mesoporous surface area and micropore volume. Here, we apply, for the first time, this method to SBA-15 systems to estimate the real surface areas attributed to the mesopores.

5.5.2 Samples to Study

For microporous samples, silicalite (MFI framework) was chosen as a candidate. We have used commercially available silicalite, provided by Union Carbide, and another synthesized by Dr. Geoffrey Tompsett, University of Massachusetts, with microwave heating. The VET framework, one of the zeolite samples prepared by Stacey Zones was also used.

As for the SBA-15 samples, we used samples that are estimated to be highly microporous based on the results from α_s plot analysis (sample preparation described in Chapter 3). As we have investigated the micropore sizes of SBA-15 samples throughout Chapters 3 and 4, we are confident that *n*-nonane (kinetic diameter of 0.43 nm) will be adsorbed onto the broadly distributed sizes of micropores that were estimated to average around 5 nm. Since argon adsorption is preferred over nitrogen, we have continued to use argon in most cases.

5.5.3 Normal-nonane Preadsorption Procedure

We followed the procedure provided by Sayari *et al.*[69] for the sequential adsorption experiments with little alteration. Argon or nitrogen adsorption isotherms were obtained from the AUTOSORB®-1-C instrument and *n*-nonane vapor adsorption was performed using the VAS.[54] Sample of 30~90 mg was placed in a glass adsorption sample cell (1/4″ outside diameter stem) with stopcock (1/4″ outside diameter stem), where the sample cell and stopcock were connected by Ultra-Torr® union (1/4″ tube outside diameter) with appropriate size Viton® o-rings. All the samples were outgassed at 300°C for 12~20 hours

prior to the adsorption experiments. *n*-nonane (99%) was obtained from Acros and used as received. Ultra high purity grade helium (for dead space calculation), nitrogen and argon gas cylinders were obtained from Merriam-Graves.

The following is the procedure of the sequential adsorption experiment:.

1. Normal argon or nitrogen adsorption was performed in AUTOSORB®-1-C.

2. With the stopcock closed, the sample cell was transferred to the VAS.

3. The sample was evacuated at room temperature for overnight with stopcock open.

4. The sample was exposed to the saturated vapor of *n*-nonane at room temperature for 2 hours, at which point the pressure of the system appears unchanging.

5. The sample was evacuated at room temperature for 2 hours, until the pressure reading from the low pressure transducer was close enough to the initial vacuum pressure.

6. With the stopcock closed, the sample cell was transferred to AUTOSORB®-1-C.

7. The sequential argon or nitrogen adsorption was performed.

Suzuki *et al.*[73, 74] and Sayari *et al.*[69] filled their sample cells with helium to a pressure of 700 Torr in step 6, for they thought this would expedite the cooling process of the zeolite to 77 K. We did not follow this procedure, since the sample cell was immersed in the coolant bath (liquid argon or nitrogen) for approximately an hour prior to the subsequent adsorption.

5.5.4 Isotherms Obtained Before and After Preadsorption

Argon or nitrogen adsorption isotherms were obtained for the designated samples (refer to Section 5.5.2) following the procedure described earlier. Data reduction of obtained isotherms was performed using ASWIN version 1.51 from AUTOSORB®-1-C instrument for BET surface area, SA_{BET} (m^2/g), BET constant, C_{BET}, α_s micropore volume, V_μ(cc/g), and BJH mesopore diameter, D_{BJH}(Å), calculations.

Commercial silicalite sample

Nitrogen adsorption isotherms at 77 K before and after *n*-nonane preadsorption are shown in Figure 26.

Microwave synthesized silicalite sample

Nitrogen adsorption isotherms at 77 K before and after *n*-nonane preadsorption are shown in Figure 27.

VET sample

Argon adsorption isotherms at 87 K before and after *n*-nonane preadsorption are shown in Figure 28.

SBA-15 sample; MW-RHP

Argon adsorption isotherms at 87 K before and after *n*-nonane preadsorption are shown in Figure 29.

SBA-15 sample; C24

Argon adsorption isotherms at 87 K before and after *n*-nonane preadsorption are shown in Figures 30.

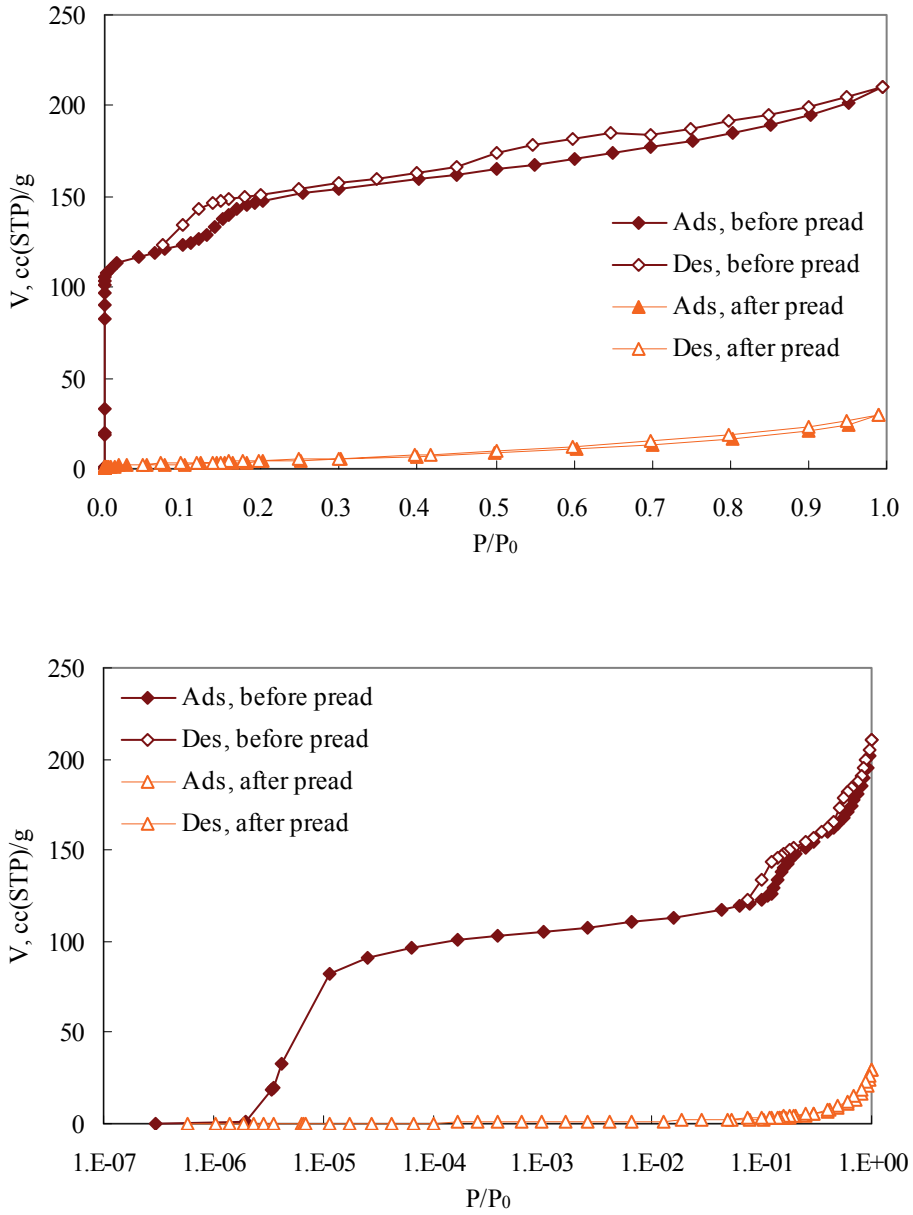

Figure 26 Nitrogen adsorption at 77 K on commercial silicalite before and after *n*-nonane preadsorption in normal scale (Top) and logarithmic scale (Bottom)

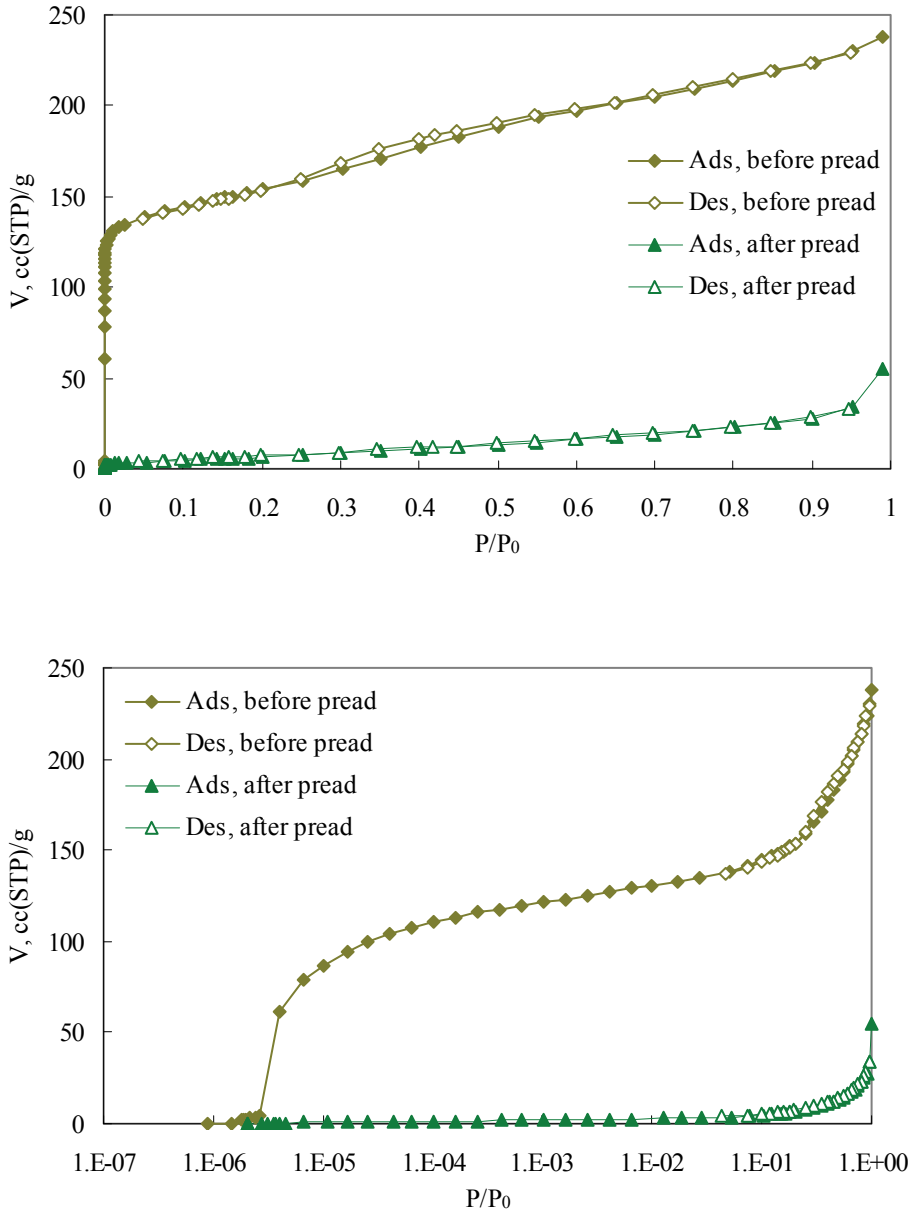

Figure 27 Nitrogen adsorption at 77 K on microwave synthesized silicalite before and after *n*-nonane preadsorption in normal scale (Top) and logarithmic scale (Bottom)

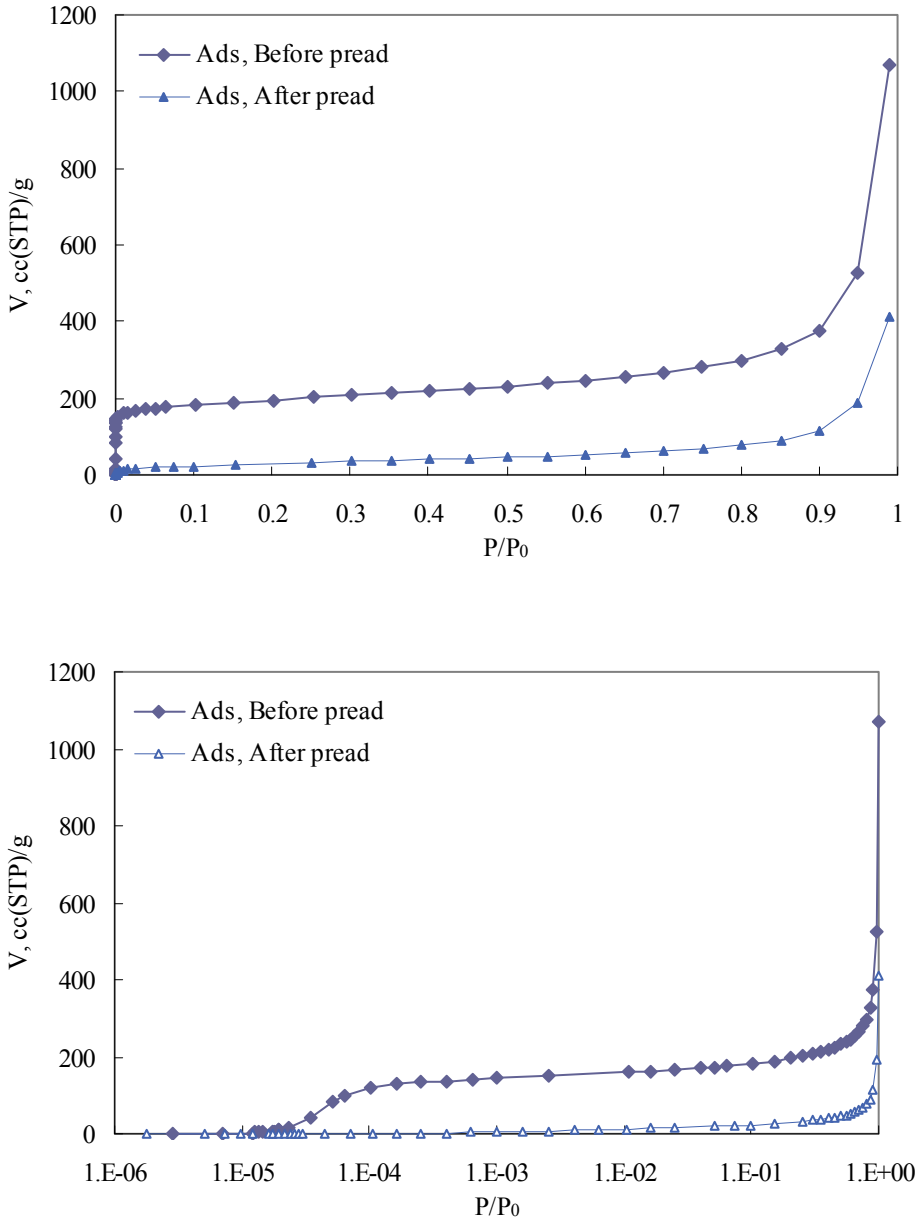

Figure 28 Argon adsorption at 87 K on VET before and after *n*-nonane preadsorption in normal scale (Top) and logarithmic scale (Bottom)

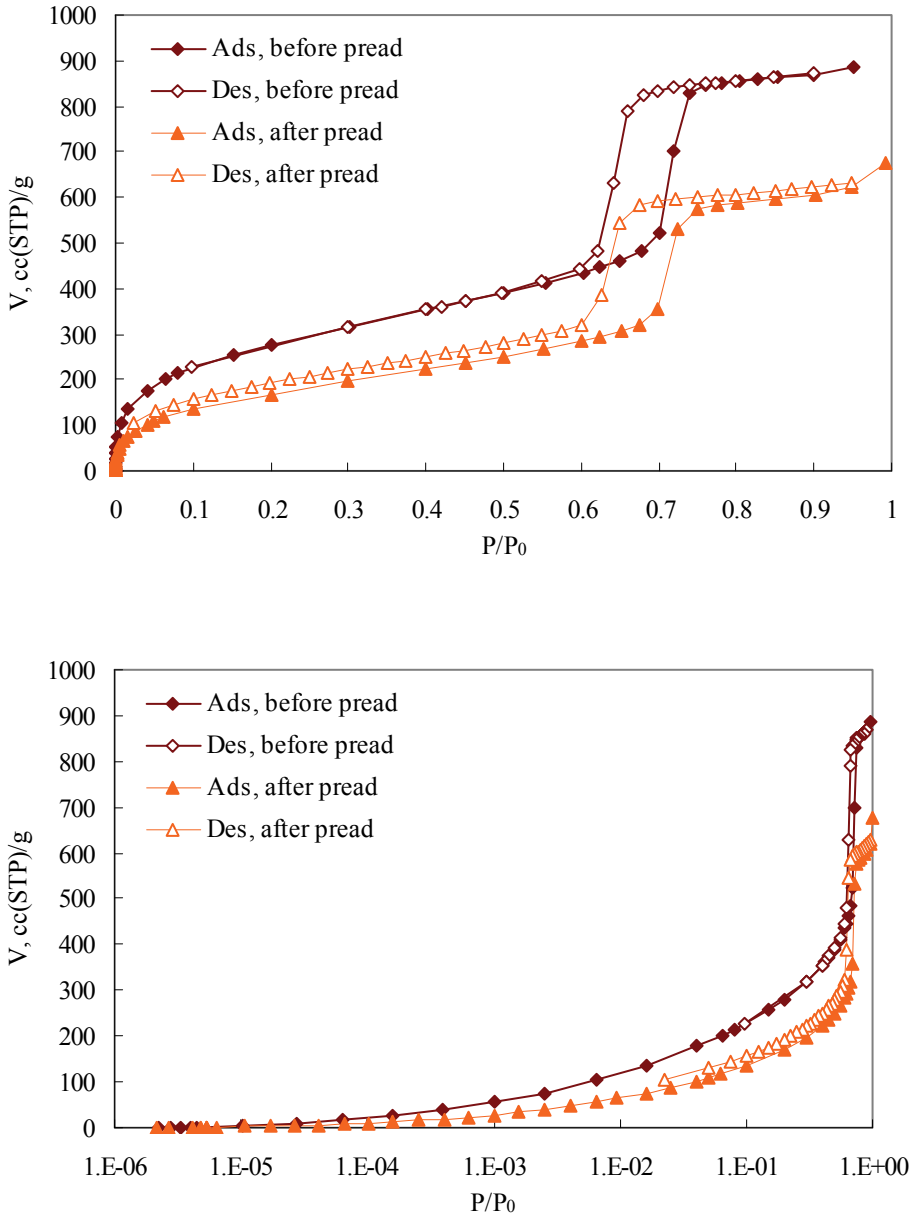

Figure 29 Argon adsorption at 87 K on MW-RHP before and after *n*-nonane preadsorption in normal scale (Top) and logarithmic scale (Bottom)

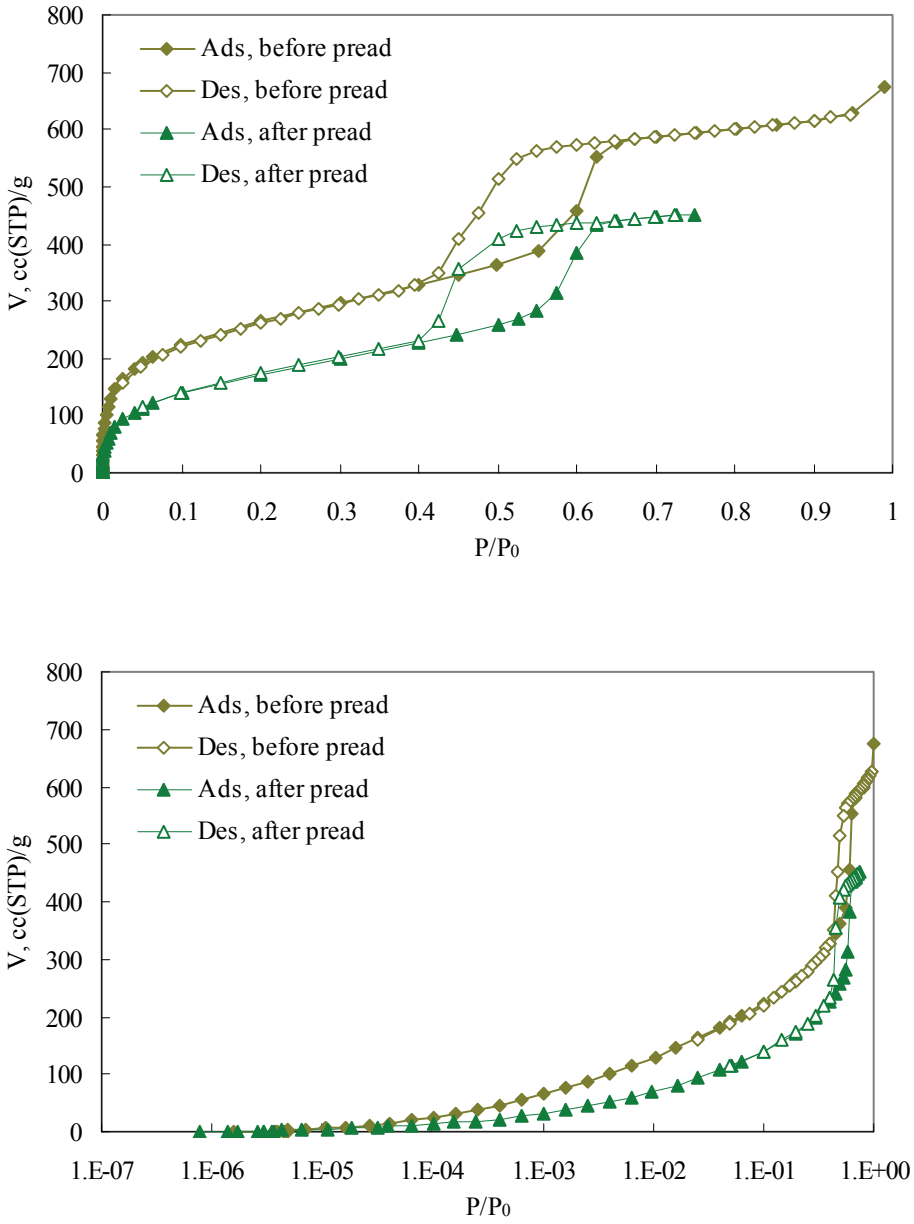

Figure 30 Argon adsorption at 87 K on C24 before and after *n*-nonane preadsorption in normal scale (Top) and logarithmic scale (Bottom)

5.5.5 Results and Discussion

More adsorption isotherm plots are available in the appendix for each sample studied in Section 5.5.4. BET surface areas, micropore volumes, and BJH mesopore sizes (for mesoporous samples) are tabulated in Table 18 for these materials.

Table 18 BET surface area, micropore volume, and BJH mesopore size calculation based on the adsorption isotherms obtained before and after n-nonane preadsorption

		SA_{BET} (m^2/g) / C_{BET}		V_μ (cc/g)[a]		D_{BJH} (Å)	
	Sample	Before	After	Before	After	Before	After
Microporous	Commercial silicalite (N2/77K)	471.1 / -98	19.1 / 98.6	0.159	-0.014		
	Microwave synthesized silicalite (N2/77K)	497.3 / -83.9	28.3 / 17.5	0.103	-0.018		
	VET (Ar/87K)	533.6 / -47.6	96.0 / 38.8	0.172	0.001		
Micro-Mesoporous SBA-15	MW-RHP (Ar/87K)	879.8 / 74.6	550.2 / 48.1	0.122	0.040	78.2	78.7
	C24 (Ar/87K)	814.9 / 130	556.1 / 53.3	0.122	0.024	57.3	53.6

[a] α_s micropore volume calculation was applied for the relative pressure range of 0.2~0.6.

The surface areas and micropore volumes were both reduced for all samples after *n*-nonane preadsorption.

For microporous samples, the BET surface area estimates were in the range of 470 ~ 530 m^2/g before the *n*-nonane preadsorption with negative BET constants. However, after preadsorption, the estimate based on BET analyses are decreased by factors of five to twenty four, and now the BET constants are within the valid applicable range (20 ~ 400). The micropore volumes are close to zero after *n*-nonane preadsorption.

For micro-mesoporous samples, before the preadsorption, the BET surface areas were approximately 800 m^2/g, but they were reduced by two thirds after preadsorption. However, micropore volumes calculated by the α_s method, after sequential adsorption, are

not negligible. This is probably partly due to the fact that micropores or even small mesopores present in the mesoporous walls are broadly distributed in size, therefore *n*-nonane might not *fill* the pore completely or desorbed during the evacuation process before the sequential argon adsorption.

From these findings, we learn that 80~95% of the BET surface area calculation for microporous materials and more than 30% of that for micro-mesoporous materials is due to the micropores present. Hence, in most cases, the calculated value of the external surface area of the zeolite, microporous material, and specific BET surface area of mesoporous material with micropores are overestimated significantly. Therefore, it is critical to exclude the micropore volume effect on the calculation of external surface area of zeolite materials and micro-mesoporous materials as well, especially when the micropore sizes are monodispersed.

5.6 Comparison

There are several methods to determine the external surface areas of microporous materials. Among them, the sequential adsorption technique seems to provide a reasonable estimation of the external surface area.

Results obtained from the sequential adsorption are compared with those from the earlier results we have obtained in this chapter. The surface areas calculated for zeolite samples are in the mid range of the results from SEM images-based geometrical analysis and modified adsorption isotherms. We believe that simply subtracting volume adsorbed to

create a modified adsorption isotherm does not solve the micropore volume effect on micro-mesoporous systems.

5.7 Summary

Sequential adsorption study was performed on pure microporous materials and mesoporous materials that have micropores in the wall. For both of the materials, after *n*-nonane preadsorption, the micropore volume effects on the BET surface areas were eliminated. We believe that the sequential adsorption enable one to measure more realistic surface areas of porous materials that have a microporous component. This technique can further be applied to multidimensional nanoporous networks such as membrane systems.

CHAPTER 6

CONCLUSION AND RECOMMENDATION FOR FUTURE WORK

6.1 Conclusions

In this study, the syntheses of micro-mesoporous material, SBA-15 with diverse structural properties were carried out using various synthesis conditions. In particular, the consequences of varying the temperature ramp rate of the precursor solution to the reaction temperature were examined. We observed that the ramp rate to the synthesis temperature has significant impact on the micropore volumes, BET surface areas and pore sizes of the obtained materials.

Empirical correlations of pore size to filling relative pressure were developed for zeolite materials with well-defined one dimensional pore structure. These correlations were employed to determine the micropore sizes of the micro-mesoporous materials. It is found that these are in close agreement with the literature values obtained from HRTEM[68] and SAXS[35] studies.

Micropore volume exclusions in the BET surface area measurements were realized to obtain the realistic surface areas of microporous materials and "multidimensional porous networks" with sequential adsorption experiment. Comparing the nitrogen or argon adsorption isotherms obtained before and after preadsorption of *n*-nonane on micropore containing substances revealed that the sequential adsorption technique would be an appropriate method to measure the external surface areas of microporous materials and the BET surface areas of mesoporous materials with micropores.

6.2 Recommended Future Works

6.2.1 Synthesis of Nanoporous Networks

As for the future synthesis work, it is recommended to synthesize SBA-15, within different heating media that shows different heat transfer rate from conventional oven or microwave oven. Currently, silicalite and NaY synthesis work is in progress with different heating media, by Ko-yeol, Choi[79]. Choi used effective heat transfer media, ethylene glycol, conventional oven, and microwave oven to study the effect of ramp rate to the synthesis temperature on the synthesis of silicalite and NaY, in terms of yield and crystallinity of synthesized samples, respectively. Similar work can be carried out for the synthesis of SBA-15 to compare the properties of the materials synthesized in conventional oven, ethylene glycol bath, and microwave oven.

Perhaps the synthesis of the ordered mesoporous silicas (OMSs) with zeolitic walls would be an ultimate goal for most researchers in the related field, since the distinct bimodal pore structure gives many advantages over pure microporous material or mesoporous materials with disordered micropore phase. Improved transports and catalytic or selectivity performances, and higher thermal and mechanical stability of the structure are achieved due to the crystalline phase of the mesopore walls. Therefore, numerous attempts been made to realize this including the works to synthesize TUD-1[80] and RMM[34, 81]. Although we have spent some amount of time to synthesize mesoporous material with microporous walls by combining the precursor solution of SBA-15 and that of silicalite, we were not successful. This might be due to the fact that two precursors are made at two extreme pH conditions. It was difficult to control the pH that would work for both structure

directing agents: SBA-15 template P123 requires acidic conditions whereas silicalite structure directing agent TPAOH requires high pH. If one is able to find a reproducible recipe to synthesize the mesoporous material with zeolitic walls, incorporating it with microwave oven synthesis is recommended, since microwave enhances the crystallization of inorganic materials.[61]

6.2.2 Adsorption Studies

Extending the sequential adsorption study to the practical system such as membrane is highly suggested. Membrane is a readily adaptable system in various applications and precise knowledge on the porosity of the material is very important for the process design. Hence, applying the sequential adsorption method to the membrane samples will be of great interest. Due to the lack of adsorption cell for membrane samples, adsorption studies of the membrane samples were not actively undertaken. Using the patented adsorption cell for membrane samples developed in professor Conner's group,[82] the adsorption experiments on membrane systems were enabled, and hence the sequential adsorption experiment can be performed in this cell. Therefore, little modification to the existing adsorption cell designed for membrane samples will facilitate the need and practically provide membrane pore structures in a relatively straightforward manner.

As for the continuing adsorption studies, it would be interesting to perform scanning curves for PSBA samples. Tompsett and Conner[83] studied the hysteresis and scanning behavior of mesoporous molecular sieves. Performing the similar scanning on each step of desorption branch would be of an interest to find the stability of hysteresis

6.2.3 Transport Studies

Transport studies will be a next step as this study of micro-mesoporous materials proceeds, since the ultimate application of the materials studied here will be its use as an adsorbent or catalyst support. An adsorptive that would adsorb onto or the reactants that would react at active sites within SBA-15, should be transported to the required surface, in the first place, in order to expect adsorption or reaction to happen. It is, as a matter of fact, critical that the target reactant and/or product of the certain reaction and the adsorbate or a target material that one wants to separate the others from, should happen fast or slow enough so that we obtain our goal of using the material for. In the past, the frequency response studies[84] were undertaken for the diffusion of aromatic hydrocarbon, from Conner's group. Moreover, these studies enable one to investigate the competitive diffusion in multidimensional nanoporous networks, which is of more practical interest. In reality, it is the mixture, rather than pure fluids, that are being transported more often than not, hence it is worthwhile for the continuation of the study for nanoporous network system.

APPENDIX A

DIAGRAM OF REACTOR VESSEL TO MONITOR THE TEMPERATURE PROFILE TO SYNTHESIZE SAMPLE C2C2

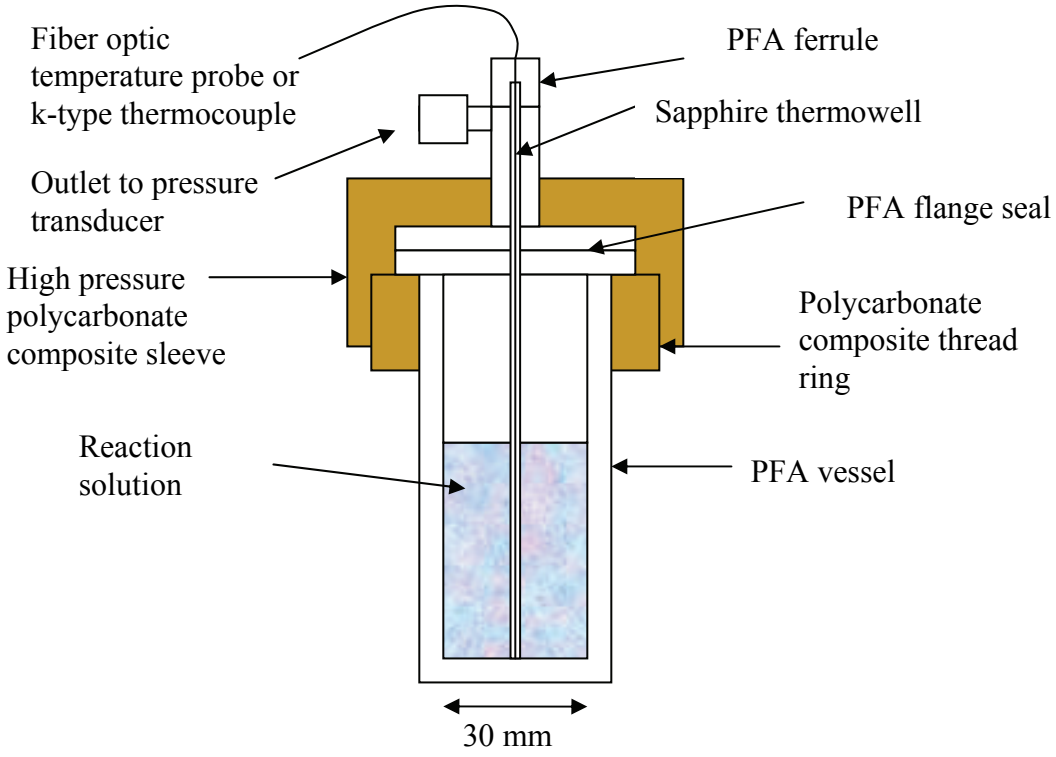

Figure 31 ACV reactor vessel from CEM Corp.

APPENDIX B

STANDARD ADSORPTION ISOTHERMS

Figure 32 is the standard adsorption isotherms that are used in this work for α_s plot. N_2 adsorption at 77 K on non-porous hydroxylated silica material was obtained from the work by Bhambhani *et al*.[37, 56] Argon adsorption at 87 K on non-porous hydroxylated silica material was obtained by Gur'yanova *et al*.[57]

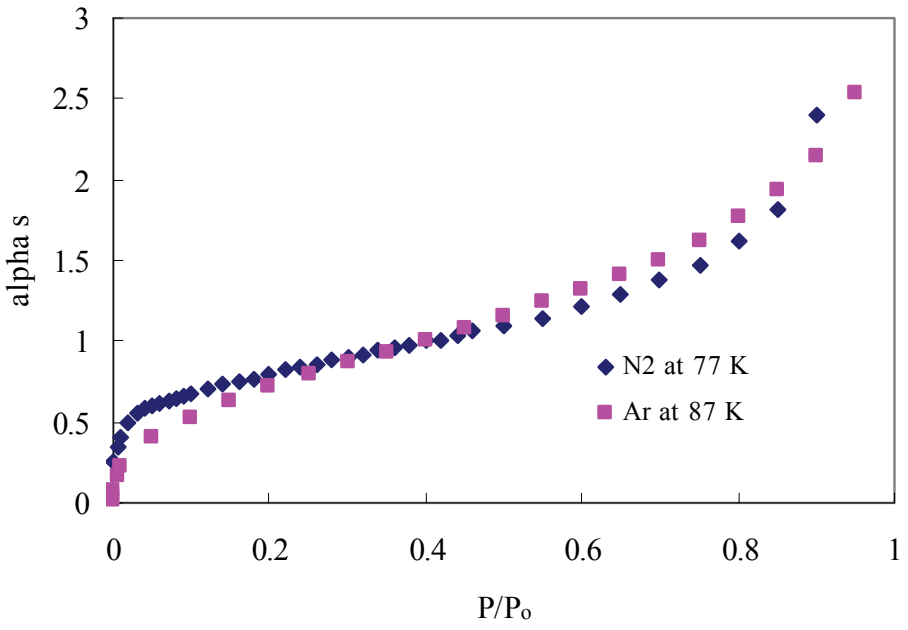

Figure 32 Standard adsorption isotherms for micropore calculation

APPENDIX C

ADDITIONAL ADSORPTION ISOTHERMS IN CHAPTER 3

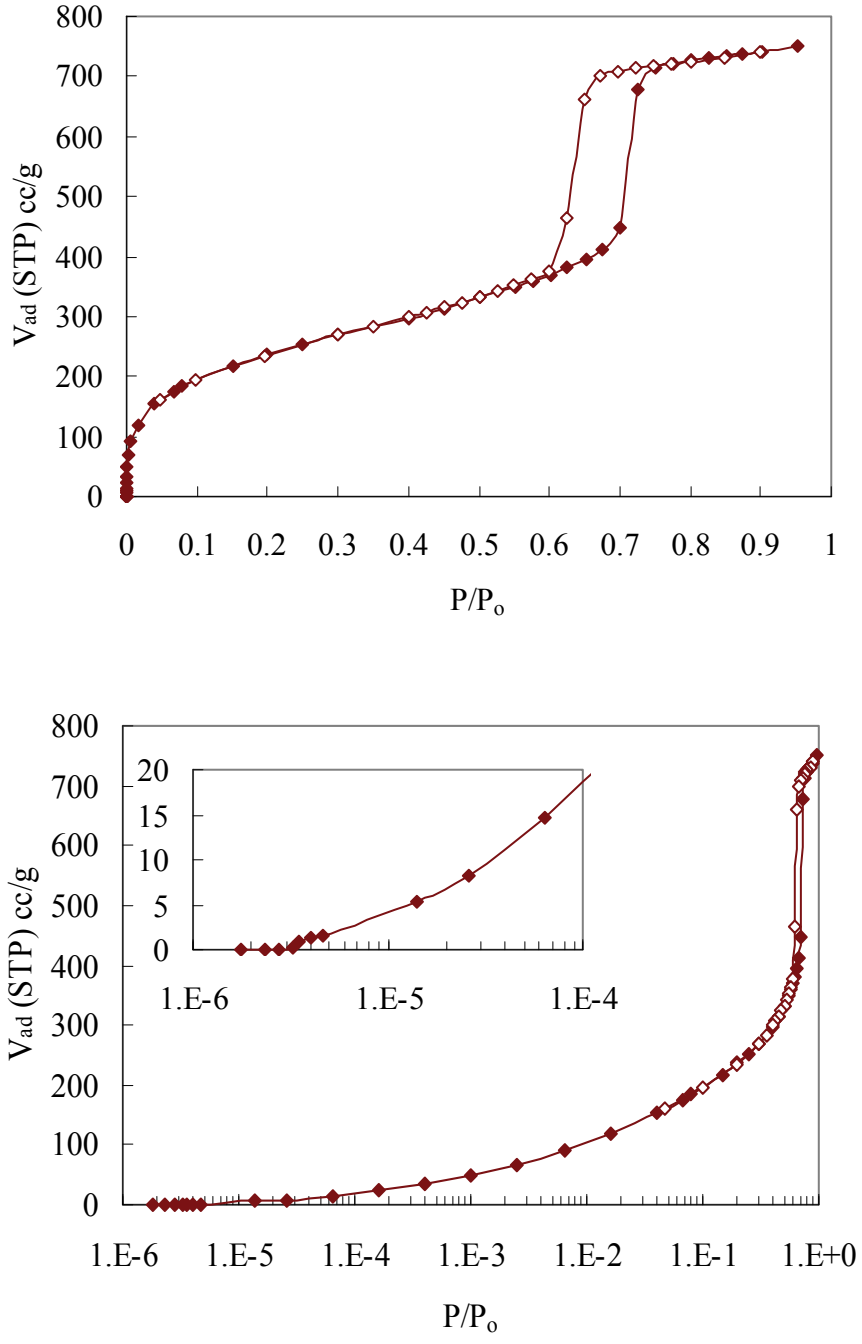

Figure 33 Argon adsorption at 87 K on MW-rhp in normal scale (Top) and logarithmic scale (Bottom)

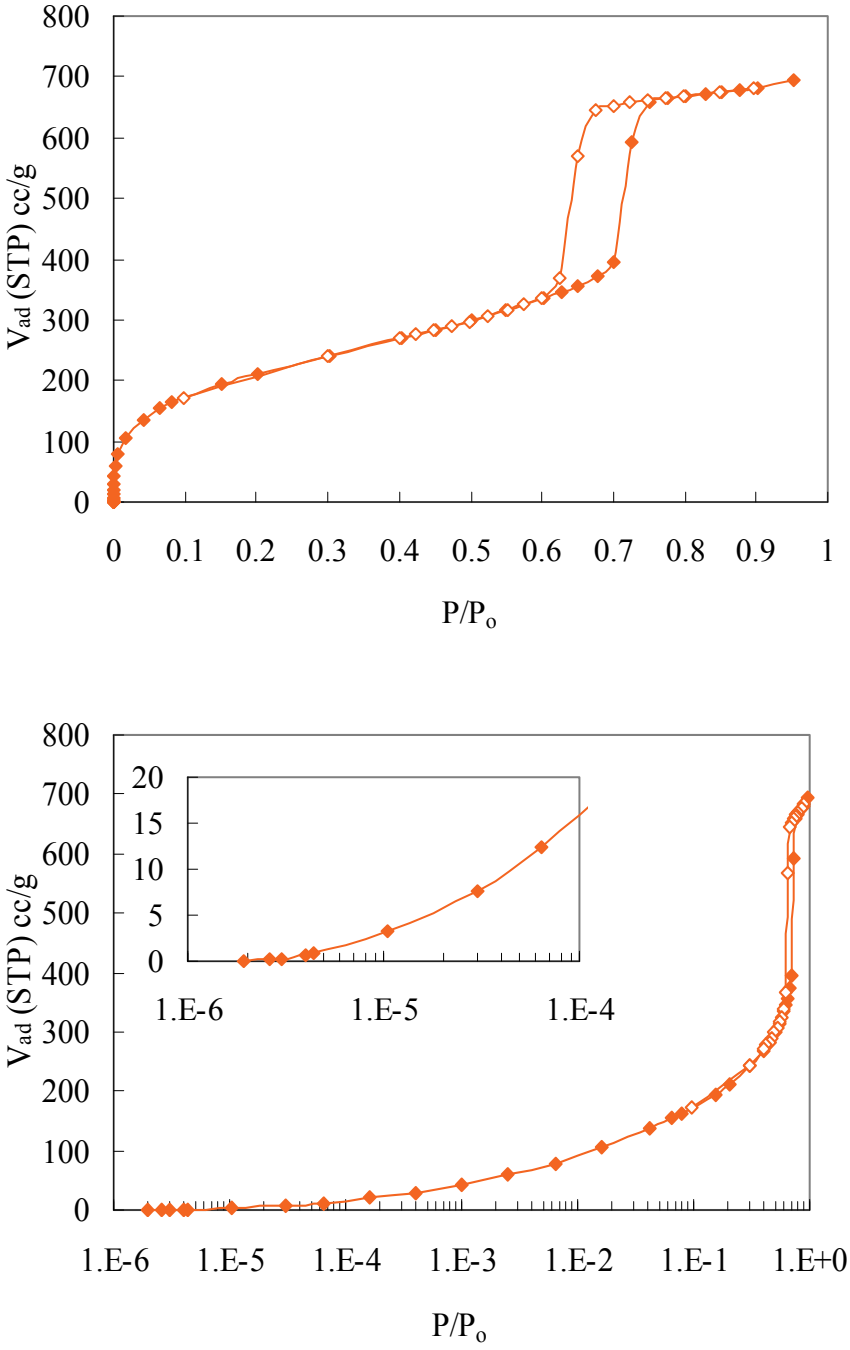

Figure 34 Argon adsorption at 87 K on MW-RHp in normal scale (Top) and logarithmic scale (Bottom)

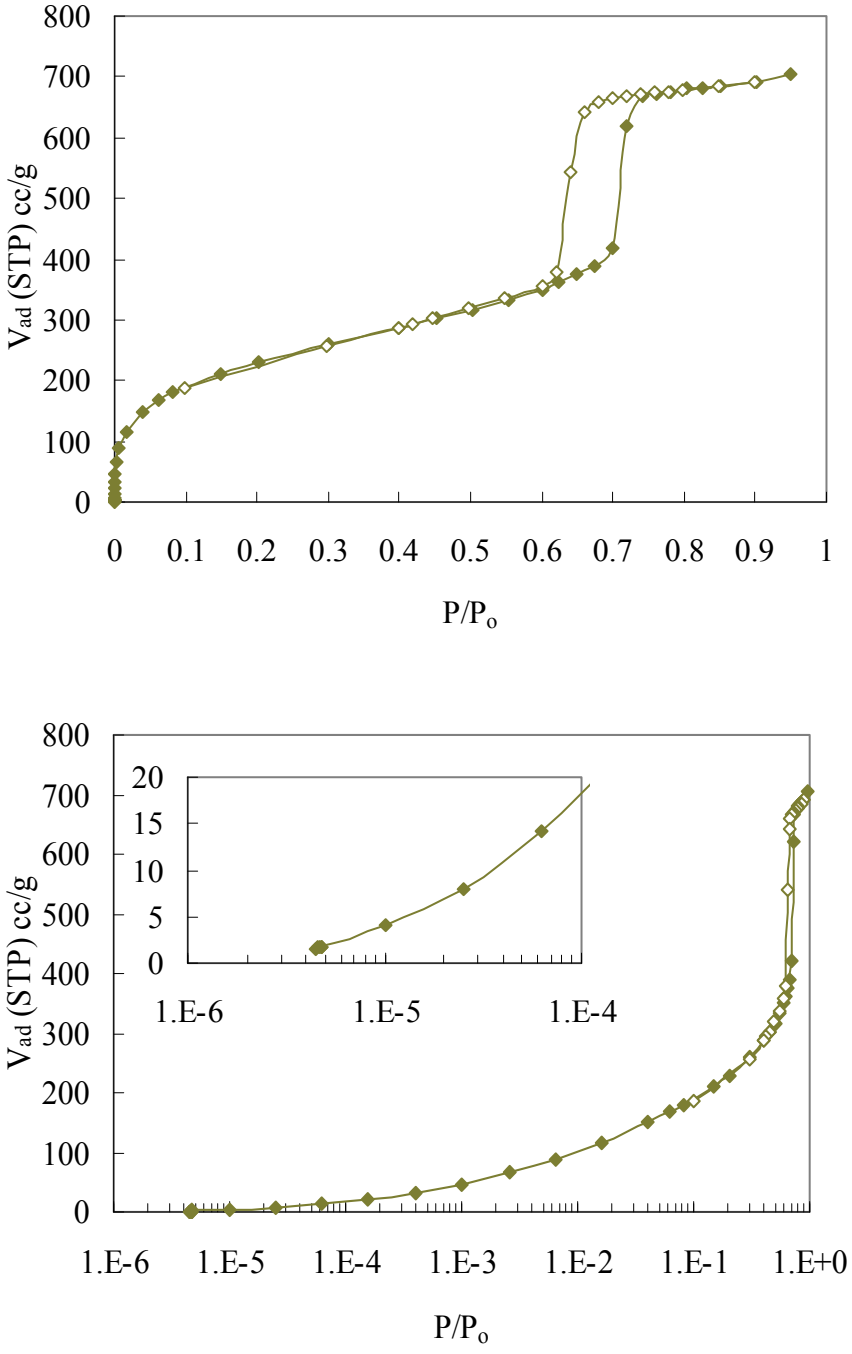

Figure 35 Argon adsorption at 87 K on MW-RhP in normal scale (Top) and logarithmic scale (Bottom)

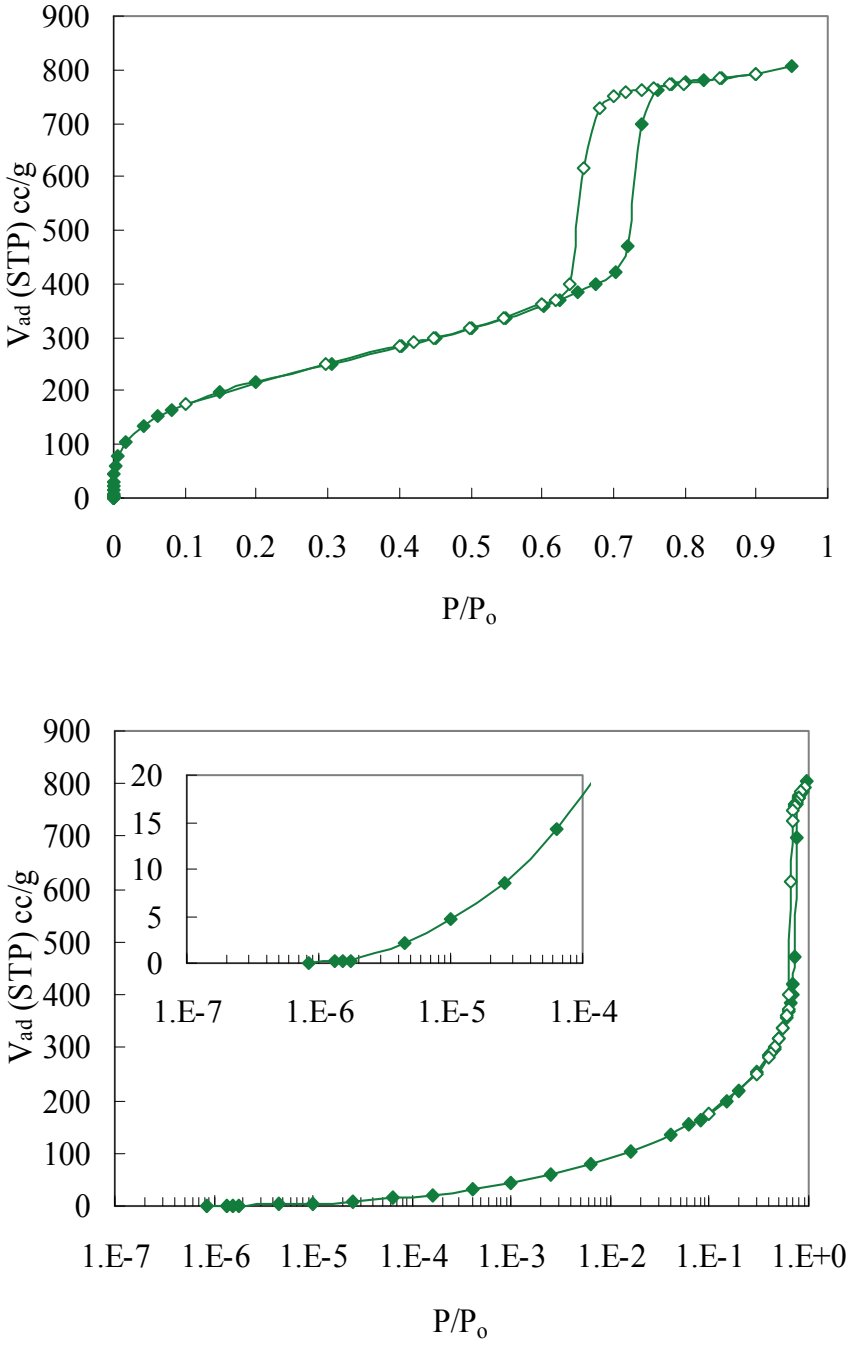

Figure 36 Argon adsorption at 87 K on MW-rHP in normal scale (Top) and logarithmic scale (Bottom)

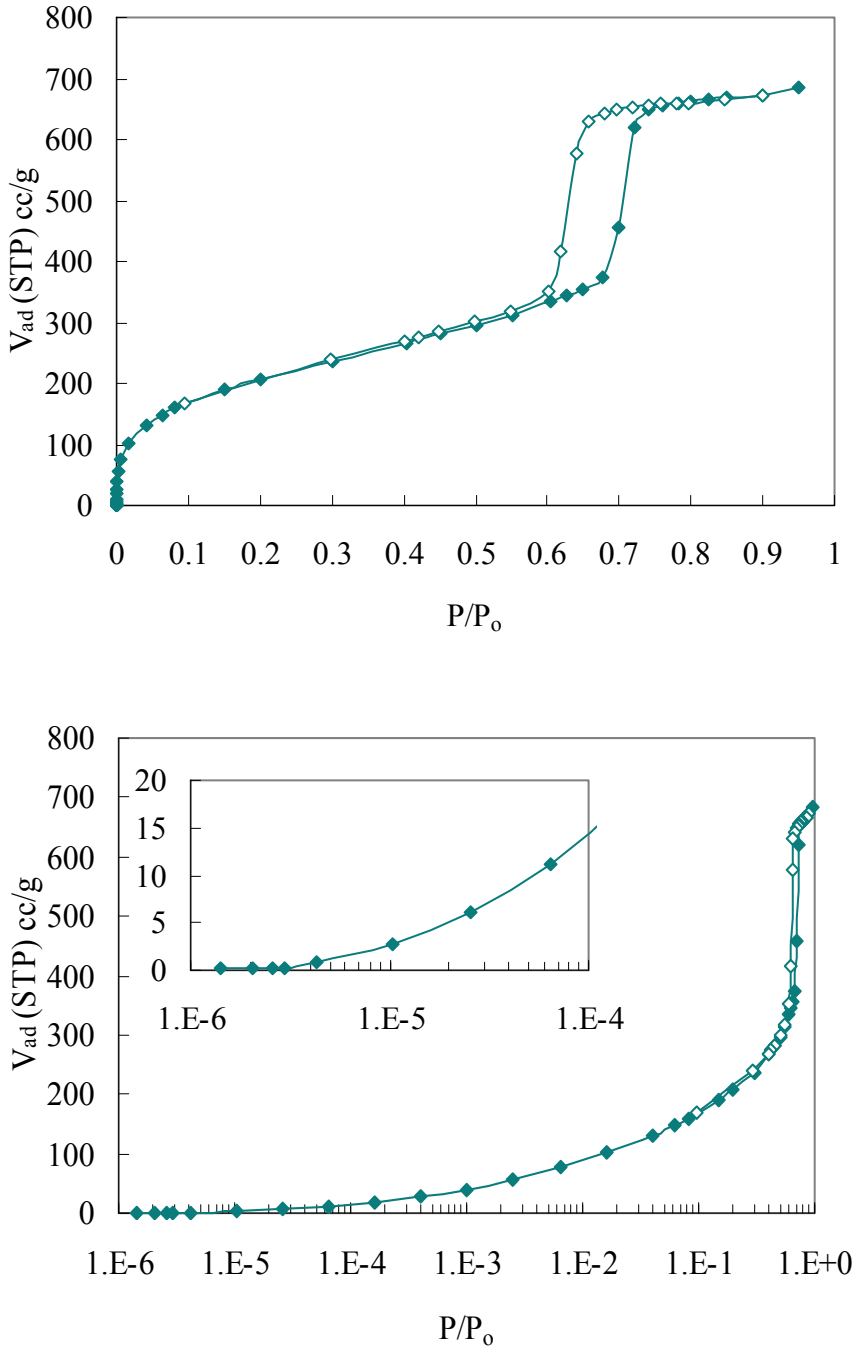

Figure 37 Argon adsorption at 87 K on MW-Rhp in normal scale (Top) and logarithmic scale (Bottom)

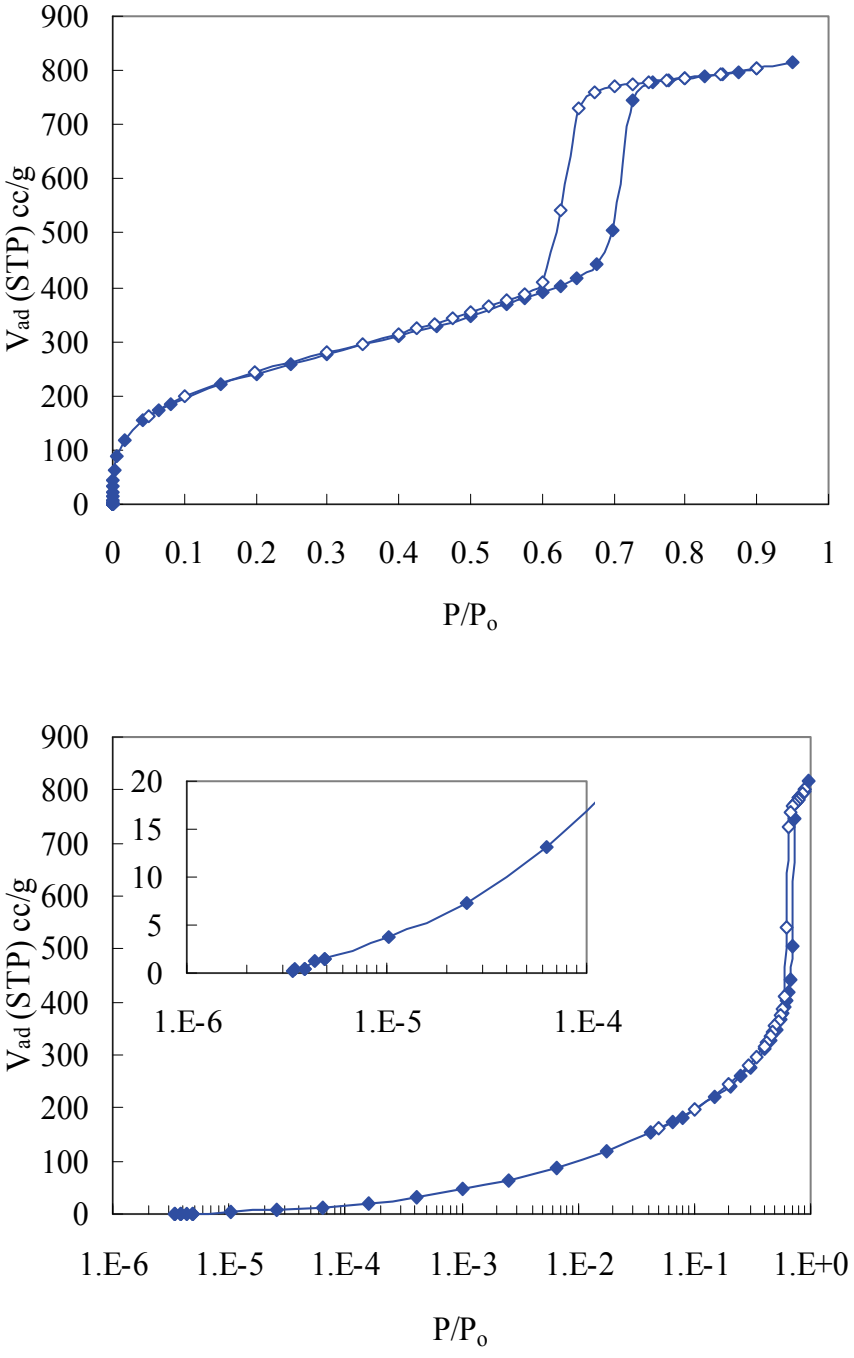

Figure 38 Argon adsorption at 87 K on MW-rHp in normal scale (Top) and logarithmic scale (Bottom)

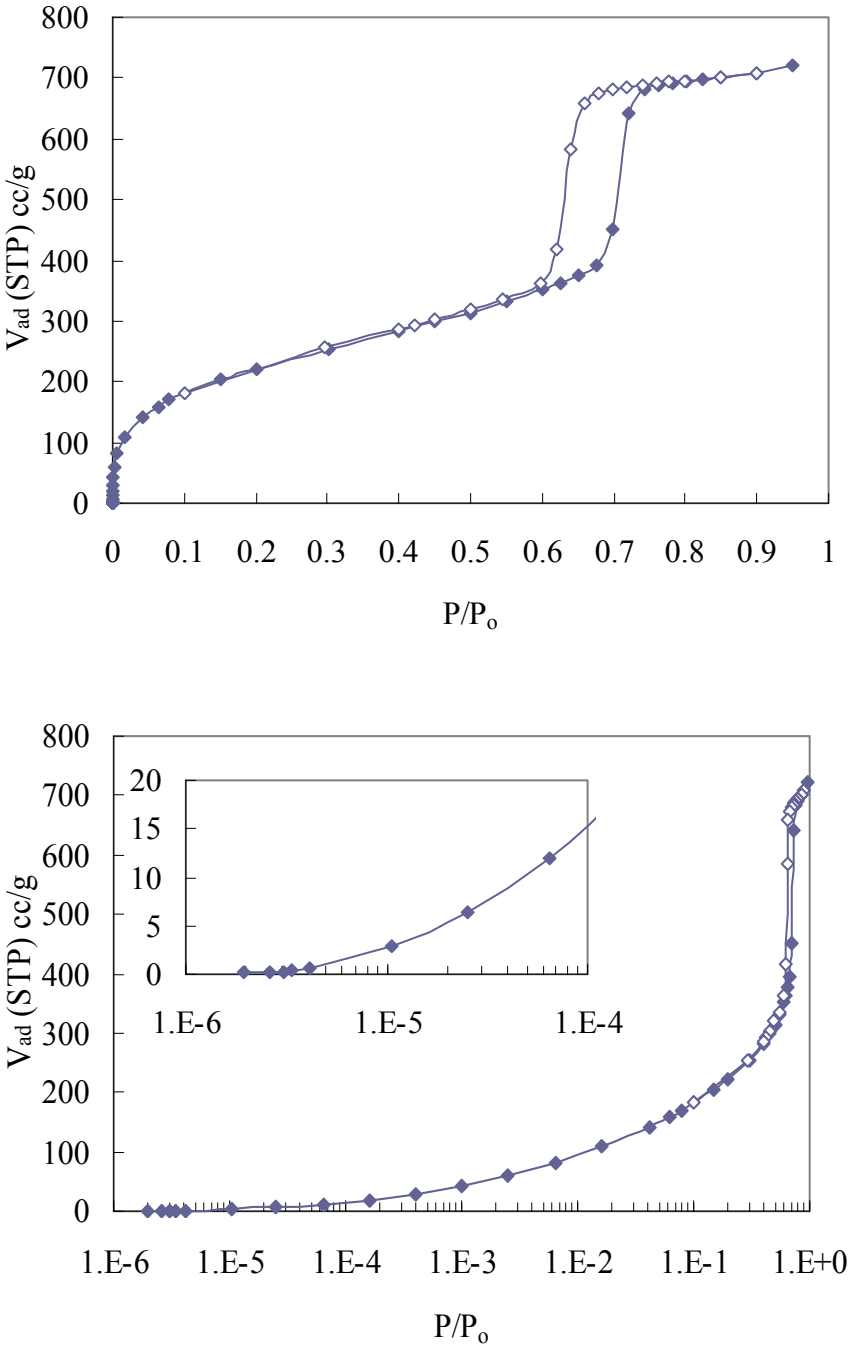

Figure 39 Argon adsorption at 87 K on MW-rhP in normal scale (Top) and logarithmic scale (Bottom)

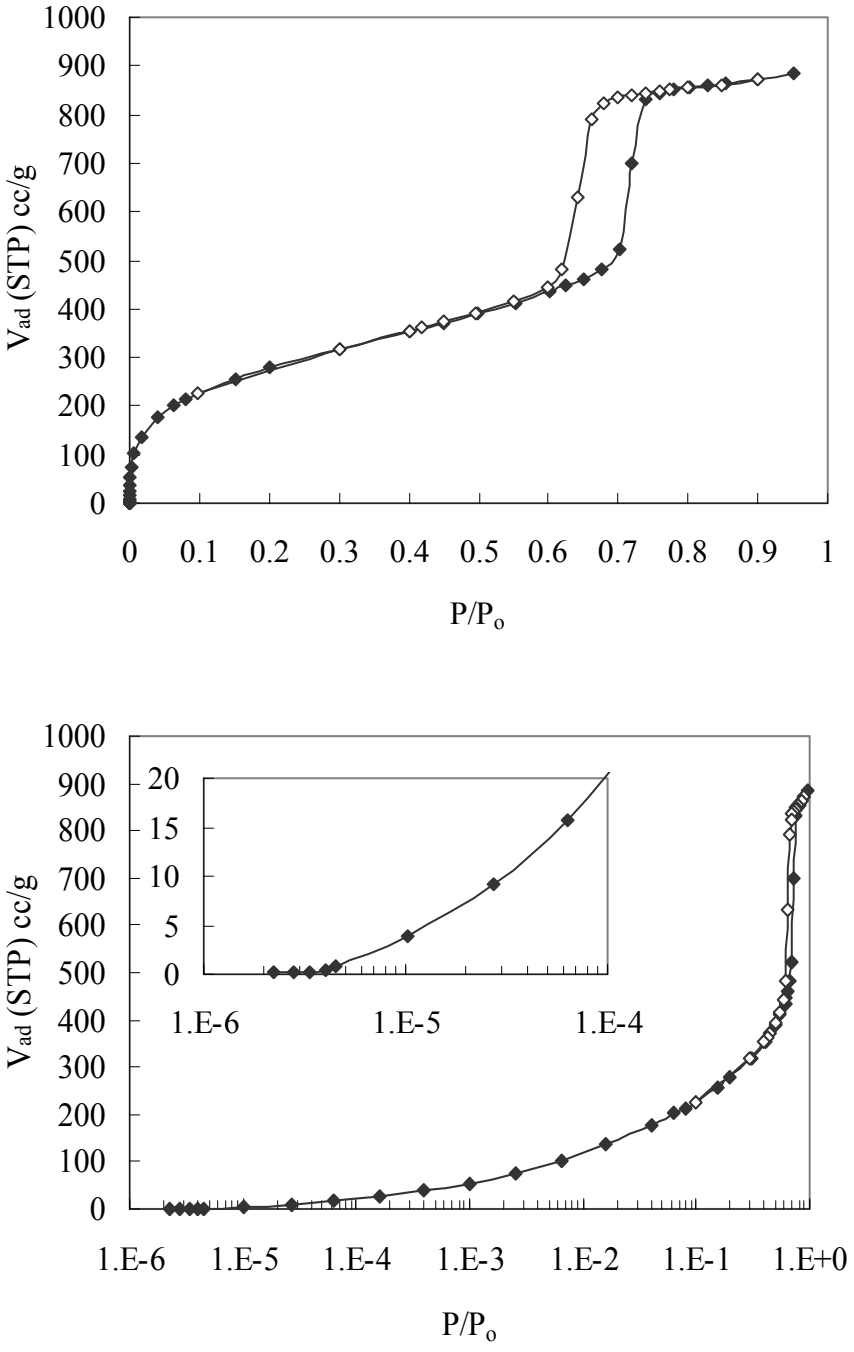

Figure 40 Argon adsorption at 87 K on MW-RHP in normal scale (Top) and logarithmic scale (Bottom)

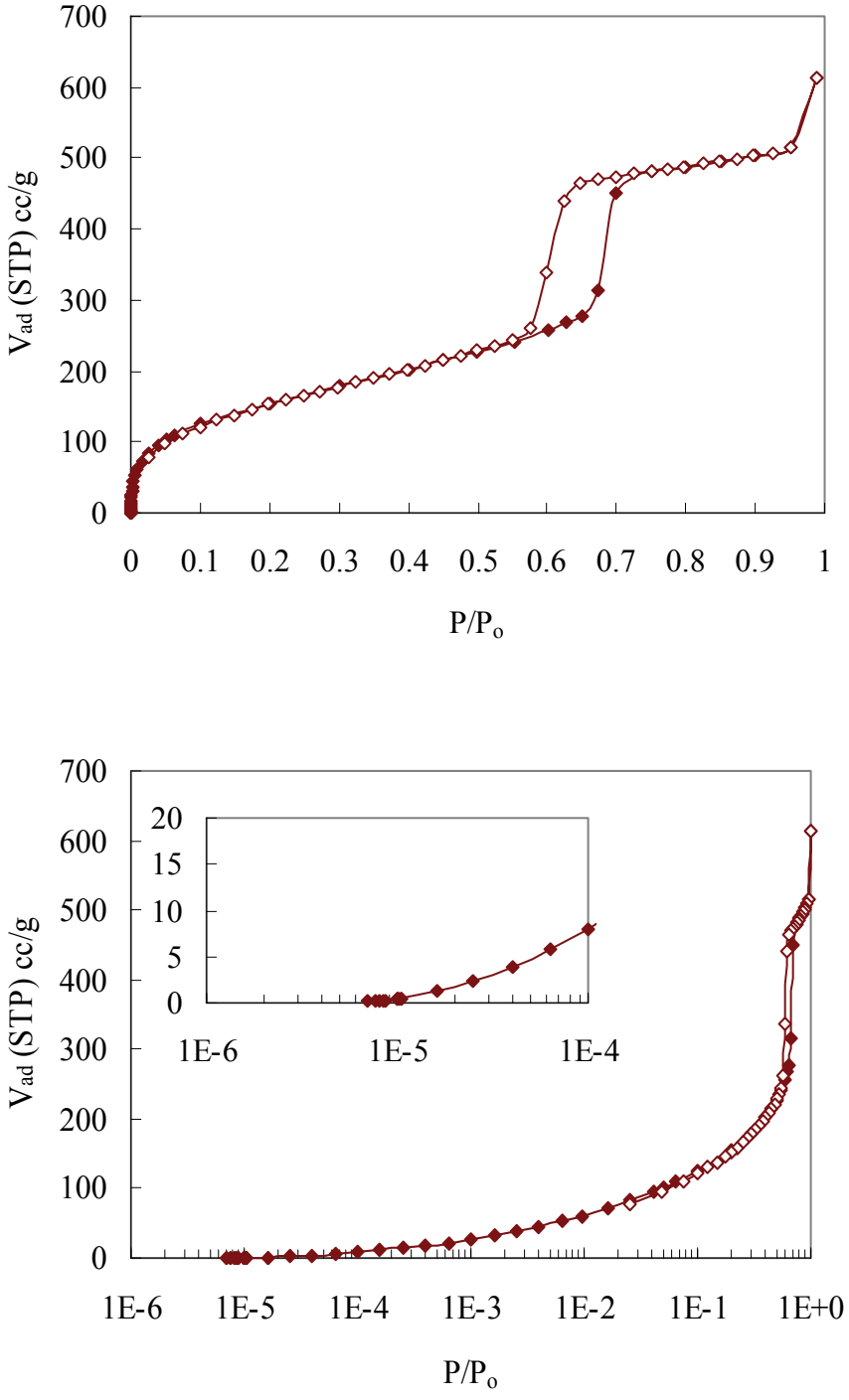

Figure 41 Argon adsorption at 87 K on C24M2 in normal scale (Top) and logarithmic scale (Bottom)

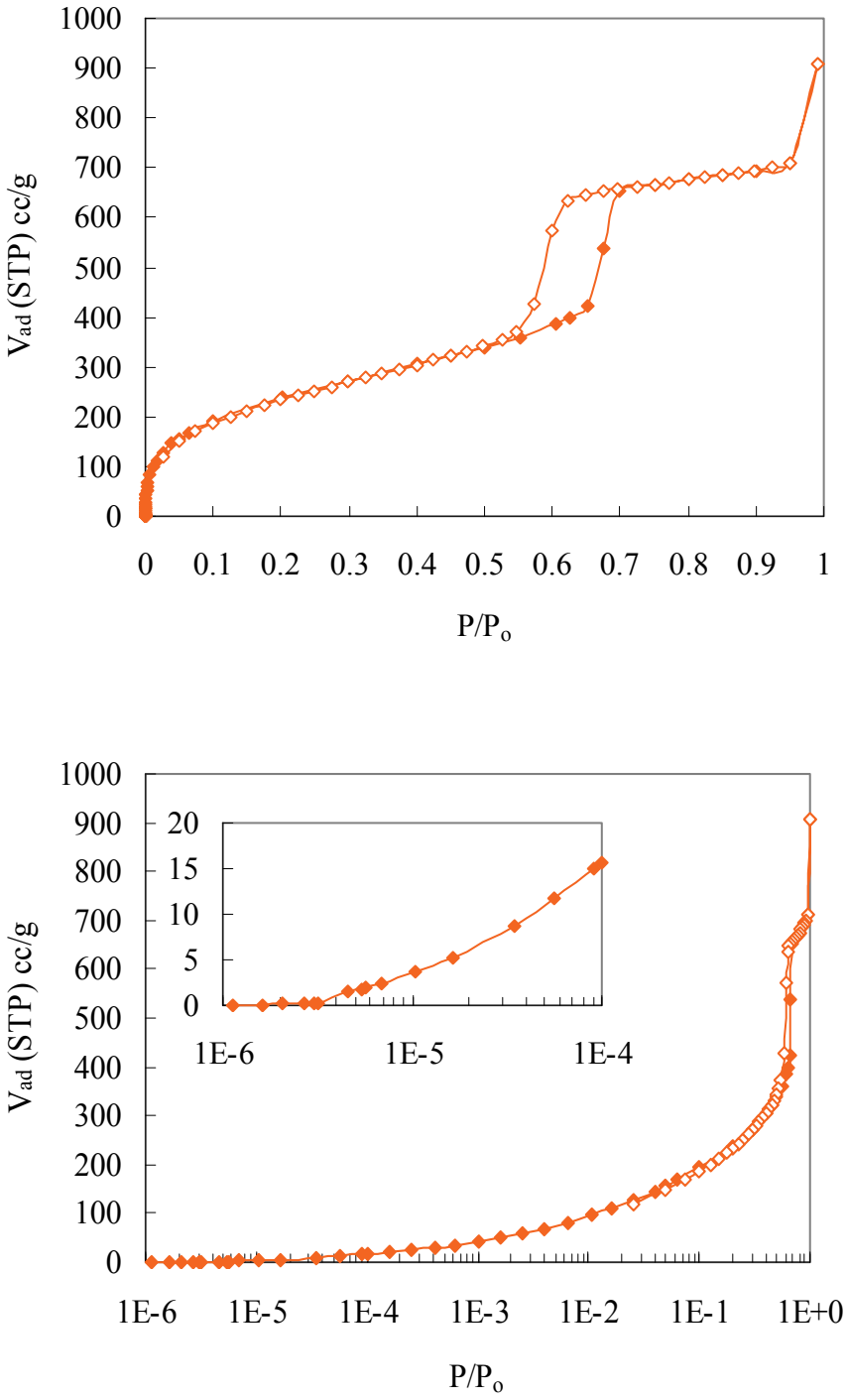

Figure 42 Argon adsorption at 87 K on C24C2 in normal scale (Top) and logarithmic scale (Bottom)

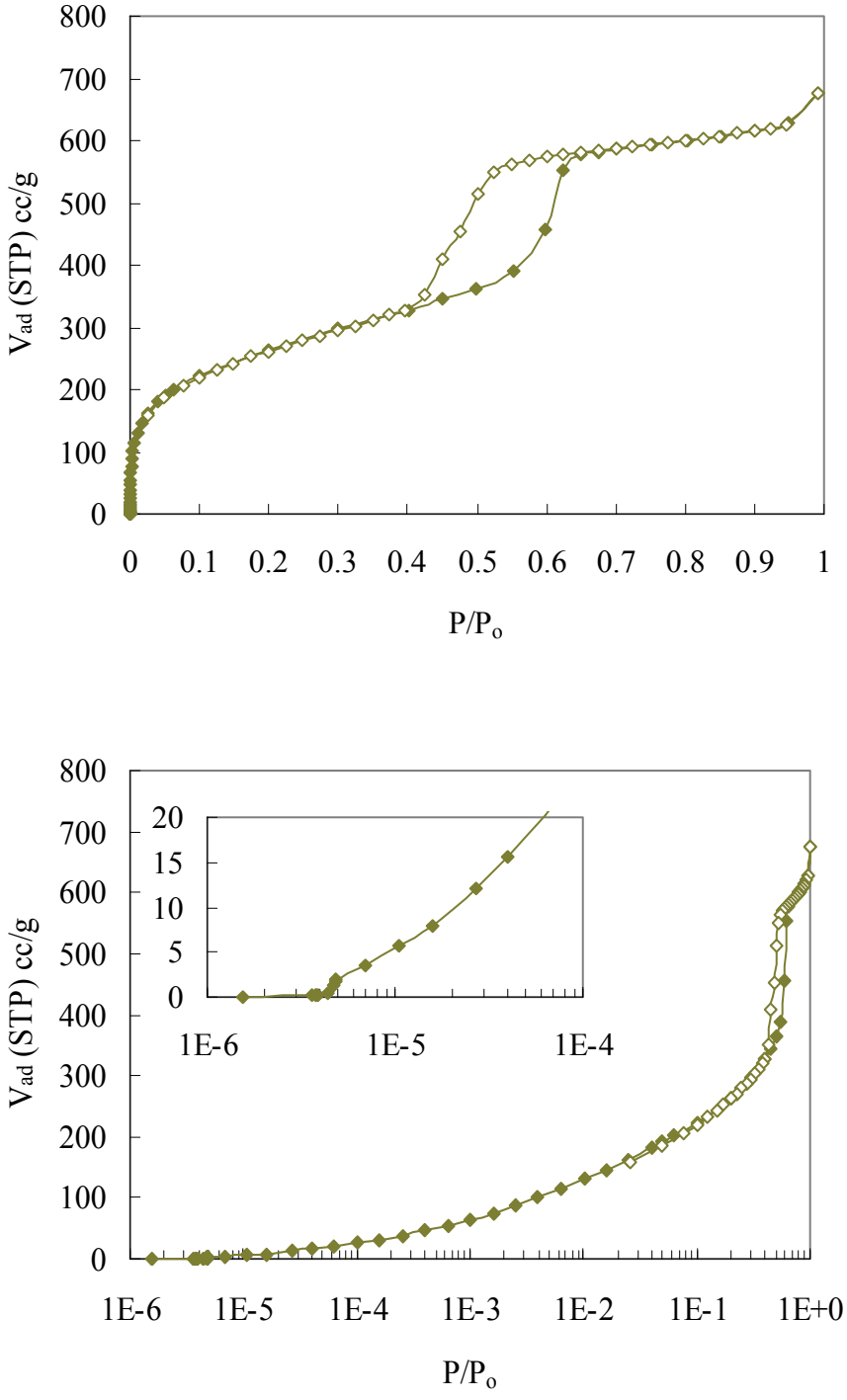

Figure 43 Argon adsorption at 87 K on C24 in normal scale (Top) and logarithmic scale (Bottom)

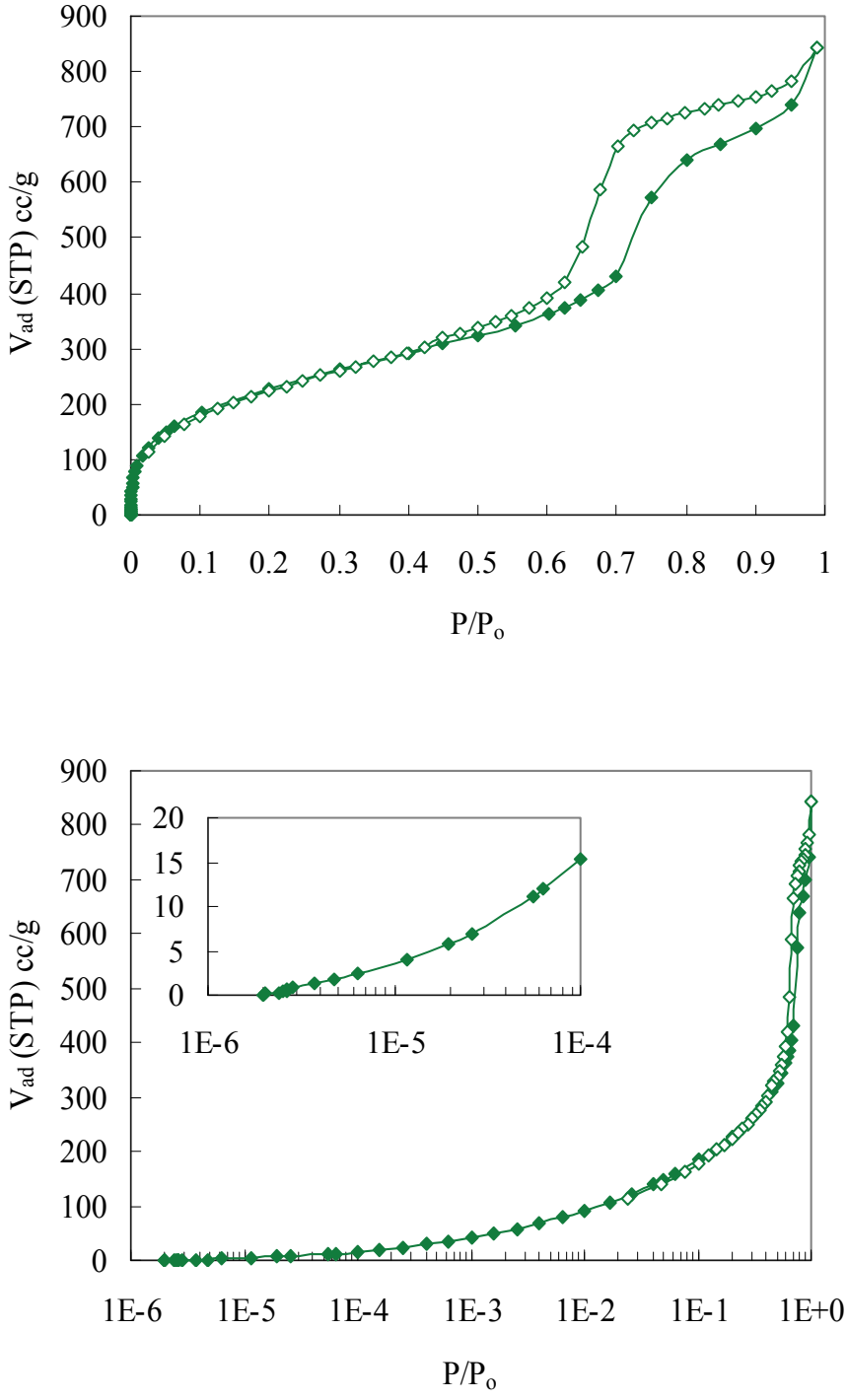

Figure 44 Argon adsorption at 87 K on M2M2 in normal scale (Top) and logarithmic scale (Bottom)

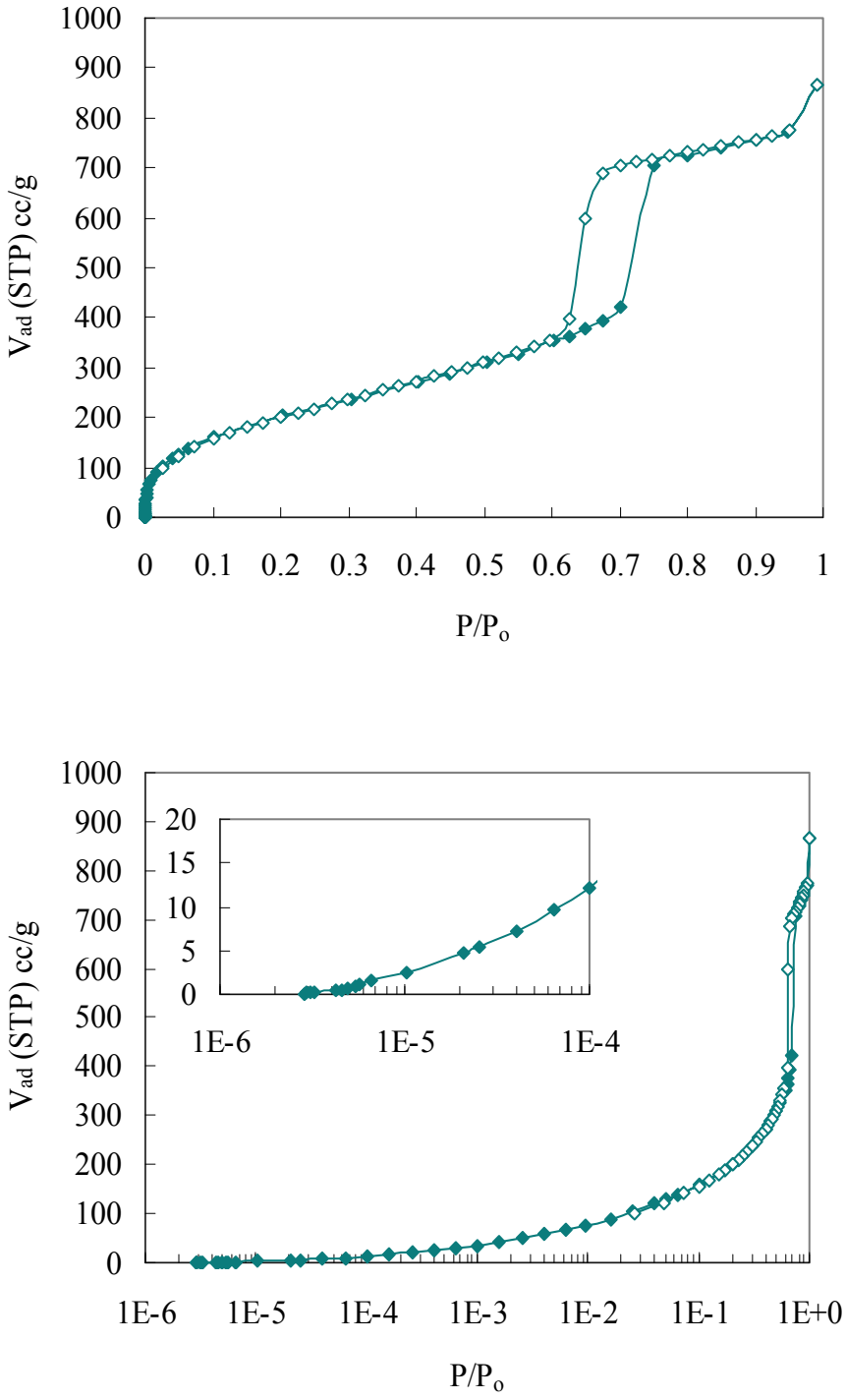

Figure 45 Argon adsorption at 87 K on C2M2 in normal scale (Top) and logarithmic scale (Bottom)

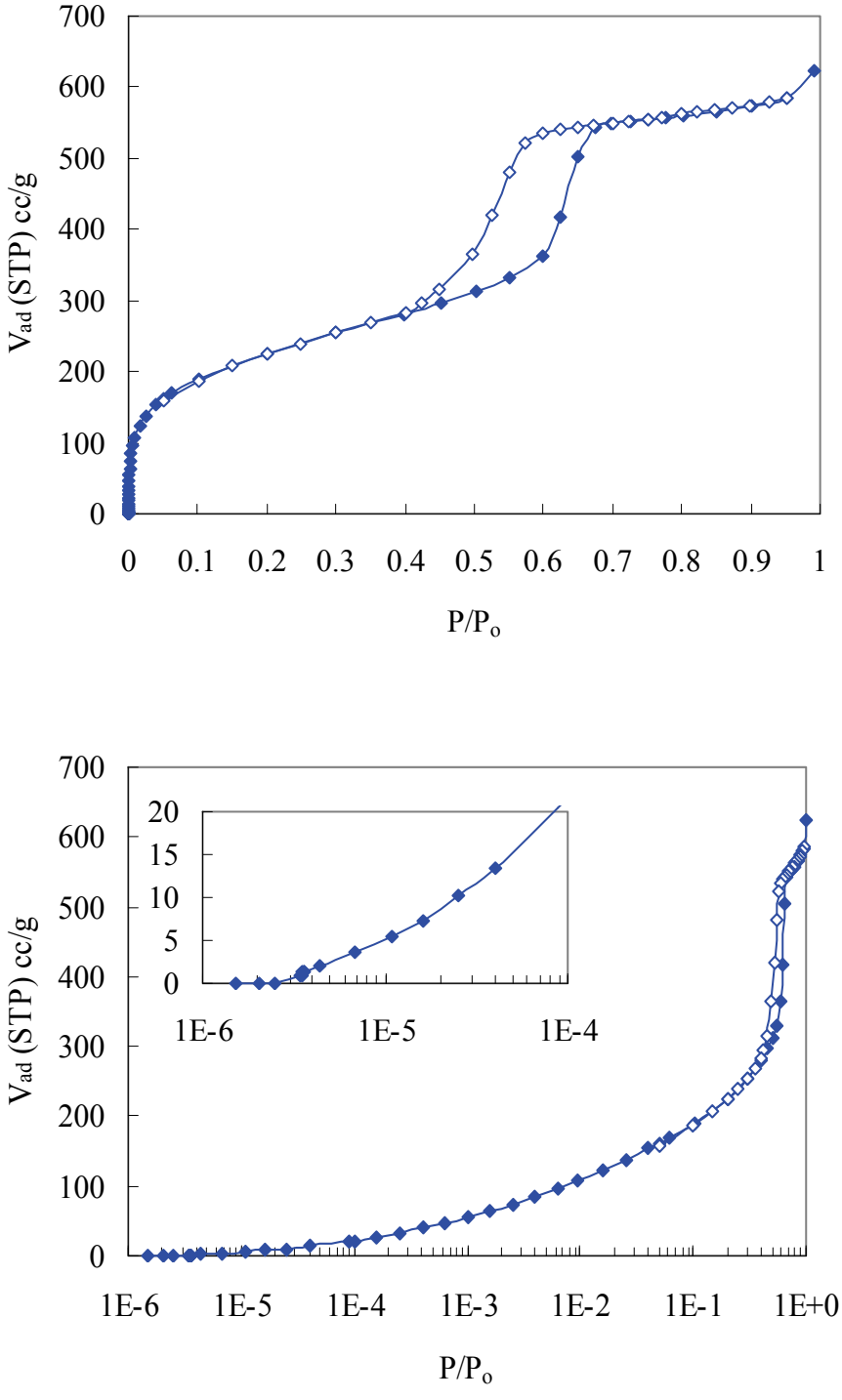

Figure 46 Argon adsorption at 87 K on C2 in normal scale (Top) and logarithmic scale (Bottom)

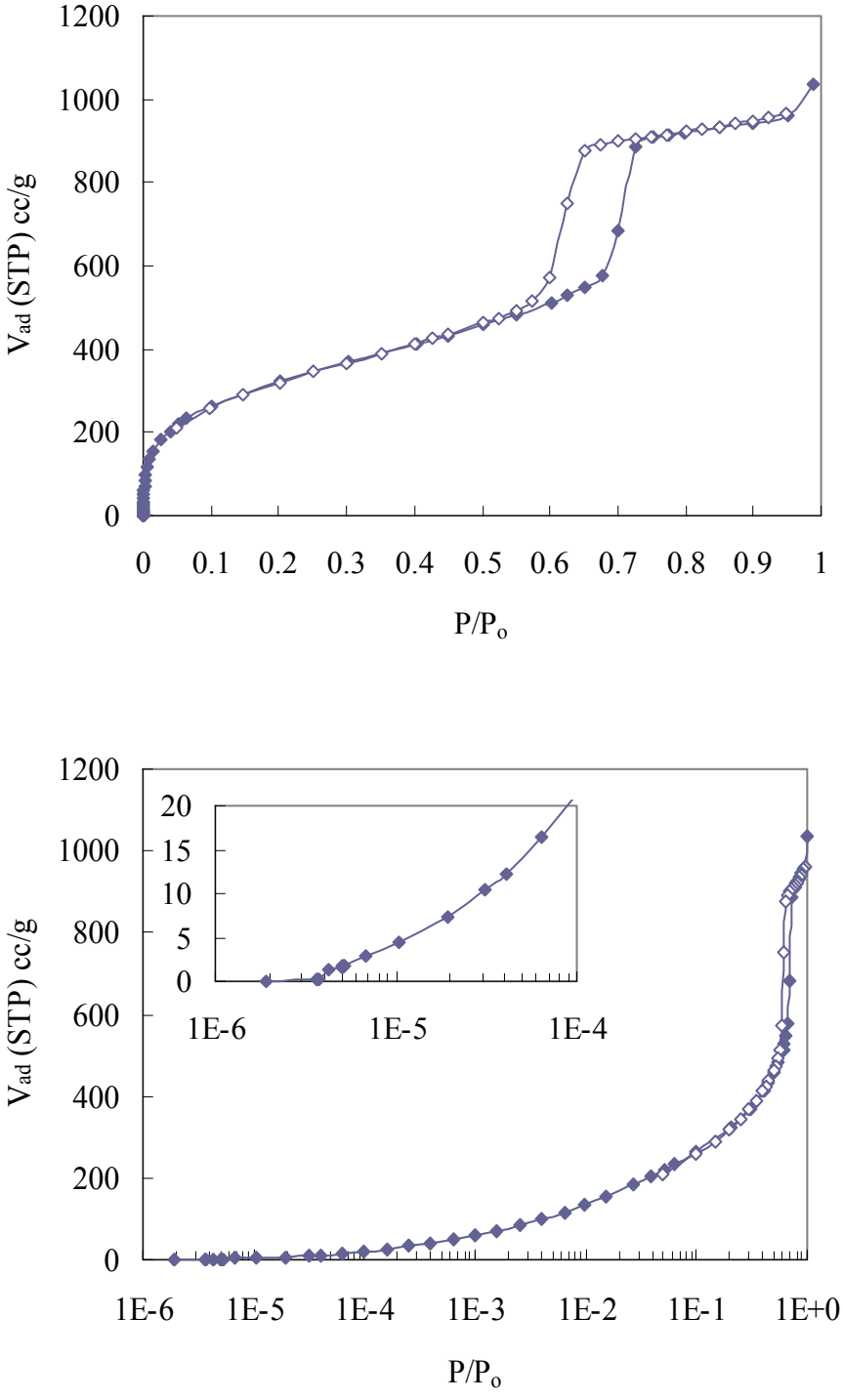

Figure 47 Argon adsorption at 87 K on C2C2 in normal scale (Top) and logarithmic scale (Bottom)

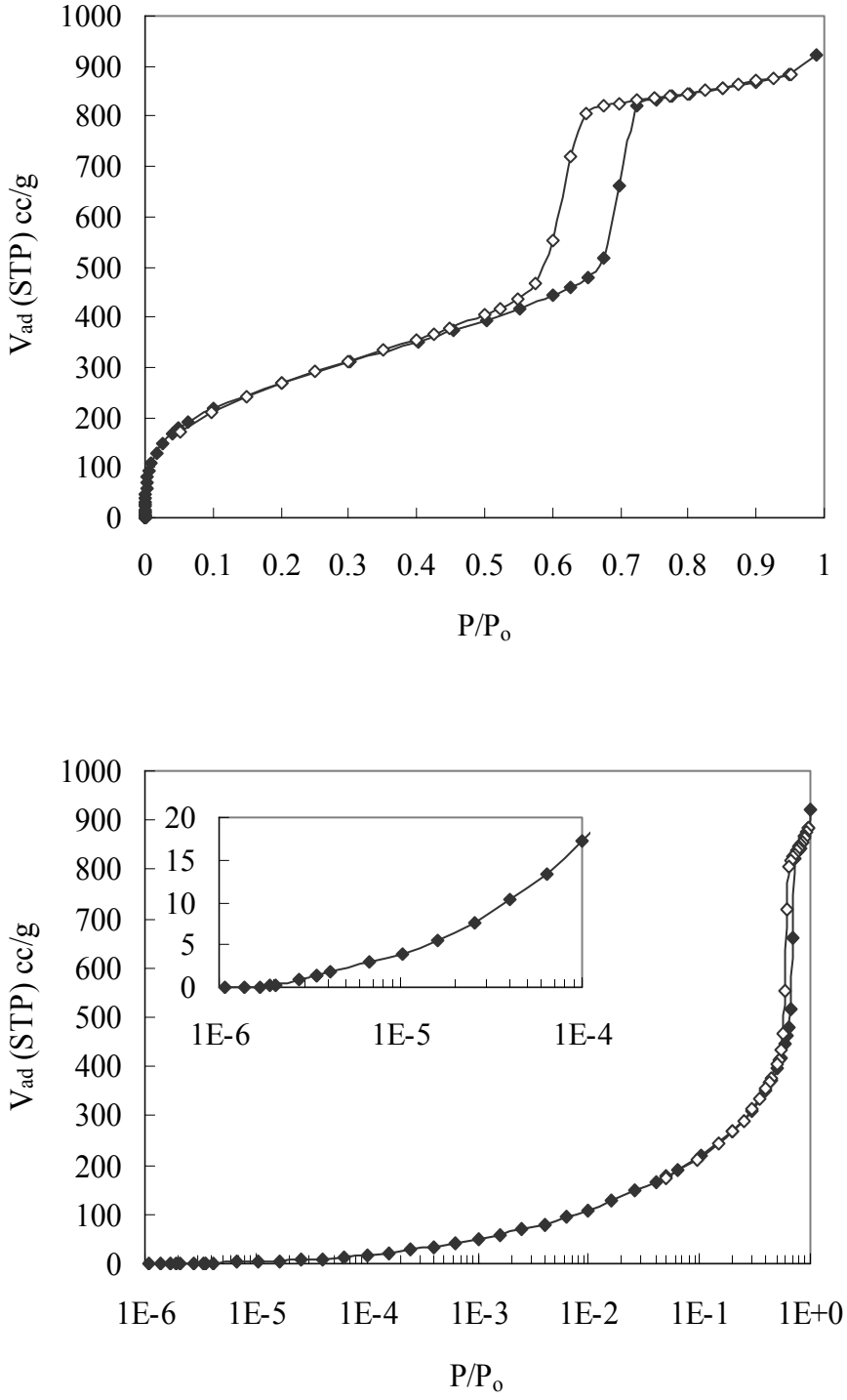

Figure 48 Argon adsorption at 87 K on C2m2 in normal scale (Top) and logarithmic scale (Bottom)

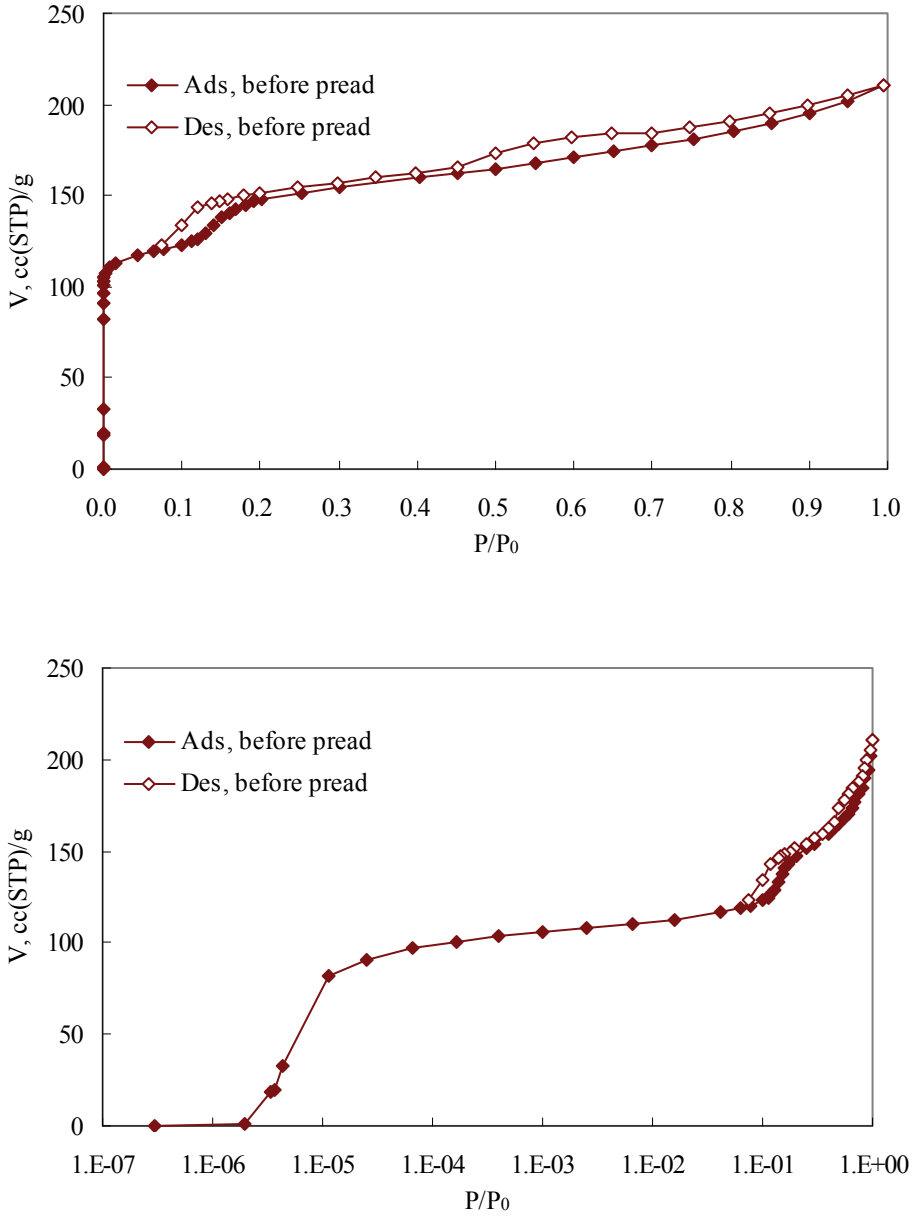

Figure 49 Nitrogen adsorption at 77 K on commercial silicalite before *n*-nonane preadsorption in normal scale (Top) and logarithmic scale (Bottom)

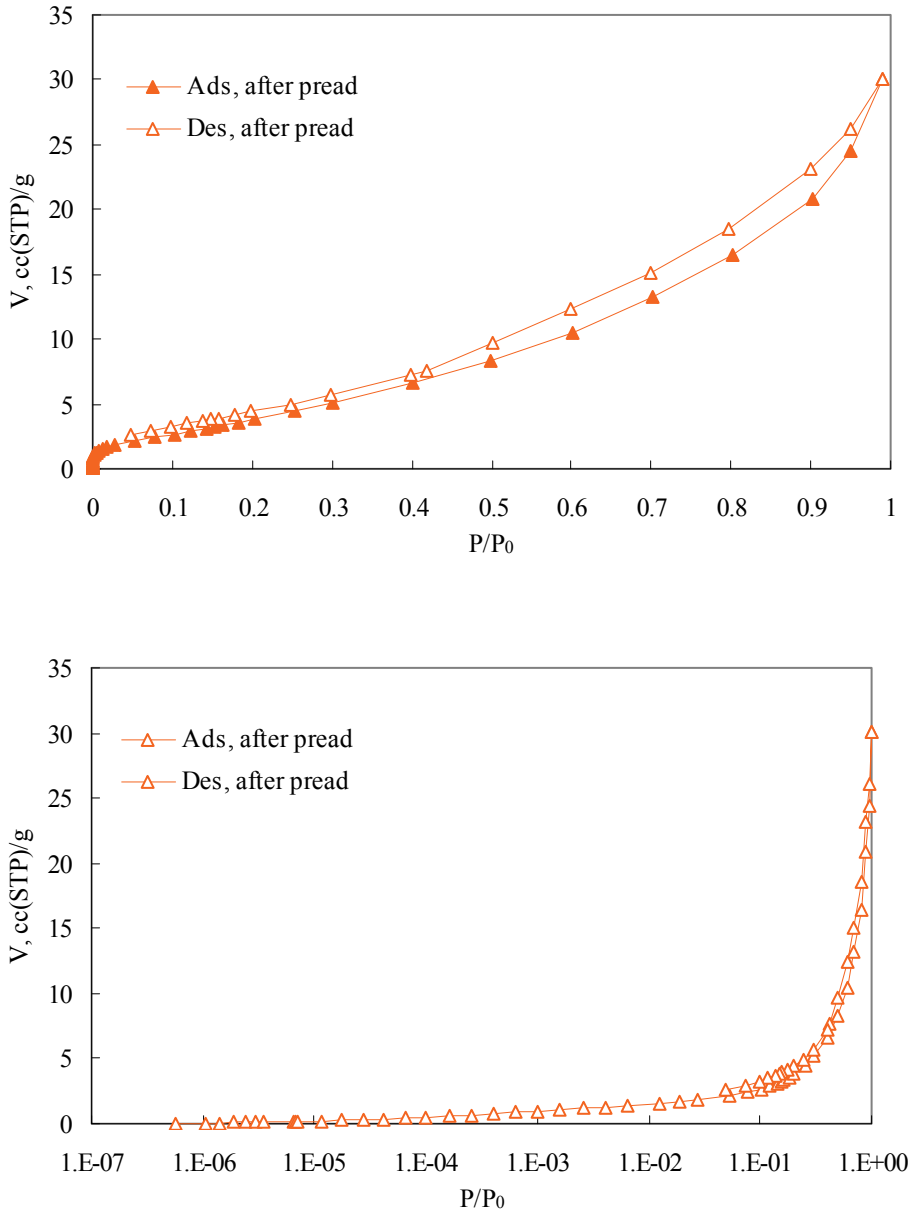

Figure 50 Nitrogen adsorption at 77 K on commercial silicalite after *n*-nonane preadsorption in normal scale (Top) and logarithmic scale (Bottom)

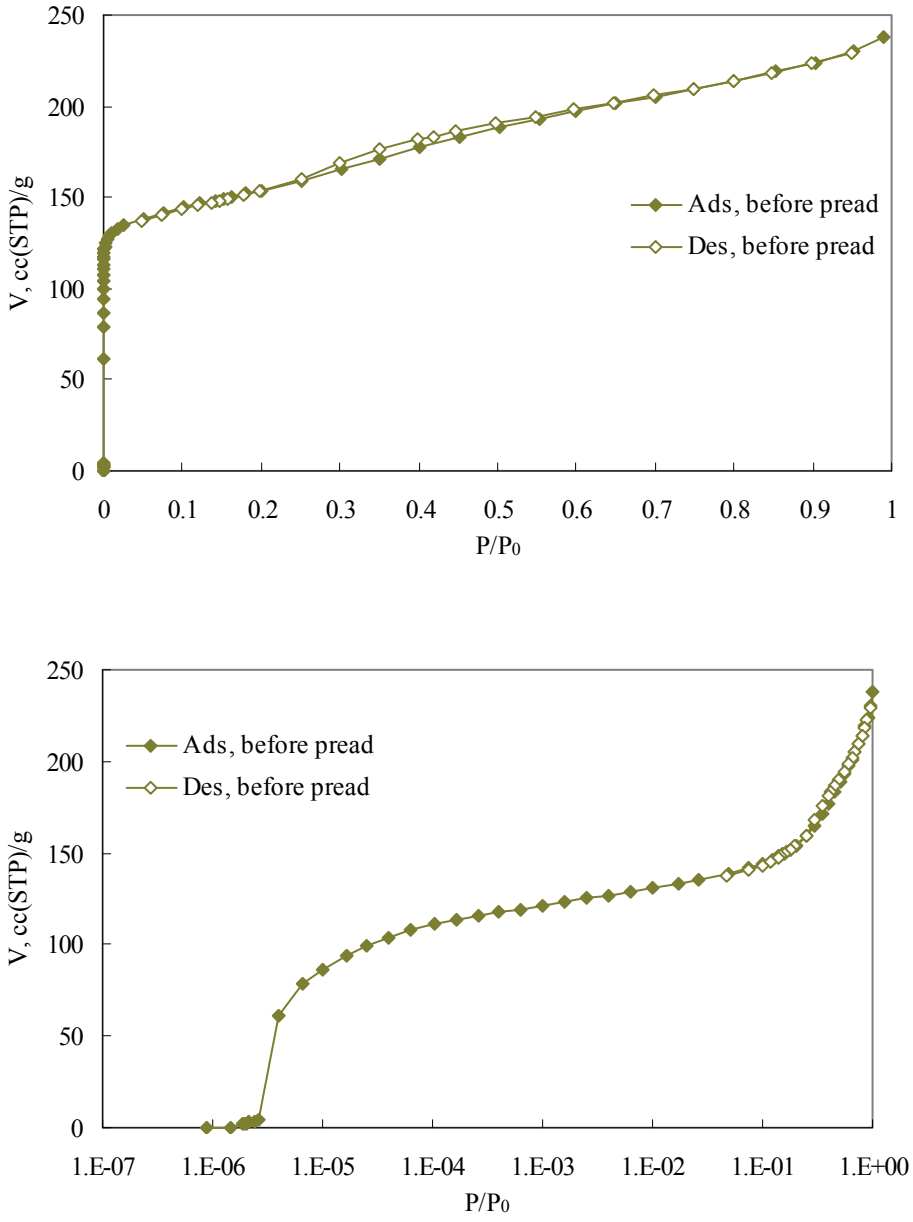

Figure 51 Nitrogen adsorption at 77 K on microwave synthesized silicalite before *n*-nonane preadsorption in normal scale (Top) and logarithmic scale (Bottom)

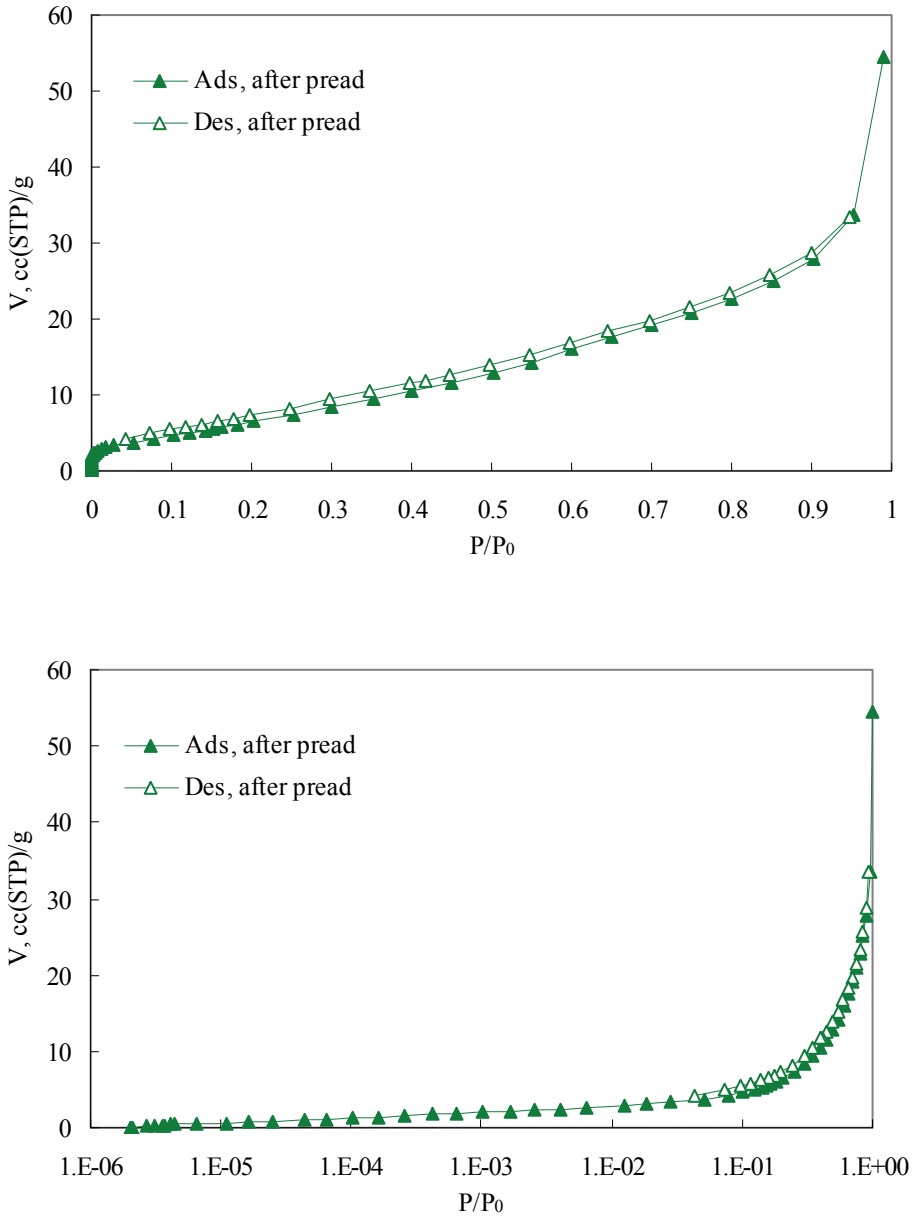

Figure 52 Nitrogen adsorption at 77 K on microwave synthesized silicalite after *n*-nonane preadsorption in normal scale (Top) and logarithmic scale (Bottom)

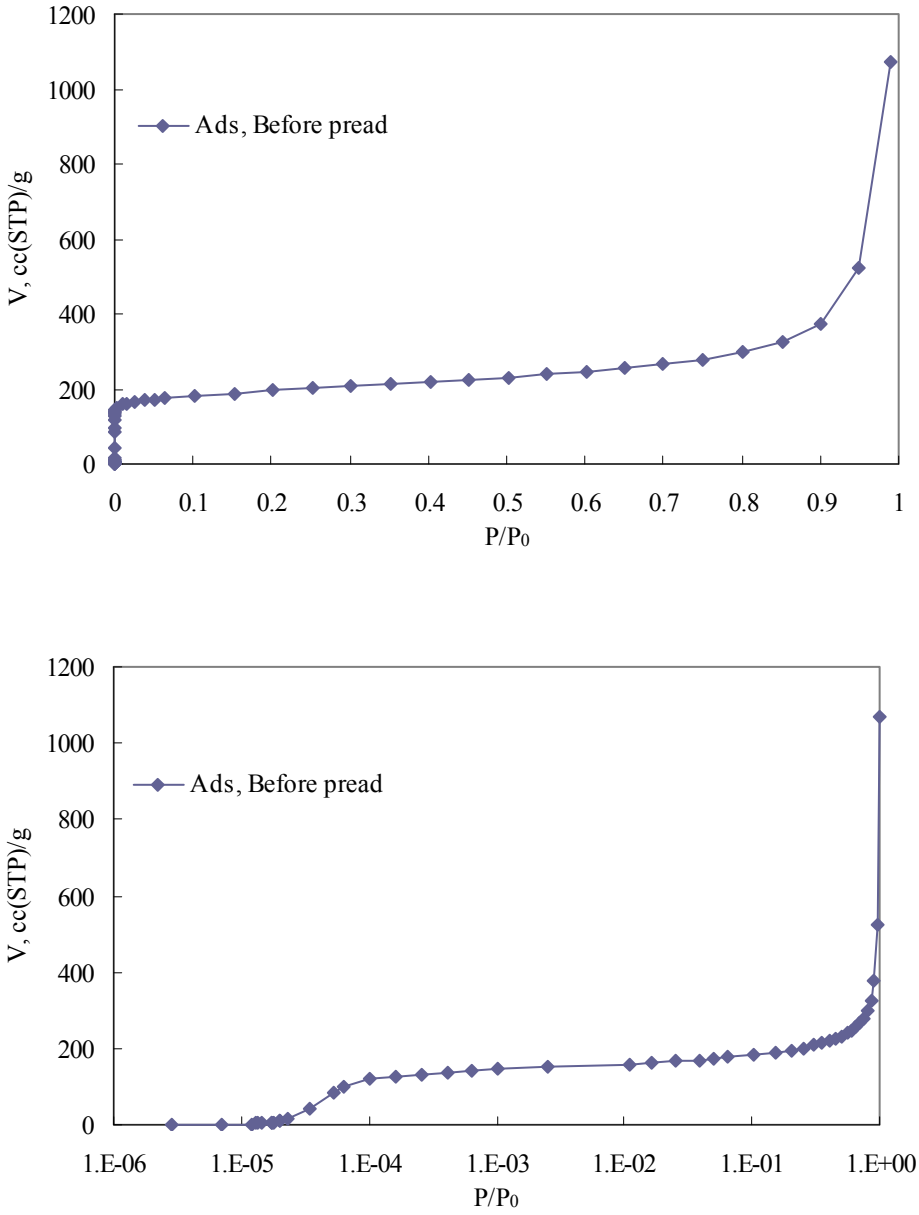

Figure 53 Argon adsorption at 87 K on VET before *n*-nonane preadsorption in normal scale (Top) and logarithmic scale (Bottom)

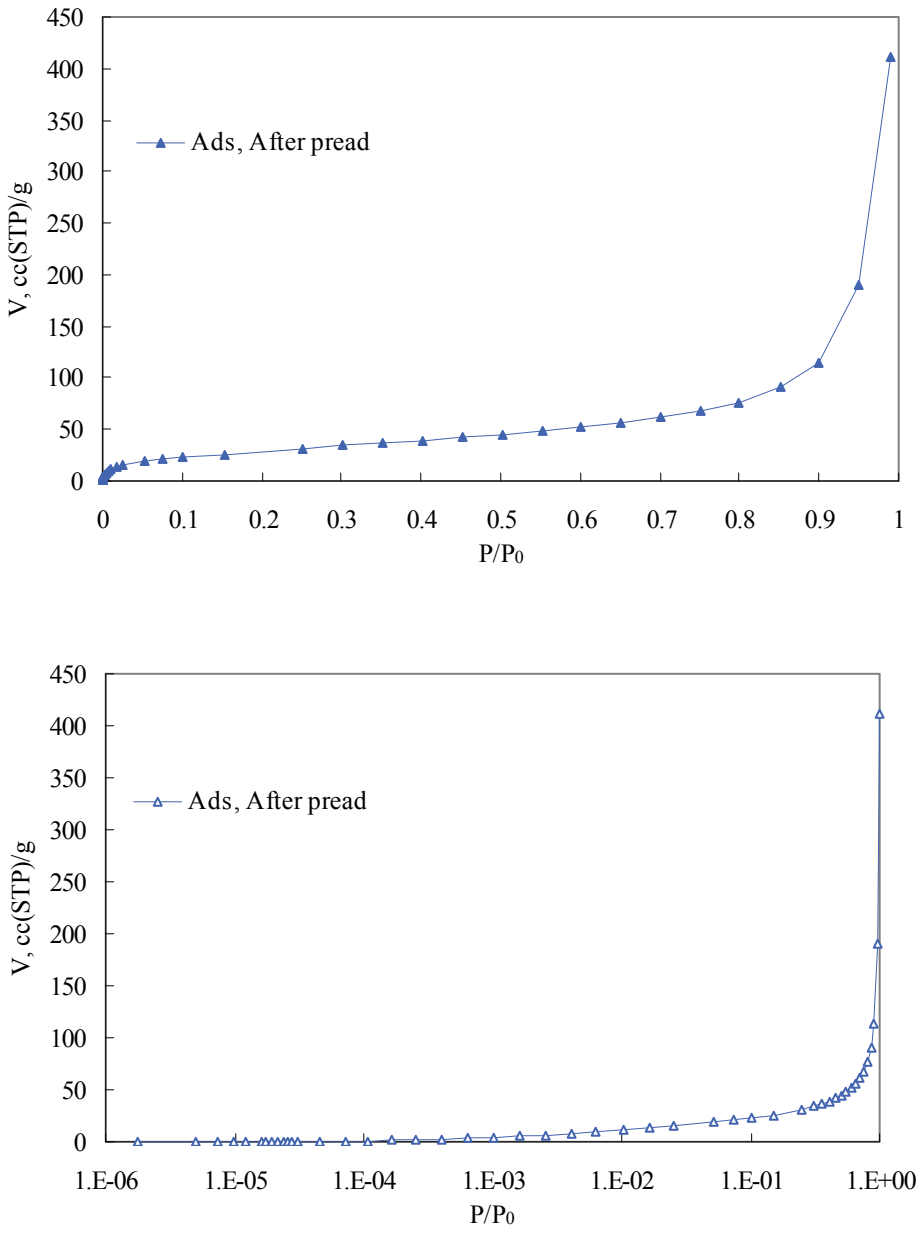

Figure 54 Argon adsorption at 87 K on VET after *n*-nonane preadsorption in normal scale (Top) and logarithmic scale (Bottom)

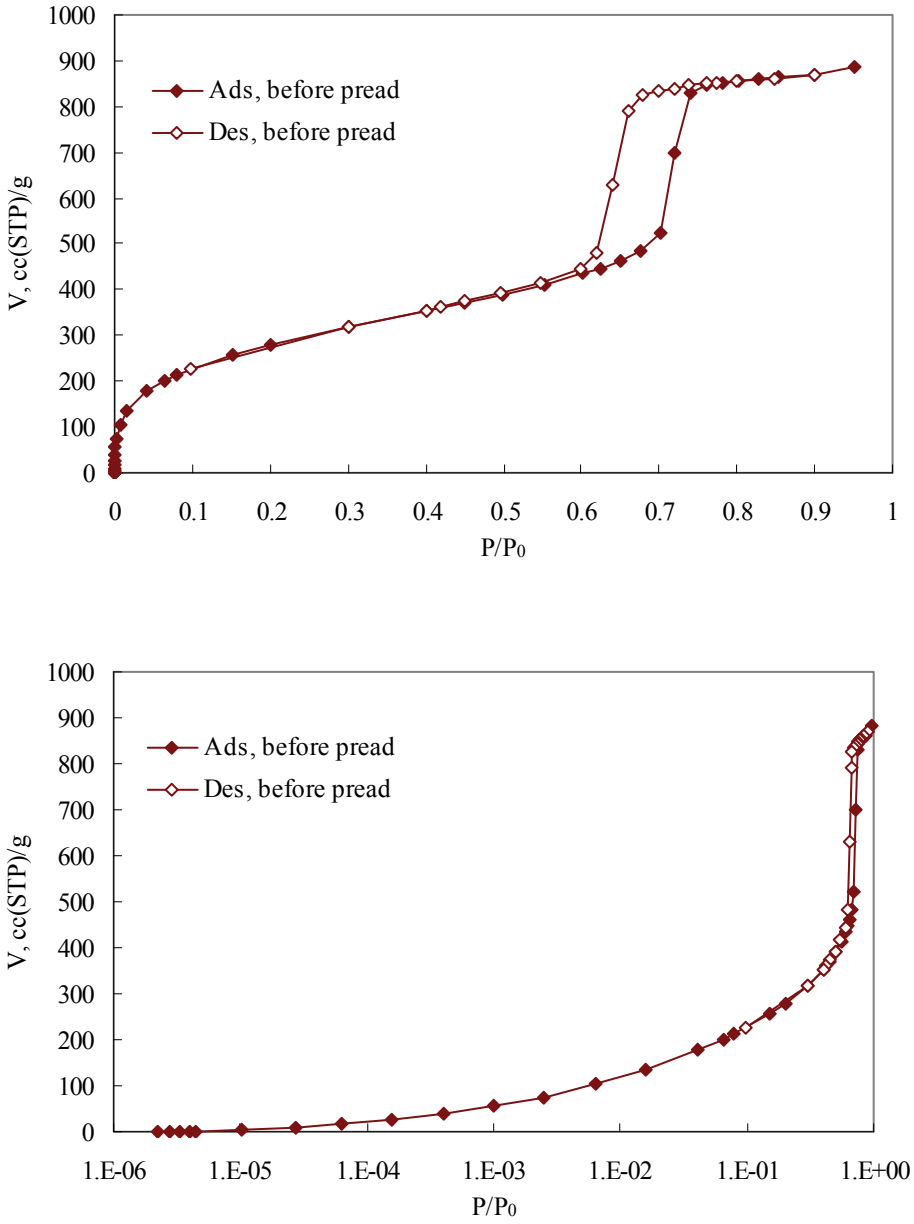

Figure 55 Argon adsorption at 87 K on MW-RHP before *n*-nonane preadsorption in normal scale (Top) and logarithmic scale (Bottom)

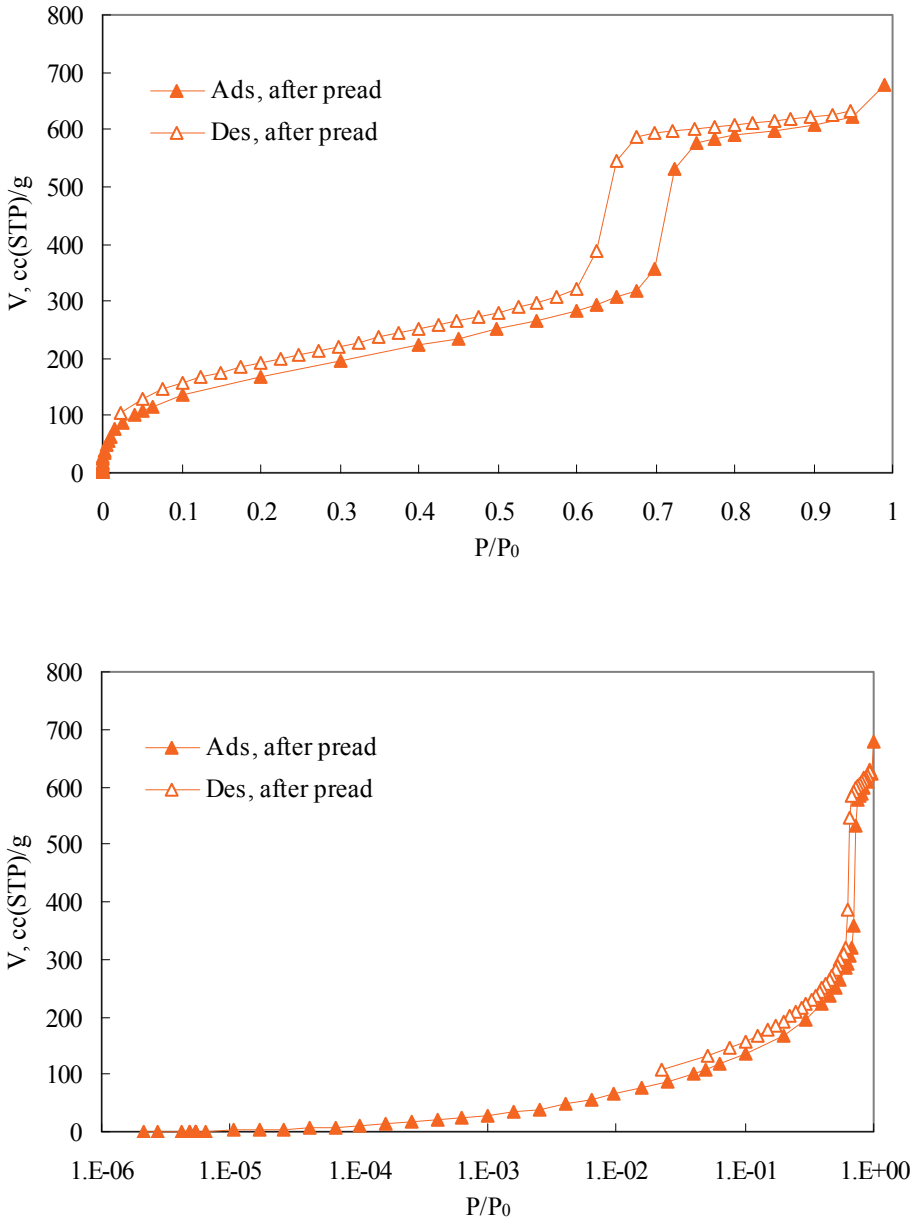

Figure 56 Argon adsorption at 87 K on MW-RHP after *n*-nonane preadsorption in normal scale (Top) and logarithmic scale (Bottom)

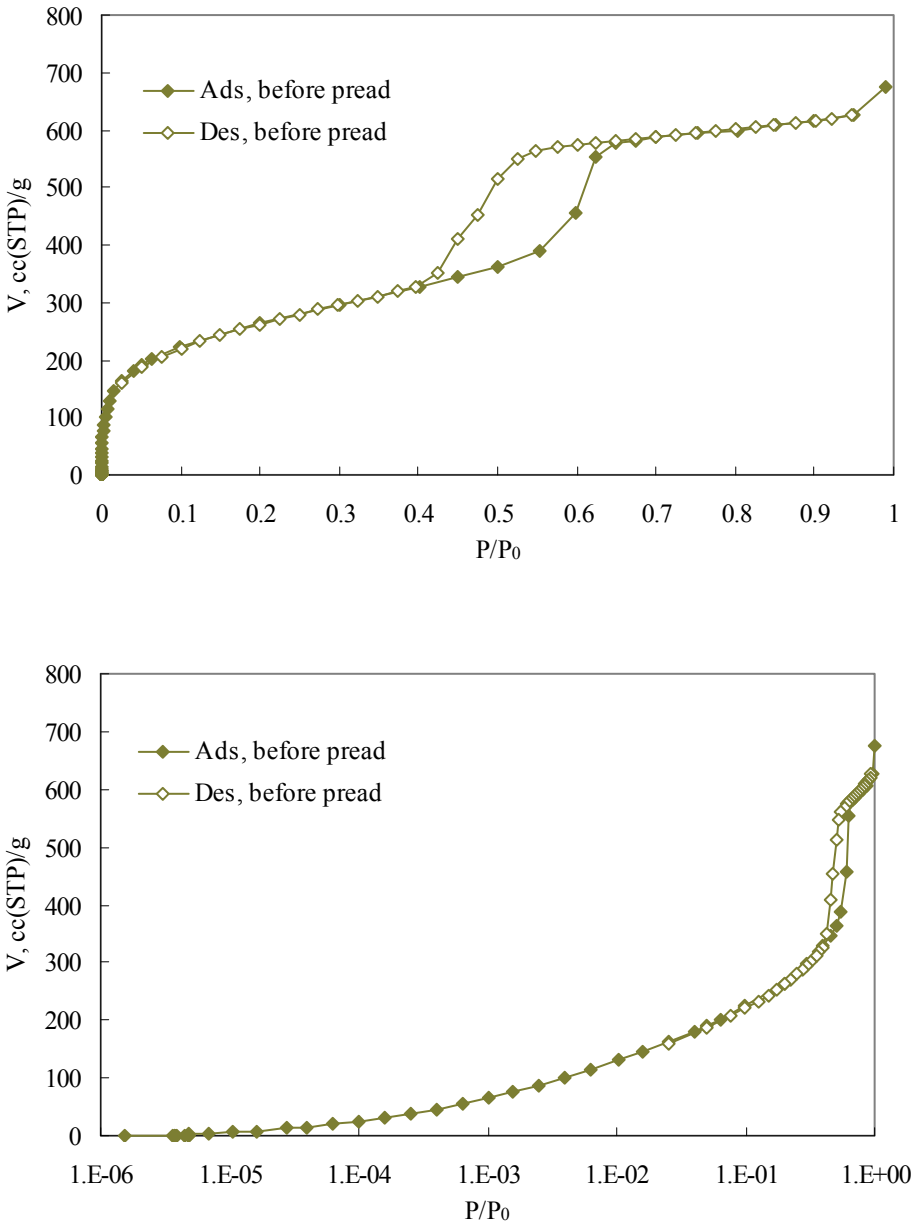

Figure 57 Argon adsorption at 87 K on C24 before *n*-nonane preadsorption in normal scale (Top) and logarithmic scale (Bottom)

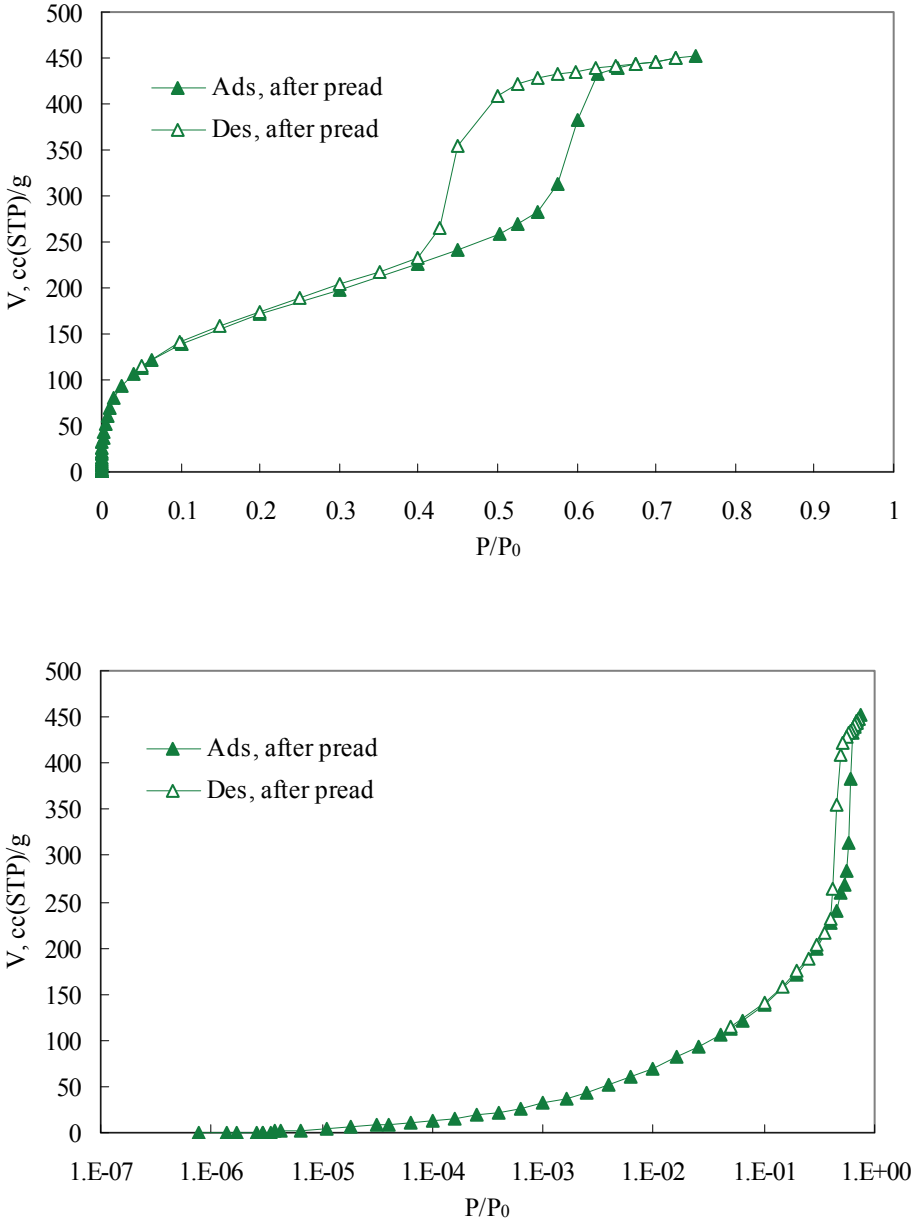

Figure 58 Argon adsorption at 87 K on C24 after *n*-nonane preadsorption in normal scale (Top) and logarithmic scale (Bottom)

BIBLIOGRAPHY

1. Dubinin, M. M., The potential theory of adsorption of gases and vapors for adsorbents with energetically nonuniform surfaces. *Chemical Reviews (Washington, DC, United States)* **1960,** 60, 235-41.

2. Anonymous, IUPAC Manual of Symbols and Terminology, Appendix 2, Pt.1,Colloid and Surface Chemistry. *Pure Applied Chemistry* **1972,** 31, 578.

3. Yanagisawa, T.; Shimizu, T.; Kuroda, K.; Kato, C., The preparation of alkyltrimethylammonium-kanemite complexes and their conversion to microporous materials. *Bulletin of the Chemical Society of Japan* **1990,** 63, (4), 988-92.

4. Beck, J. S.; Vartuli, J. C.; Roth, W. J.; Leonowicz, M. E.; Kresge, C. T.; Schmitt, K. D.; Chu, C. T. W.; Olson, D. H.; Sheppard, E. W.; et al., A new family of mesoporous molecular sieves prepared with liquid crystal templates. *Journal of the American Chemical Society* **1992,** 114, (27), 10834-43.

5. Kresge, C. T.; Leonowicz, M. E.; Roth, W. J.; Vartuli, J. C.; Beck, J. S., Ordered mesoporous molecular sieves synthesized by a liquid-crystal template mechanism. *Nature (London, United Kingdom)* **1992,** 359, (6397), 710-12.

6. Beck, J. S.; Vartuli, J. C., Recent advances in the synthesis, characterization and applications of mesoporous molecular sieves. *Current Opinion in Solid State & Materials Science* **1996,** 1, (1), 76-87.

7. Beck, J. S.; Calabro, D. C.; McCullen, S. B.; Pelrine, B. P.; Schmitt, K. D.; Vartuli, J. C. Method for functionalizing synthetic mesoporous crystalline material. 91-718056 5145816, 19910620., 1992.

8. Zhao, D.; Feng, J.; Huo, Q.; Melosh, N.; Frederickson, G. H.; Chmelka, B. F.; Stucky, G. D., Triblock copolymer syntheses of mesoporous silica with periodic 50 to 300 angstrom pores. *Science (Washington, D. C.)* **1998,** 279, (5350), 548-552.

9. Zhao, D.; Huo, Q.; Feng, J.; Chmelka, B. F.; Stucky, G. D., Nonionic triblock and star diblock copolymer and oligomeric surfactant syntheses of highly ordered, hydrothermally stable, mesoporous silica structures. *Journal of the American Chemical Society* **1998,** 120, (24), 6024-6036.

10. Ryoo, R.; Ko, C. H.; Kruk, M.; Antochshuk, V.; Jaroniec, M., Block-Copolymer-Templated Ordered Mesoporous Silica: Array of Uniform Mesopores or Mesopore-Micropore Network? *Journal of Physical Chemistry B* **2000,** 104, (48), 11465-11471.

11. Imperor-Clerc, M.; Davidson, P.; Davidson, A., Existence of a microporous corona around the mesopores of silica-based SBA-15 materials templated by triblock copolymers. *Journal of the American Chemical Society* **2000,** 122, (48), 11925-11933.

12. Van Grieken, R.; Calleja, G.; Stucky, G. D.; Melero, J. A.; Garcia, R. A.; Iglesias, J., Supercritical Fluid Extraction of a Nonionic Surfactant Template from SBA-15 Materials and Consequences on the Porous Structure. *Langmuir* **2003,** 19, (9), 3966-3973.

13. Tian, B.; Liu, X.; Yu, C.; Gao, F.; Luo, Q.; Xie, S.; Tu, B.; Zhao, D., Microwave assisted template removal of siliceous porous materials. *Chemical Communications (Cambridge, United Kingdom)* **2002**, (11), 1186-1187.

14. Khodakov, A. Y.; Zholobenko, V. L.; Imperor-Clerc, M.; Durand, D., Characterization of the Initial Stages of SBA-15 Synthesis by in Situ Time-Resolved Small-Angle X-ray Scattering. *Journal of Physical Chemistry B* **2005,** 109, (48), 22780-22790.

15. Alfredsson, V.; Amenitsch, H.; Flodström, K.; Linden, M.; Teixeira, C. V.; Wennerstroem, H., In-situ studies of the formation mechanism of SBA-15. *Studies in Surface Science and Catalysis* **2005,** 156, (Nanoporous Materials IV), 69-74.

16. Flodström, K.; Teixeira, C. V.; Amenitsch, H.; Alfredsson, V.; Linden, M., In Situ Synchrotron Small-Angle X-ray Scattering/X-ray Diffraction Study of the Formation of SBA-15 Mesoporous Silica. *Langmuir* **2004,** 20, (12), 4885-4891.

17. Flodström, K.; Wennerstroem, H.; Alfredsson, V., Mechanism of Mesoporous Silica Formation. A Time-Resolved NMR and TEM Study of Silica-Block Copolymer Aggregation. *Langmuir* **2004,** 20, (3), 680-688.

18. Ruthstein, S.; Frydman, V.; Kababya, S.; Landau, M.; Goldfarb, D., Study of the Formation of the Mesoporous Material SBA-15 by EPR Spectroscopy. *Journal of Physical Chemistry B* **2003,** 107, (8), 1739-1748.

19. Fulvio, P. F.; Pikus, S.; Jaroniec, M., Short-time synthesis of SBA-15 using various silica sources. *Journal of Colloid and Interface Science* **2005,** 287, (2), 717-720.

20. Fulvio, P. F.; Pikus, S.; Jaroniec, M., Tailoring properties of SBA-15 materials by controlling conditions of hydrothermal synthesis. *Journal of Materials Chemistry* **2005,** 15, (47), 5049-5053.

21. Choi, M.; Heo, W.; Kleitz, F.; Ryoo, R., Facile synthesis of high quality mesoporous SBA-15 with enhanced control of the porous network connectivity and wall thickness. *Chemical Communications (Cambridge, United Kingdom)* **2003**, (12), 1340-1341.

22. Galarneau, A.; Cambon, H.; Di Renzo, F.; Ryoo, R.; Choi, M.; Fajula, F., Microporosity and connections between pores in SBA-15 mesostructured silicas as a function of the temperature of synthesis. *New Journal of Chemistry* **2003,** 27, (1), 73-79.

23. Kruk, M.; Jaroniec, M.; Ko, C. H.; Ryoo, R., Characterization of the Porous Structure of SBA-15. *Chemistry of Materials* **2000,** 12, (7), 1961-1968.

24. Ravikovitch, P. I.; Neimark, A. V., Characterization of Micro- and Mesoporosity in SBA-15 Materials from Adsorption Data by the NLDFT Method. *Journal of Physical Chemistry B* **2001,** 105, (29), 6817-6823.

25. Hung, S.-C.; Lin, H.-P.; Mou, C.-Y., One-step synthesis of mesoporous silica SBA-15 with ultra-high microporosity. *Studies in Surface Science and Catalysis* **2003,** 146, (Nanotechnology in Mesostructured Materials), 105-108.

26. Newalkar, B. L.; Komarneni, S., Simplified synthesis of micropore-free mesoporous silica, SBA-15, under microwave-hydrothermal conditions. *Chemical Communications (Cambridge, United Kingdom)* **2002**, (16), 1774-1775.

27. Kipkemboi, P.; Fogden, A.; Alfredsson, V.; Flodstroem, K., Triblock Copolymers as Templates in Mesoporous Silica Formation: Structural Dependence on Polymer Chain Length and Synthesis Temperature. *Langmuir* **2001,** 17, (17), 5398-5402.

28. Galarneau, A.; Cambon, H.; Di Renzo, F.; Fajula, F., True Microporosity and Surface Area of Mesoporous SBA-15 Silicas as a Function of Synthesis Temperature. *Langmuir* **2001,** 17, (26), 8328-8335.

29. Miyazawa, K.; Inagaki, S., Control of the microporosity within the pore walls of ordered mesoporous silica SBA-15. *Chemical Communications (Cambridge)* **2000**, (21), 2121-2122.

30. Jönsson, B.; Lindman, B.; Holmberg, K.; Kronberg, B., *Surfactants and Polymers in Aqueous Solution*. ed.; 1998; 'Vol.' p 438 pp.

31. Janssen, A. H.; Van Der Voort, P.; Koster, A. J.; de Jong, K. P., A 3D-TEM study of the shape of mesopores in SBA-15 and modified SBA-15 materials. *Chemical Communications (Cambridge, United Kingdom)* **2002**, (15), 1632-1633.

32. Van Der Voort, P.; Ravikovitch, P. I.; De Jong, K. P.; Benjelloun, M.; Van Bavel, E.; Janssen, A. H.; Neimark, A. V.; Weckhuysen, B. M.; Vansant, E. F., A New Templated Ordered Structure with Combined Micro- and Mesopores and Internal Silica Nanocapsules. *Journal of Physical Chemistry B* **2002,** 106, (23), 5873-5877.

33. Van Bavel, E.; Cool, P.; Aerts, K.; Vansant, E. F., Plugged Hexagonal Templated Silica (PHTS): An In-Depth Study of the Structural Characteristics. *Journal of Physical Chemistry B* **2004,** 108, (17), 5263-5268.

34. Sonwane, C. G.; Li, Q., Molecular Simulation of RMM: Ordered Mesoporous SBA-15 Type Material Having Microporous ZSM-5 Walls. *Journal of Physical Chemistry B* **2005,** 109, (38), 17993-17997.

35. Göltner, C. G.; Smarsly, B.; Berton, B.; Antonietti, M., On the Microporous Nature of Mesoporous Molecular Sieves. *Chemistry of Materials* **2001,** 13, (5), 1617-1624.

36. Jun, S.; Joo, S. H.; Ryoo, R.; Kruk, M.; Jaroniec, M.; Liu, Z.; Ohsuna, T.; Terasaki, O., Synthesis of New, Nanoporous Carbon with Hexagonally Ordered Mesostructure. *Journal of the American Chemical Society* **2000,** 122, (43), 10712-10713.

37. Gregg, S. J.; Sing, K. S. W., *Adsorption, Surface Area and Porosity*. 2nd ed.; 1982; 'Vol.' p 1~303.

38. Ravikovitch, P. I.; Vishnyakov, A.; Russo, R.; Neimark, A. V., Unified approach to pore size characterization of microporous carbonaceous materials from N2, Ar, and CO2 adsorption isotherms. *Langmuir* **2000,** 16, (5), 2311-2320.

39. Storck, S.; Bretinger, H.; Maier, W. F., Characterization of micro- and mesoporous solids by physisorption methods and pore-size analysis. *Applied Catalysis, A: General* **1998,** 174, (1-2), 137-146.

40. Venero, A. F.; Chiou, J. N., Characterization of zeolites by gas adsorption at low pressures. *Materials Research Society Symposium Proceedings* **1988,** 111, (Microstruct. Prop. Catal.), 235-40.

41. Brunauer, S.; Emmett, P. H.; Teller, E., Adsorption of gases in multimolecular layers. *Journal of the American Chemical Society* **1938,** 60, 309-19.

42. Horvath, G.; Kawazoe, K., Method for the calculation of effective pore size distribution in molecular sieve carbon. *Journal of Chemical Engineering of Japan* **1983,** 16, (6), 470-5.

43. Saito, A.; Foley, H. C., Curvature and parametric sensitivity in models for adsorption in micropores. *AIChE Journal* **1991,** 37, (3), 429-36.

44. Lippens, B. C.; de Boer, J. H., Pore systems in catalysts. V. The t-method. *Journal of Catalysis* **1965,** 4, (3), 319-23.

45. Lippens, B. C.; Linsen, B. G.; de Boer, J. H., Pore systems in catalysts. I. Adsorption of nitrogen; apparatus and calculation. *Journal of Catalysis* **1964,** 3, (1), 32-7.

46. Halsey, G., Physical adsorption on nonuniform surfaces. *Journal of Chemical Physics* **1948,** 16, 931-7.

47. Groen, J. C.; Peffer, L. A. A.; Perez-Ramirez, J., Pore size determination in modified micro- and mesoporous materials. Pitfalls and limitations in gas adsorption data analysis. *Microporous and Mesoporous Materials* **2003,** 60, (1-3), 1-17.

48. Everett, D. H., Capillary condensation. *Charact. Porous Solids, Proc. Symp.* **1979**, 229-51.

49. Liu, H.; Zhang, L.; Seaton, N. A., Analysis of sorption hysteresis in mesoporous solids using a pore network model. *Journal of Colloid and Interface Science* **1993,** 156, (2), 285-93.

50. Ravikovitch, P. I.; Domhnaill, S. C. O.; Neimark, A. V.; Schueth, F.; Unger, K. K., Capillary Hysteresis in Nanopores: Theoretical and Experimental Studies of Nitrogen Adsorption on MCM-41. *Langmuir* **1995,** 11, (12), 4765-72.

51. Barrett, E. P.; Joyner, L. G.; Halenda, P. P., The determination of pore volume and area distributions in porous substances. I. Computations from nitrogen isotherms. *Journal of the American Chemical Society* **1951,** 73, 373-80.

52. Kruk, M.; Jaroniec, M., Accurate Method for Calculating Mesopore Size Distributions from Argon Adsorption Data at 87 K Developed Using Model MCM-41 Materials. *Chemistry of Materials* **2000,** 12, (1), 222-230.

53. Neimark, A. V.; Ravikovitch, P. I., Capillary condensation in MMS and pore structure characterization. *Microporous and Mesoporous Materials* **2001,** 44-45, 697-707.

54. Vallee, S. J.; Conner, W. C., Microwaves and Sorption on Oxides: A Surface Temperature Investigation. *Journal of Physical Chemistry B* **2006,** 110, (31), 15459-15470.

55. Flodström, K.; Alfredsson, V., Influence of the block length of triblock copolymers on the formation of mesoporous silica. *Microporous and Mesoporous Materials* **2003,** 59, (2-3), 167-176.

56. Bhambhani, M. R.; Cutting, P. A.; Sing, K. S. W.; Turk, D. H., Analysis of nitrogen adsorption isotherms on porous and nonporous silicas by the BET [Brunauer-Emmett-Teller] and as methods. *Journal of Colloid and Interface Science* **1972,** 38, (1), 109-17.

57. Gur'yanova, L. N.; Gur'yanov, V. V., Analysis of the adsorption isotherms of nitrogen and argon on nonporous and very porous silica. II. Adsorption of argon on hydroxylated silica. *Zhurnal Fizicheskoi Khimii* **1989,** 63, (2), 426-31.

58. Luan, Z.; Hartmann, M.; Zhao, D.; Zhou, W.; Kevan, L., Alumination and Ion Exchange of Mesoporous SBA-15 Molecular Sieves. *Chemistry of Materials* **1999,** 11, (6), 1621-1627.

59. Newalkar, B. L.; Komarneni, S.; Katsuki, H., Rapid synthesis of mesoporous SBA-15 molecular sieve by a microwave-hydrothermal process. *Chemical Communications (Cambridge)* **2000**, (23), 2389-2390.

60. Newalkar, B. L.; Komarneni, S., Control over Microporosity of Ordered Microporous-Mesoporous Silica SBA-15 Framework under Microwave-Hydrothermal Conditions: Effect of Salt Addition. *Chemistry of Materials* **2001,** 13, (12), 4573-4579.

61. Tompsett, G. A.; Conner, W. C.; Yngvesson, K. S., Microwave synthesis of nanoporous materials. *ChemPhysChem* **2006,** 7, (2), 296-319.

62. Baerlocher, C.; Meier, W.; Olson, D., *Atlas of Zeolite Framework Types*. 5th Revised ed.; Elsevier: 2001; 'Vol.' p 1-308.

63. Anon., Database of Zeolite Structures http://www.iza-structure.org/databases/

64. Maglara, E. MSc Thesis. University of Massachusetts, Amherst, 1994.

65. Cook, M.; Conner, W. C., How big are the pores of zeolites? *Proceedings of the International Zeolite Conference, 12th, Baltimore, July 5-10, 1998* **1999,** 1, 409-414.

66. Liang, S. C., The calculation of thermal transpiration. *Journal of Physical Chemistry* **1953,** 57, 910-11.

67. Cheng, L. S.; Yang, R. T., Predicting isotherms in micropores for different molecules and temperatures from a known isotherm by improved Horvath-Kawazoe equations. *Adsorption* **1995,** 1, (3), 187-96.

68. Liu, J.; Zhang, X.; Han, Y.; Xiao, F. S., Direct Observation of Nanorange Ordered Microporosity within Mesoporous Molecular Sieves. *Chemistry of Materials* **2002,** 14, (6), 2536-2540.

69. Sayari, A.; Crusson, E.; Kaliaguine, S.; Brown, J. R., External surface areas of H-ZSM 5 zeolites. *Langmuir* **1991,** 7, (2), 314-17.

70. Chang, C. D.; Silvestri, A. J., The conversion of methanol and other O-compounds to hydrocarbons over zeolite catalysts. *Journal of Catalysis* **1977,** 47, (2), 249-59.

71. Chen, N. Y.; Kaeding, W. W.; Dwyer, F. G., Para-directed aromatic reactions over shape-selective molecular sieve zeolite catalysts. *Journal of the American Chemical Society* **1979,** 101, (22), 6783-4.

72. Weisz, P. B., Molecular shape selective catalysis. *Studies in Surface Science and Catalysis* **1981,** 7, (Pt. A, New Horiz. Catal.), 3-20.

73. Suzuki, I.; Oki, S.; Namba, S., Determination of external surface areas of zeolites. *Journal of Catalysis* **1986,** 100, (1), 219-27.

74. Suzuki, I.; Namba, S.; Yashima, T., Determination of external surface area of ZSM-5 type zeolite. *Journal of Catalysis* **1983,** 81, (2), 485-8.

75. Liu, Z.; Ottaviani, M. F.; Abrams, L.; Lei, X.; Turro, N. J., Characterization of the External Surface of Silicalites Employing Electron Paramagnetic Resonance. *Journal of Physical Chemistry A* **2004,** 108, (39), 8040-8047.

76. Gregg, S. J.; Langford, J. F., Evaluation of microporosity, with special reference to a carbon black. *Transactions of the Faraday Society* **1969,** 65, (5), 1394-400.

77. Carrott, P. J. M.; Drummond, F. C.; Kenny, M. B.; Roberts, R. A.; Sing, K. S. W., Desorption of n-nonane from microporous carbons. *Colloids and Surfaces* **1989,** 37, 1-13.

78. Kondratyuk, P.; Yates, J. T., Desorption kinetic detection of different adsorption sites on opened carbon single walled nanotubes: The adsorption of n-nonane and CCl4. *Chemical Physics Letters* **2005,** 410, (4-6), 324-329.

79. Choi, K.-Y.; Tompsett, G.; Conner, W. C., Microwave synthesis engineering - Power delivery and energy efficiency. *Green Chemistry* **2007,** In preparation.

80. Waller, P.; Shan, Z.; Marchese, L.; Tartaglione, G.; Zhou, W.; Jansen, J. C.; Maschmeyer, T., Zeolite nanocrystals inside mesoporous TUD-1: A high-performance catalytic composite. *Chemistry--A European Journal* **2004,** 10, (20), 4970-4976.

81. Sakthivel, A.; Huang, S.-J.; Chen, W.-H.; Lan, Z.-H.; Chen, K.-H.; Kim, T.-W.; Ryoo, R.; Chiang, A. S. T.; Liu, S.-B., Replication of Mesoporous Aluminosilicate Molecular Sieves (RMMs) with Zeolite Framework from Mesoporous Carbons (CMKs). *Chemistry of Materials* **2004,** 16, (16), 3168-3175.

82. Hammond, K. D.; Tompsett, G. A.; Auerbach, S. M.; Conner, W. C., Jr., Physical Adsorption Analysis of Intact Supported MFI Zeolite Membranes. *Langmuir*, ACS ASAP.

83. Tompsett, G. A.; Krogh, L.; Griffin, D. W.; Conner, W. C., Hysteresis and Scanning Behavior of Mesoporous Molecular Sieves. *Langmuir* **2005,** 21, (18), 8214-8225.

84. Turner, M. D.; Capron, L.; Laurence, R. L.; Conner, W. C., The design and construction of a frequency response apparatus to investigate diffusion in zeolites. *Review of Scientific Instruments* **2001,** 72, (12), 4424-4433.